論文 / 著書情報
Article / Book Information

題目(和文)	安全性と快適性を改善した手首・前腕のリハビリテーションのための装着型ロボットの運動力学解析および設計
Title(English)	Kineto-Static Analysis and Design of Wearable Robot for Wrist and Forearm Rehabilitation with Improved Safety and Comfort
著者(和文)	Liu Ying-Chi
Author(English)	Ying-Chi Liu
出典(和文)	学位:博士（工学）, 学位授与機関:東京工業大学, 報告番号:甲第12181号, 授与年月日:2022年9月22日, 学位の種別:課程博士, 審査員:武田 行生,菅原 雄介,岩附 信行,岡田 昌史,三浦 智
Citation(English)	Degree:Doctor (Engineering), Conferring organization: Tokyo Institute of Technology, Report number:甲第12181号, Conferred date:2022/9/22, Degree Type:Course doctor, Examiner:,,,,
学位種別(和文)	博士論文
Type(English)	Doctoral Thesis

Kineto-Static Analysis and Design of Wearable Robot for Wrist and Forearm Rehabilitation with Improved Safety and Comfort

安全性と快適性を改善した手首・前腕のリハビリテーションのための装着型ロボットの運動力学解析および設計

by

Ying-Chi Liu

DISSERTATION

Presented to
The Graduate major of Mechanical Engineering,
The Department of Mechanical Engineering,
The School of Engineering of Tokyo Institute of Technology
in partial fulfillment of the requirements
for the degree of

DOCTOR OF ENGINEERING

Tokyo Institute of Technology

August 2022

Approved by:

Nobuyuki Iwatsuki
Professor, Dr. Eng.
Department of Mechanical Engineering
School of Engineering

Masafumi Okada
Professor, Dr. Eng.
Department of Mechanical Engineering
School of Engineering

Satoshi Miura
Associate Professor (Lecturer), Dr. Eng.
Department of Mechanical Engineering
School of Engineering

Yusuke Sugahara
Associate Professor [Academic Supervisor], Dr. Eng.
Department of Mechanical Engineering
School of Engineering

Yukio Takeda
Professor [Academic Supervisor], Dr. Eng.
Department of Mechanical Engineering
School of Engineering

Abstract

This dissertation focuses on the development of a wearable hybrid robot for wrist and forearm rehabilitation. The design requirements of rehabilitation robots are not only to achieve the required rehabilitation functions, but also to ensure the safety and comfort of users. To achieve this goal, firstly, a design methodology is proposed that integrates the human and the robot as a whole system in the design process. Therefore, both the human and the robot are considered together to obtain a better design with reduced interaction forces/-torques between the human and robot. With the consideration of the effects of soft and deformable characteristics of human limb, the designer can follow this methodology to design a wearable robot with consideration of the comfort and safety. Taking a 1-DOF wrist rehabilitation planar robot as an example, through kineto-static analysis on this robot, the effects of the initial offset and the use of compliant components are discussed. Then, addition of passive joints to the robot for joint misalignment compensation is analyzed. Through the optimal design, the robot can further ensure the comfort and safety of the user. Finally, the influence of the soft characteristics of human limbs is investigated.

Secondly, a human-robot dynamic model of a rehabilitation robot is developed to further understand the behavior of human soft tissues in rehabilitation movements. The deformations of human soft parts with nonlinear stiffness behavior is addressed. The soft properties of human tissues may reduce the rehabilitation outcomes and result in discomfort of the user. In addition, the utilization of the soft nature of human body is investigated to design a compact rehabilitation robot.

The proposed design is portable and safer due to its portability and ability to compensate for joint misalignment, which is suitable for in-home rehabilitation, which allow the patient to do rehabilitation in a safer environment as their home without spending time and money to go to the hospital.

Next, in order to support more DOFs of wrist rehabilitation movements, the 3-RPS parallel robot is considered as a wrist rehabilitation robot. The 3-RPS robot is a lower-mobility parallel robot which can generate 3 DOFs motions and has a simpler structure compared with full-mobility parallel robot (6 DOFs). However, the parasitic motions of 3-RPS robot in the constrained DOFs may have undesirable effects on performing rehabilitation movements and the comfort of use. The robot is analyzed with consideration of the parasitic motion, initial offsets and the soft characteristic of the human limb. The architecture optimization for a 3-RPS parallel rehabilitation robot is performed, and the optimization goal is to have reduced applied forces and torques to the human limb, which is beneficial for the safety and comfort of users.

Finally, a wearable parallel-serial hybrid robot is proposed for wrist and forearm rehabilitation. The novel mechanisms for joint misalignment compensation are designed to improve the comfort and safety of the user while performing required motion. The robot is lightweight and portable. An experimental study to evaluate the performance of the robot and the comfortability of the user is conducted. The results of the analysis show that the proposed design can meet the rehabilitation requirements. In addition, based on user feedback of an experimental study, the proposed design is modified and improved.

Contents

List of Tables

List of Figures

Nomenclature

ADL Activities of daily living

BP Base platform of 3-RPS

C Center of wrist joint

DOF Degree of Freedom

GA Genetic Algorithm

H Hand attached point

MP Moving platform of 3-RPS robot

N Number of calculations

O Center of robot joint

P Prismatic joint

ROM Range of motion

R Revolute joint

SUS System Usability Scale

S Spherical joint

a_i Radius of base platform of 3-RPS

b_i Radius of moving platform of 3-RPS

d_x Translational deformation along x-axis

d_y Translational deformation along y-axis

d_z Translational deformation along z-axis

d_{tot} Total deformation of human tissues

F_d Unwanted force

i Number of the link

J Jacobian matrix

k_{r} Rotational spring coefficient

k_{tot} Total spring coefficient

k_{t} Translational spring coefficient

l_f Forearm link

l_h Hand link

P_x Parasitic motion along x-axis

P_y Parasitic motion along y-axis

r Link length of planar robot

t Time

T_{in} Input torque

T_{out} Output torque

TI Transmission Index

x	Offset along x-axis
y	Offset along y-axis
α	Angle for the arrangement of revolute joints
δ	Misalignment between forearm and cuff rotation axes
ϵ	Rotation angle of robot output link
η_z	Rotational deformation angle
$\mathcal{F}$	External wrench
$\mathcal{V}$	End-effector twist
ϕ	Parasitic motion about z-axis
ψ	Rotation angle of radial/ulnar deviation movement
τ	Joint forces/torques
θ	Rotation angle of flexion/extension movement

Chapter 1

Introduction

1.1 Background

According to estimates by the World Health Organization (WHO) in 2018, stroke is the first and second leading cause of death in Japan and Taiwan, respectively [1]. Stroke can lead to long-term disability and loss of motor function [2], especially for the increasing elderly population in the aging society. A stroke occurs when part of the brain is deprived of oxygen and can be classified as ischemic stroke and hemorrhagic stroke. The former is due to blockage of blood vessels in the brain, and the latter is due to a bleed in the brain. Either of them can eventually cause brain damage, causing a bunch of brain cells to die and can be fatal. Many stroke survivors suffer from the damage caused by a stroke [3], such as the loss of arm function or muscle weakness and spasticity due to patient's inability to receive or integrate signals from the brain. In addition, they often experience loss of strength on one side of their body, called hemiparesis, making it difficult to walk or balance standing.

Patients with neurological lesions require rehabilitation to restore lost functional capacity, muscle strength, coordination, and shorten

the recovery period [4]. Rehabilitation therapy includes intensive, repetitive, long duration exercises and task-oriented treatment, which stimulate the patient's brain and activates the neuroplastic response [5–7]. Through the rehabilitation therapy, the brain will be retrained and forced to create new neural connections, which has a positive effect on recovery [8,9]. Rehabilitation is an effective way to help patients regain their independence of performing activities of daily living (ADL) and improve their quality of life. However, conventional rehabilitation therapy requires the patient to be treated by a well-trained therapist on a one-to-one treatment as shown in Figure 1.1. This treatment is time-consuming and labor-intensive. Therefore, its effectiveness is limited due to the shortage of the therapists [10].

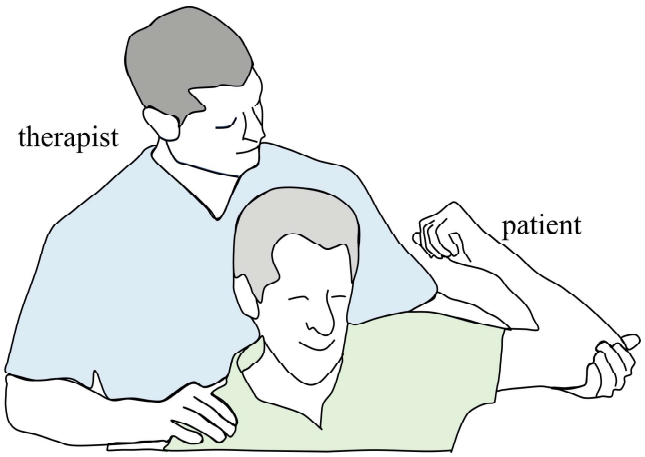

Figure 1.1: A one-to-one conventional rehabilitation therapy.

To overcome this issue, robot-assisted therapy can be an alternative solution to assist rehabilitation therapists. Current rehabilitation robots are not designed to completely replace rehabilitation therapists since the therapists have multiple communications with patients and these interactions are truly beneficial for the treatment [11]. However, robots can provide highly intensive and continuous treatment

to reduce the significant workload of therapists [12]. Moreover, with telecommunication technology and rehabilitation robots with the consideration of safety and portable design, in-home rehabilitation can be achieved, as depicted in Figure 1.2, which allows patients to further reduce the inconveniences, time and cost of needing to go to a hospital for rehabilitation while receiving instructions and advice from therapists via telecommunication [13, 14].

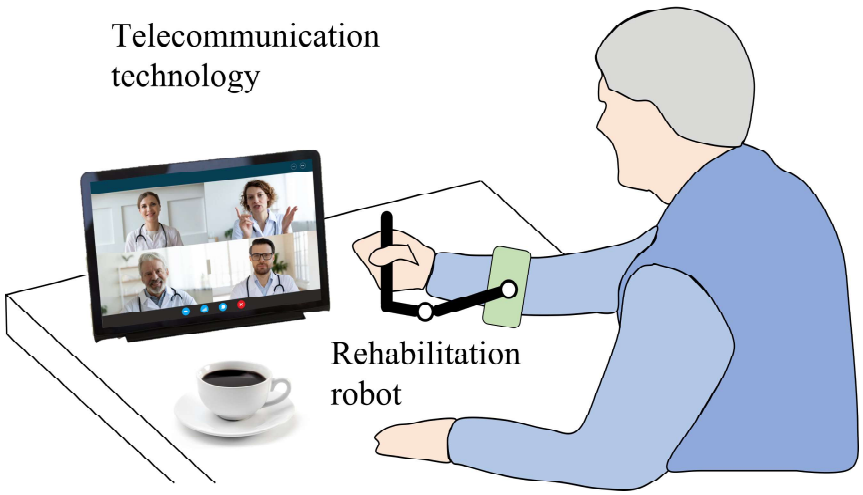

Figure 1.2: Robot-assisted therapy for in-home rehabilitation.

1.2 Robot-Assisted Rehabilitation Devices

The need for physical rehabilitation has increased due to the aging of the world population and the rising prevalence of chronic diseases, leading to the development of a variety of rehabilitation robots over the last four decades [15–17]. A comprehensive analysis was performed by Norouzi-Gheidari et al. [18] and they found the robot-assisted therapy could be effective in assisting rehabilitation. In addition, some robots have already been commercialized and used in practice for rehabilitation treatment. The aim of rehabilitation robotics comes

from their ability to performing repetitive and intensive rehabilitation treatments for impaired limbs over a longer period of time. Furthermore, robots also enable to monitor the patient's movements, and the recorded data can be used by therapists to evaluate the effects of treatment and rehabilitation outcome of patients. In the meantime, with the advancement of entertaining assistance technology such as Augmented Reality (AR) and Virtual Reality (VR) tools, connected to rehabilitation robotics [19], patients can experience increasing sense of immersion and are more willing to participate in rehabilitation towards improved recovery results [20].

1.2.1 The Classifications of Rehabilitation Robots

Rehabilitation robots are generally classified into two categories, based on their mechanical structures: end-effector type robots and exoskeleton type robots as shown in Figure 1.3. The end-effector type is connected to the distal part of the human limb, such as the palm. And the posture of the human limb is changed through the movement of the contacted end-effector. The advantage of the end-effector type robots is the relatively simpler structure and the ability to adapt to different lengths of the user's limb. However, this type of robot can only ensure the end of the limb to a target position, but not the movement of an individual joint of the limb. In addition, it is not possible to control the applied torque to the target joint, which may cause the risk of the joint to be injured by the exceeding torque. The exoskeleton type has a structure similar to the human limbs and is in contact with the limb through attachments such as cuffs or straps at multiple connection points. Exoskeletons can provide direct force or torque to specific impaired joints which are thought to be beneficial for rehabilitation. They require correct alignment between human and robot joints to

avoid unwanted force generated, which will be discussed later in Section 1.3. Rehabilitation robots can also be classified in many ways

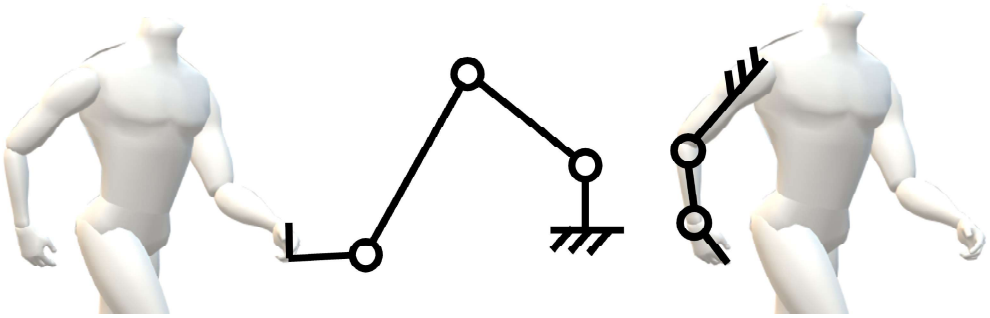

(a) end-effector type (b) exoskeleton type

Figure 1.3: Classifications of rehabilitation robots.

based on different points of view. For the linkage configuration such as serial, parallel and hybrid. For the method of actuation such as electric, pneumatic, and hydraulic. For the type of assistance such as active, passive, and interactive. More details are described in [17, 21].

1.2.2 Review of the Upper-limb Rehabilitation Robots

The ability to move one's upper limbs is crucial for activities of daily living. Approximately between 50% and 70% of stroke patients experience some symptoms of upper limb dysfunction [22]. The loss of upper limb function will cause patients to be unable to live independently, especially the wrist and forearm movements are related to many basic ADL (activities of daily living). A variety of rehabilitation robots have been developed, analyzed, or even used for practical treatment [15, 16, 21, 23]. Some significant researches are presented below by their mechanical structural classification.

Examples of upper-limb end-effector type robots include MIT-MANUS [24, 25], MIME [26, 27], GENTLE/s [28], Bi-Manus-Track [29], REHAROB [30], ARM guide [31]. The MIT-MANUS project was started

in 1989 with the development of a device to assist people perform upper-limb rehabilitation exercises. The system was designed for wrist and forearm movements. Users need to grab a joystick-like handle and perform specific actions to complete tasks displayed on the monitor, just like playing a video game. MIT-MANUS has been commercialized with positive results in clinical trials. In 2002, Mirror image movement enabler (MIME) was tested and designed for shoulder and elbow movements. The users are seated in a wheelchair and a Puma 560 robot was used to move their limb. Different types of assistance mode were applied to improve user's muscles strength and limb movements. However, safety concerns may be raised by the use of industrial robots interacting with humans. In 2003, GENTLE/s system was developed by applying haptic interface and VR technology for the upper-limb rehabilitation movements following human-like trajectories. This did enhance the user's willingness to use the robot and obtained positive feedback from patients by the clinical research. Bi-Manus-Track was designed for wrist flexion/extension and forearm pronation/supination. The system is simple, low-cost and can provide bilateral exercises for both healthy and impaired limb, which can promote functional recovery because it stimulated both sides of the brain. REHAROB therapeutic system was developed for the movements of shoulder and elbow. The system used two 6-DOFs industrial robots to perform the exercise guided by the therapist. During the rehabilitation process, the system will record the trajectories and move the user's limb at a constant speed. However, there are still safety concerns regarding the use of industrial robotic arms with the users. ARM guide is a simple and low-cost rehabilitation robot with only one motor for evaluating and training the impaired arm. The user is attached their arm to a splint and moves their arm along the linear guide of the

robot. However, the system cannot accurately measure the constraint forces according to the trajectory difference between ARM guide and the natural, unperturbed reaching movements of human.

Examples of upper-limb exoskeleton type robots includes MAHI [32, 33], ARMin [34–36], T-WREX [37], Dampace [38], RUPERT [39], SUEFUL-7 [40], L-EXOS [41], CADEN-7 [42]. MAHI was a 5-DOFs exoskeleton with both electrical motors and cable drives for power transmission. Unlike wearable ones that only attached to the user's body (see Figure 1.3b), MAHI was affixed to a rigid base, therefore, part of reaction forces of the system can be transferred to the ground (see Figure 1.4). The system was designed for elbow, forearm and wrist rehabilitation movements with VR and haptic applications in the rehabilitation sessions. MAHI II had further improvements over MAHI on reduction of backlash and singularities, increased output torques and better ergonomics design. ARMin was developed through an iterative design process and was considered as one of the mature exoskeleton type rehabilitation robots. The system was designed to provide 7 DOFs for the rehabilitation of whole upper-limb, including wrist, forearm, elbow and shoulder joints. It also applied a coupling mechanism to deal with the misalignment between robot and anatomical joint axes of shoulder. ARMin was commercialized as the name of Armeo Power and the rehabilitation effectiveness had been proven by many clinical studies. However, the robotic arm of the system was grounded so it can not be portable. T-WREX was an upper-limb rehabilitation robot with 5 DOFs. The system had mechanisms for gravity compensation for the upper-limb to perform gravity-supported exercises. T-WREX was commercialized by the name of Armeo Spring. However, the pneumatic actuators used in the system may cause some control challenges for their nonlinear behavior and delayed response. In 2007, Dampace

was developed as an exoskeleton for force-coordinator trainer for the upper limb. The system has two translational DOFs for shoulder joint misalignment compensation. Therefore, Dampace was considered as having a self-aligning feature. RUPERT was designed to provide 4 DOFs by using pneumatic muscles for movements of shoulder, elbow, forearm and wrist. The links of the system can be adjusted to adapt to different limb lengths and the movements of user can be assessed in real-time. SUEFUL-7 was developed as an exoskeleton for upper-limb which was mounted on the wheelchair. It applied the control method by using both the upper-limb posture and EMG signals to control the robot in real-time. However, the system was still bulky and not portable due to the robot was fixed to a stationary pole. In 2007, L-EXOS was developed to provide 5 DOFs for upper-limb movements. As a tendon driven wearable robot, the actuators were placed out of the moving parts of the robot and the weight of the exoskeleton can be reduced. Another cable-driven exoskeleton called CANDEN-7 had been developed as an exoskeleton with 7 DOFs for upper-limb. The system considered the range of motion (ROM) of all joints of upper limb so it can achieve almost all ROM required for ADL. However, it cannot be portable because of its heavy weight and large size.

In Table 1.1, some robotic devices for upper limb rehabilitation are summarized in terms of the supported movements, DOFs, type, and characteristics.

1.3 The Requirement and Design Challenge

In recent years, more and more attention has been paid to the development of exoskeleton type rehabilitation robots, especially their wearable feature has the potential benefits for in-home rehabilitation

Table 1.1: Robotic devices for upper limb rehabilitation.

System Name	Supported Movements	DOF	Type	Characteristics
MIT-MANUS	HD, WR, FA	5	EE	Planar manipulator; Integrated with VR
MIME	EL, SD	6	EE	Mounted on wheelchair
GENTLE/s	FA, EL, SD	6	EE	Support movements following human-like trajectories
Bi-Manus-Track	WR(FE), FA(PS)	2	EE	Provide bilateral exercises for both limbs
REHAROB	EL, SD	12	EE	Integrated with two industrial robotic arms.
ARM guide	EL, SD	3	EE	Simple and low-cost.
MAHI	WR(FE-RUD), FA(PS), EL(FE)	5	EXO	Cable-driven; Reduced weight; Integrated with VR
ARMin	FG(GR), WR(FE), FA(PS), EL(FE), SD(FE-AA-IER)	7	EXO	Cable-driven; Reduced weight; Coupling mechanisms for joint misalignment compensation
T-WREX	FG(GR), EL(FE), SD(FE-AA-IER)	5	EXO	Mounted on wheelchair; Use pneumatic actuators
Dampace	EL(FE), SD(FE-AA-IER)	4	EXO	Two translational DOFs for misalignment compensation
RUPERT	WR(FE), FA(PS), EL(FE), SD(FE-AA)	5	EXO	Assessment of rehabilitation movements in real-time
SUEFUL-7	WR(FE-RUD), FA(PS), EL(FE), SD(FE-AA-IER)	7	EXO	Mounted on wheelchair; Use EMG signal for control
L-EXOS	FA(PS), EL(FE), SD(FE-AA-IER)	5	EXO	Cable-driven; Reduced weight
CADEN-7	WR(FE-RUD), FA(PS), EL(FE), SD(FE-AA-IER)	7	EXO	Cable-driven; Reduced weight; Support ROM of ADL.

Abbreviations: GR: grasp & release, FE: flexion & extension, RUD: radial & ulnar deviation, PS: pronation & supination, AA: abduction & adduction, IER: internal & external rotation, DOF: degree of freedom, EMG: electromyography.

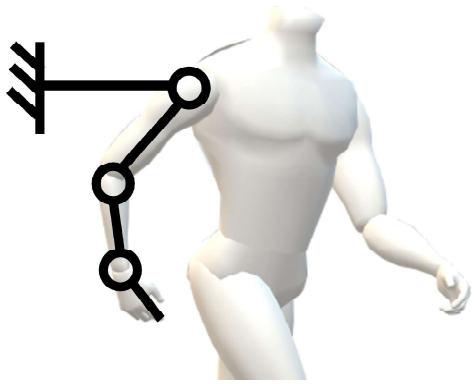

Figure 1.4: The concept of the grounded exoskeleton.

compared to those fixed on the ground, which are usually larger and heavier [16]. In addition, since rehabilitation usually takes a long time, it is important for robots to be light-weight. Heavy weights tend to make the wearer feel tired because of the increased energy consumption and muscle fatigue. Furthermore, since the robots are worn on a patient' s limbs, the robot joints need to be carefully aligned with the human joints in order to avoid misalignment between the two joints, which may cause the generation of unwanted forces [43]. Unwanted forces should be reduced throughout the design process since they might cause the user to feel uncomfortable or even painfully. Tucan et al. [44] indicate that the focus should be on the guaranteed safety of the medical device and the design should follow a risk assessment process to identify and overcome the risks. Indeed, a safe rehabilitation robot should offer movement support without causing the user any discomfort, pain, or movement disturbance. If the user feels uncomfortable when using the robot, it will significantly lower the user' s willingness to use it and thus reduce the rehabilitation effects [45]. How to address the misalignment issue has been the subject of several studies. However, due to the complex structure of human joints and

the soft nature of the human body, ensuring joint alignment remains a challenging issue for robot-assisted therapy [43].

1.3.1 Joint Misalignment Compensation

Joint misalignment is a misalignment between the joint rotation axis of the human and robot joint, and therefore a displacement exists between them [43]. Joint misalignment happens for a variety of reasons. One of them is about the design of exoskeleton robots that the robot joints do not support all the DOF of the human joints. If kinematic mismatch exists between the exoskeleton and the human arm, joint misalignment cannot be avoided. In addition, it is not easy to define the accurate position of the rotation axis of the human joint, therefore, initial offset is often expected to exist. Furthermore, the axis of rotation of the human joint is not fixed but slightly migrates during the movements of the limb, which increases the challenge of the proper alignment.

According to the study by Näf et al. [43], joint misalignment compensation strategies mainly include manual adjustment, the use of compliant elements and the addition of passive joints. First, manual adjustment is adopted by many rehabilitation devices, although this method only ensures good initial alignment. It requires precise measurement of the position of the user's joints and therefore requires a professional and skillful approach to measure. In addition, due to the difference in the length of the user's limb, it usually takes time to adjust the misalignment, which often results in a significant increase in wearing time. Second, the use of compliant elements, such as flexible links or joints, can allow for small deformations to reduce joint misalignment effects. However, this approach can only compensate for part of the joint misalignment. Third, by adding passive joints into

the robot can compensate joint misalignment effect, and this strategy has also been applied by many researchers [46–51]. However, the added joints and links increase the weight and complexity of the robot. In this thesis, the addition of passive joints is applied to compensate for misalignment and apply the deformable properties of the human body, which the detail will be discussed in the next subsection, as an addition passive joint and attempt to solve the disadvantages of increasing weight and complexity.

1.3.2 Characteristics of Human Tissues

Wearable rehabilitation robots for the upper limb are usually fixed to the arm at several fixations through cuffs or straps. Human tissues are soft and highly deformable due to the low stiffness. The characteristics of human soft tissues, such as skin and muscle, have been studied through a number of in-vitro and in-vivo experiments [52, 53]. The stiffness of human tissue varies in different parts of the body and is affected by age. Rocon et al. have presented a strain stress curve of the soft tissues at a point of the forearm and observed highly nonlinear and hysteresis behavior [54]. For wearable robots, it is important to understand the tissue deformation during the rehabilitation, because it is directly related to the safety and comfort of the user. However, so far, the effect of the soft tissue in rehabilitation with robots has not been fully clarified through research. In this dissertation, the effects of human soft tissue on the movement of rehabilitation robot are analyzed and the design of the robot for reduced forces/torques to the human body is applied to improve the safety and comfort of the user.

The relationship between the applied force/torque on soft tissues and the discomfort is complex and not clearly defined. Since the comfort of using the wearable robot highly depends on human's feelings,

which is very sensitive to the deformation of soft tissues. Also, the shear forces on skin can easily cause pain [55]. Especially the human pain threshold is related to human soft tissues and some studies have combined peak pressure, pressure gradients and contact area to define discomfort [56]. However, the results are very different depending on the testing location of the human body. Due to the complex structure of human tissue and many variables affecting the outcome including skin moisture, measurement locations and age of the subject [57, 58], making it difficult to obtain convincing data. In addition, not only the magnitude of the force makes the user uncomfortable, but also the frequency and duration of the force can affect user's feeling. For example, with regard to wearable rehabilitation robots, since the rehabilitation is a long and repetitive process, even relatively small forces/torques applied to human body may cause discomfort or even injury to the user.

1.3.3 Functional Requirements

In general, robot-assisted therapy includes two main application fields: providing physical therapy and supporting to perform some ADLs. Two requirements are focused: the first is the precise rehabilitation movements of the robot for rehabilitation treatment; the second is ensuring the safety and comfort. In order to perform many ADLs, FE and RUD movements of the wrist and PS movements of the forearm are necessary as depicted in Figure 1.5a, and some basic movements of ADL also need to include FE movements of the elbow, such as eating with a spoon or drinking a cup of tea as illustrated in Figure 1.5b. This dissertation mainly focuses on providing physical therapy, however, supporting to perform some ADLs is also beneficial for the rehabilitation.

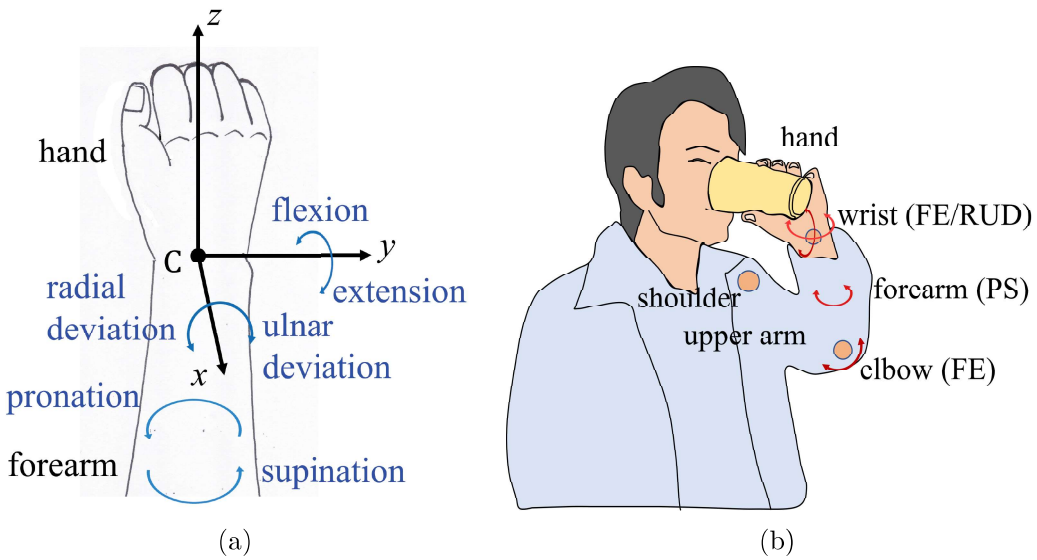

Figure 1.5: (a) Rehabilitation movements; (b) ADL movements.

In addition, the wearable and portable features of the robot are also valuable properties, since with these features, the users do not require to go the hospital or the medical center for rehabilitation. Therefore, it can benefit for in-home rehabilitation, especially in the current severe COVID-19 epidemic, to perform the rehabilitation in a safe environment is necessary and important. As a wearable robot, it is worn by the user, therefore, to design considering lightweight, portable, comfort, and safety is required. One potential risk is the misalignment of robot and human joints, which can have serious impacts on comfort and safety, as unwanted forces are generated. Some rehabilitation robots are designed considering wrist, elbow or shoulder alignment [43], however, the alignment for the forearm PS motion is often ignored.

The PS movement of the forearm plays an important role in the functionality of the upper limb, and if it is hindered, it will have a serious impact on performing ADLs. For robot-assisted rehabilitation of

forearm PS movement, it is usually achieved by rotating the rigid links or attachments which are fixed to the forearm and rotated around the rotation axis of robot. However, the PS movement is a complex movement that couples the rotation between humerus, ulna and radius. The rotation is around an axis that runs from the head of the radius to the head of the ulna. In other words, the axis of rotation is not purely straight along the forearm. On the other hand, the rotation axis of the forearm is not constant during the movements [59]. Therefore, in such a situation, joint misalignment may easily occur which leads to generation of the unwanted forces and cause safety problems.

The second requirement is related to safety and comfort with consideration of the wearable robot is directly contacted with the human body. Due to the softness of the human body, the deformation of the human body has a number of effects on the robot's ability. To analyze and understand the effects of the deformation is important and with consideration of reducing these effects in the early design phase can help to design safer rehabilitation robots and reduce the cost of design modifications. This dissertation considers the soft characteristics of human limb and how the misalignment between human and robot joints affecting the safety and comfort. In general, safety and comfort are related and influenced to each other, however they are not the same. Safety refers to the absence of hazards or dangers and guarantees of security under certain conditions. Safety should be considered as the highest priority requirement when the robot interacts with the human [60]. Comfort, on the other hand, is when the user does not feel pain or constraint, and has a feeling of contentment during the movements. As mentioned in Subsection 1.3.2, the comfort of the user cannot be easily defined and measured.

In the field of industrial robotics, safety issues are usually related to

bruising from the impacts, clamping by the rigid links or end-effector tools, cutting by the sharp edges of the robot [61], which involve a wider scope of issues. For applications of the wearable rehabilitation robots described in this dissertation, the safety issues will be focused on reducing the forces/torques applied to the human body which is directly related to risk avoidance. A simple and effective way to ensure safety is to analyze whether the force applied to human exceeds the human pain tolerance in the design phase. According to [62], the pain tolerance threshold value of 10 N on the measurement of upper arm against static normal force was obtained by an experimental study. In addition, according to [63], the forearm is more sensitive to the shear force than the normal force. Also, the average shear force for sensing the force stimulus is about half of the normal force. Therefore, 5 N of shear force is set as pain tolerance threshold value to ensure the safety, which will be discussed in detail in Subsection 2.5.2. Furthermore, the validation of the design of the prototype related to safety and comfort is done by human experiments. With this point of view, effective solutions are provided to improve comfort and safety of the user when using the wearable robot.

1.4 Design Methodology

To address these challenges, firstly, the proposed design methodology is introduced and the concept of the dynamic pair which is used in the methodology is described. The special feature of the proposed design methodology is that it takes into account the soft properties of the human body in the design process. Through the kineto-static analysis of the whole human-robot system, the design can achieve not only meeting the requirement of rehabilitation function, but also ensuring

the comfort and safety of the user. Then, the proposed prototype is evaluated through experimental study and the effectiveness of the methodology is validated.

The core of this design methodology is the concept of the dynamic pair, which was proposed by Takeda et al. [64]. Instead of considering the human-machine connection as an ideal rigid constraint, the connection part is modelled as a dynamic pair to represent the coupling between the human body and the robot, as shown in Figure 1.6. Then, both the human limb and the rehabilitation robot as a whole system can be analyzed. The dynamic pair contains many mechanical behaviors, including type of motion (rotation or translation), type of actuation (passive or active) and some mechanical properties (spring coefficient, damping coefficient, etc). By incorporating the dynamic pair into the design, it is expected that it will more accurately reflect the actual situations in which wearable rehabilitation robots are used. In addition, the corresponding designs based on the analysis results can be made to ensure the effectiveness and safety of the robot.

1.4.1 Proposed design methodology

The design methodology is divided into three phases and has eight stages. The designer will be able to design a prototype of a wearable rehabilitation robot by following the steps of this design methodology. Figure 1.7 shows the process of the design methodology.

The phase 1 is the preparation work to identify the requirements before starting the design. This phase consists of two stages, including determining the supported joints and the ROM of target joint movements. This requires referring to actual rehabilitation exercises or consulting with a professional therapist. Then to determine how to attach the robot to the human limb and how many connections are

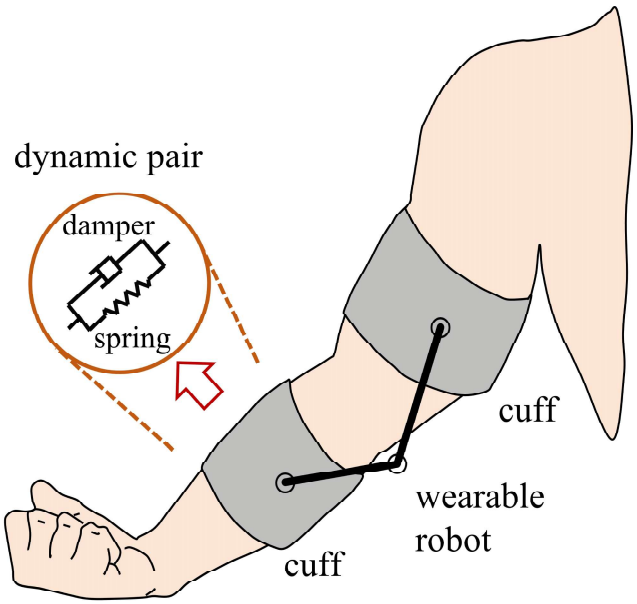

Figure 1.6: The concept of dynamic pair.

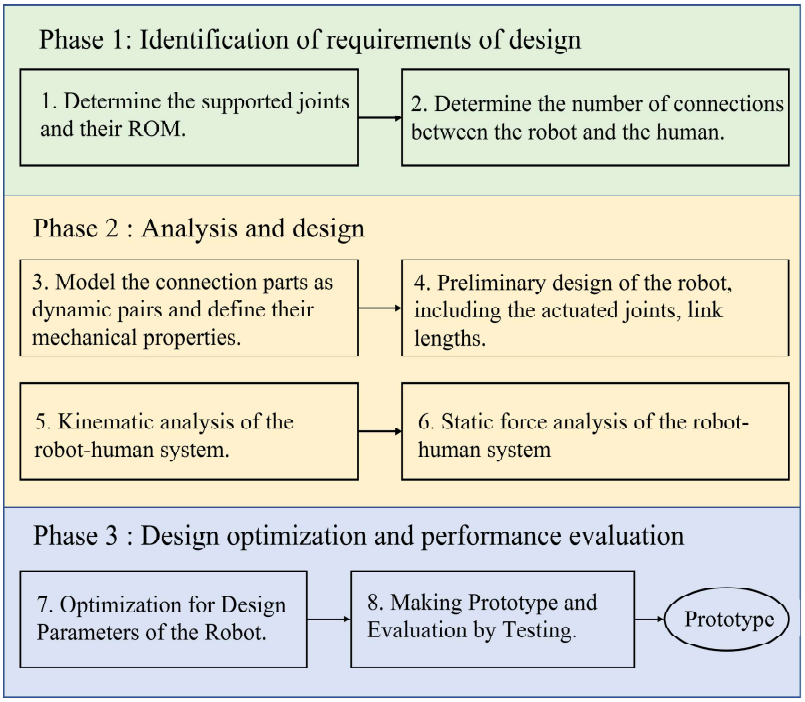

Figure 1.7: The design methodology of the wearable rehabilitation robot.

needed. This requires consideration of user comfort and wearing convenience with ergonomic design. After this phase, the requirements of the design can be obtained.

The phase 2 is mainly the process of analysis and design, which consists of four stages. The first is to apply the dynamic pairs to model the connections parts and determine their mechanical properties including movement type, spring and damping coefficients, and so on. Next, the basic features of the robot are designed including the actuation, types of joints, and the link lengths. Then, with the preliminary design, the kinematic analysis can be conducted to examine the robot's movements. Finally, the static force analysis of the robot-human system is performed to find the forces/torques at each joint and connection. After this phase, a preliminary design of the robot with analyzed results can be achieved.

The phase 3 is the optimal design and performance evaluation of the robot, which consists of 2 sages. Firstly, the optimal design process is conducted with the target objective function. The objective function can be set according to the design requirements. For example, this study is focused on reducing the forces/torques applied to the human limb. Through optimization process, the design parameters can be determined. The next stage is to evaluate the current optimal design of the robot. There are many evaluation criteria to verify the robot. One of the most effective ways is to actually obtain the feedback from users through experiments and modify the design according to the feedback. After this phase, a prototype with the consideration of soft characteristics of human body can be established. By using this methodology, it is an effective way to design a wearable robot with improved safety and comfort.

1.4.2 Scope and Limitation of the Design Methodology

The design methodology can be used as a design process based on the following assumptions:
1. The connection components such as cuffs or braces are tightly attached to the human limb without any slippages.
2. The rehabilitation movement is considered to be quasi-static so that the dynamic effect is not taken into account.

In addition, some important and appealing features such as lightweight, portability, and control strategies are not discussed in this methodology.

1.5 Motivation and Objective

The soft nature of the human body has many effects on the use of wearable rehabilitation robots. These effects may be related to reduced or obstructed range of motion of the robot to affect rehabilitation outcome, or decrease comfort or safety in use, resulting in reduced user's willingness to use the devices. However, most rehabilitation robots do not take into account the softness of the human body at the beginning of the design phase and without consideration of the force and displacement effects on the human body into the design.

In order to clarify how to consider the softness of human limb, and how the softness affects the performance of the robot and comfort of the use while comparing the effects of additional passive joints for misalignment compensation and related issues such as parasitic motions and initial offsets. This dissertation focuses on kineto-static analysis and design of wearable rehabilitation robot for wrist and forearm rehabilitation. A design methodology is proposed with the consideration of human-robot interface behaviors and integrated the connection parts

into the overall design of the rehabilitation robot. Although the design of rehabilitation robots requires consideration of many aspects, such as performance, low cost, volume, and wearable convenience, this design approach focuses on providing effective rehabilitative function while ensuring comfort and safety, which are essential for the user's willingness to use the rehabilitation robot. By applying the proposed design approach, a wearable hybrid robot with comfort and safety for forearm and wrist rehabilitation will be developed.

The concept of the wearable hybrid robot is shown in Figure 1.8. Specifically, the 3-R$\underline{P}$S parallel module is aimed at flexion/extension (FE) and radial/ulnar deviation (RUD) movements of the wrist and the serial module targets pronation and supination (PS) movements of the forearm. In general, serial robots have a larger workspace and are designed in a more intuitive way to provide assistive torques for human joints. Also, due to their relatively smaller size and simpler kinematics, they have been widely used in the field of rehabilitation. Compared with serial robots, parallel robots have some appealing mechanical features such as a relatively stable performance within the entire workspace and smaller configuration changes according to movement, which are a benefit to users' safety. Furthermore, with excellent position accuracy, greater payload capacity, and higher stiffness, parallel robots are considered as a good candidate with better rehabilitation capabilities.

The parallel robots for wrist rehabilitation usually have at least two degrees of freedom (DOFs) for wrist movements in flexion/extension (FE) and radial/ulnar deviation (RUD) movements, some of which can achieve pronation/supination (PS) movements of the forearm [15, 16]. In addition, the 3-R$\underline{P}$S parallel robot used in this dissertation is a lower-mobility parallel robot. This type of robot has attracted much

attention in recent years [65]. They have less than 6 DOFs, thereby reducing the linkages and actuators needed to perform the required tasks while reducing costs and having a simpler structure for in-home rehabilitation. However, the parasitic motions of the lower-mobility parallel robot are the undesired motions in the constrained DOF of the robot, which is considered to be detrimental to many applications, and its impact cannot be ignored. Further details will be discussed in Chapter 4.

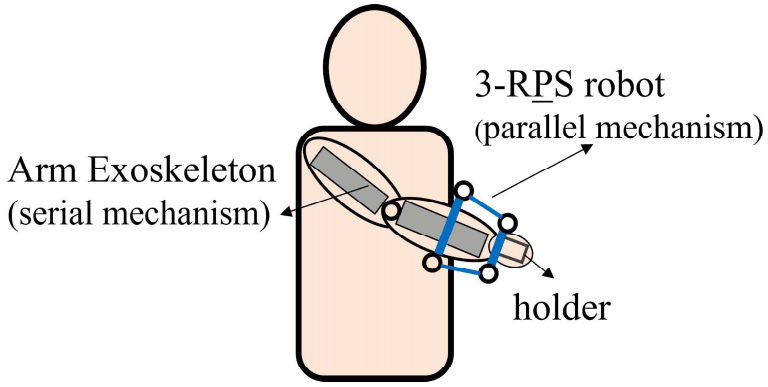

Figure 1.8: The concept of a wearable hybrid robot.

1.6 Outline of the Dissertation

The rest of the dissertation is organized as follows. In Chapter 2, the kineto-static analysis of a 1-DOF wrist rehabilitation robot is presented and the influence of initial offset and compliance elements are discussed. In addition, four cases of design are investigated for joint misalignment compensation. Moreover, a human-robot model is developed to further understand the effect and behavior of human soft tissues when using a wearable robot. In Chapter 3, the kineto-static analysis of the 3-RPS parallel robot is examined and the parasitic motions of the 3-RPS robot are calculated. In addition, by including the

human limb into the robot design, an optimal design process is conducted to minimize the forces and torques applied to the human limbs to improve the safety and comfort. In Chapter 4, a wearable hybrid robot for forearm and wrist rehabilitation is proposed. Moreover, an experimental study is conducted for evaluating the proposed design. In Chapter 5, the conclusion of this dissertation is summarized with discussions of the possible future work to continue research in this field.

Chapter 2

Analysis and Modeling of Human-Robot System

In this chapter, starting with a simple one-degree-of-freedom (1-DOF) wrist rehabilitation robot, the use of compliance and the addition of passive joints for joint misalignment compensation are introduced. In detail, firstly, a kineto-static analysis on a planar wearable rehabilitation robot for wrist flexion/extension (FE) movement is presented and the effects of the initial offset and the use of compliant components is investigated. Secondly, the consideration of the additional passive joints to the robot which forms a planar four-bar mechanism which includes human wrist joint, to compensate for joint misalignment. The optimized design contributes to the comfort and safety of the user. Lastly, the influence of the soft characteristics of human limbs is investigated. This soft property, causing the movement of the braces, results in reducing the angular range of the wrist, which should be considered when designing a wearable robot with the comfort and safety of the patients.

2.1 Objective

The goal of this chapter is to apply the proposed design methodology to create the modeling of a 1-DOF robotic system. The modeling of the interface between human and robot is investigated for four cases. Kineto-static analysis for each case is done for analyzing the joint misalignment compensation by additional passive joints and the effect of human soft tissue within a wearable robot. Finally, a human-robot model is established for further understanding the influence of the deformation of the human soft tissues when using a wearable rehabilitation robot.

2.2 Assumptions and Limitation

In this chapter, the following assumptions are made for the analysis:

1. The rehabilitation movements are restricted in the plane, and the movements outside of the plane are ignored.
2. The handle of the robot is firmly grasped by the user's hand, and the effect of the fingers is neglected.
3. The displacement of the human soft tissue is considered only as a translation without rotation and the slippage of the connection between robot and human is not considered.
4. The rehabilitation process is considered to be quasi-static so that the dynamic effects are not taken into account. This means that the model of the human parts has a spring-like behavior and can be modeled as a spring.

For the limitation, only a planar robot is considered in this chapter and the deformation of human soft tissues is also restricted within the plane.

2.3 Analytical Models

In this section, the following four models are introduced, and the proposed design methodology is applied to build the analytical model (R: revolute joint; P: prismatic joint) .
Case 1: 4R model, the addition of passive joints in the robot for misalignment compensation.
Case 2: 3R+1P model, consideration of misalignment and introduction of spring characteristics of hand.
Case 3: 4R+1P model, the addition of passive joints for misalignment compensation and consideration of human soft tissue effects.
Case 4: 3R+1P model, a simplified model of Case 3.

2.3.1 Case 1: 4R model

It has been proven that adding passive joints to the robot is an effective way to compensate for the misalignment of human-robot joints, despite the fact that it also may increase the size and weight of the exoskeleton [50, 51]. Inspired by these studies, the passive joints to be added can be revolute joints or prismatic joints. In order to achieve a more compact design and lower friction mechanism, the revolute joints are used as added passive joints instead of prismatic joint. The conceptual figure of the RRRR four-bar linkage is shown in Figure 2.1a. The hand is attached to the output link of the robot at point H. Also, the analytical model of the RRRR four-bar linkage is depicted in Figure 2.1b. Here, as illustrated in Figure 2.2, three passive revolute joints were applied to form a planar four-bar linkage, where R and R_a denote revolute and active revolute joints, respectively. Through Gruebler' s equation, the degree of freedom (DOF) of the mechanism

can be determined as follows:

$$F = \lambda(n - 1 - j) + \sum_{i=1}^{j} f_i \tag{2.1}$$

where λ is the DOF of the motion space, n is the total number of links, j is the total number of joints, and f_i is the DOF of each joint. Once the exoskeleton is connected to the forearm as seen in Figure 2.2a, the human wrist is viewed as a virtual revolute joint to form a closed chain. By substituting $\lambda = 3$, $n = 4$, and $j = 4$ into Equation (2.1), it yields that the DOF of the mechanism is one. This indicates that regardless of the robot's dimensions, the rehabilitation of the wrist joint may be accomplished with a single input from the active revolute joint. Therefore, this mechanism can be adapted to the variation of rotation axis position of the wrist joint. In other words, this fact can be explained by considering the situation of the detachment of the exoskeleton from the human forearm depicted in Figure 2.2b. In this situation, the mechanism becomes an open chain and its DOF becomes three, which is the maximum DOF of planar mechanism. As a result, the hand can be connected to the distal link BC of this robot at any position within the reachable region.

Next, the length of each link of the crank-rocker four-bar linkage can be determined by geometric analysis. As shown in Figure 2.3, $\Delta\theta$ represents the rotation angle range for the output rocker link (r_4). By using Equation (2.2) below, if the lengths of the fixed link r_1 and actuated link r_2 are known, the lengths of the coupler link r_3 and the rocker link r_4 can be obtained for the given rotation angle range. Since the link lengths of the four-bar linkage would have an impact on the static performance of the mechanism. Thus, the optimization should be done to obtain the optimal link lengths, which will be discussed

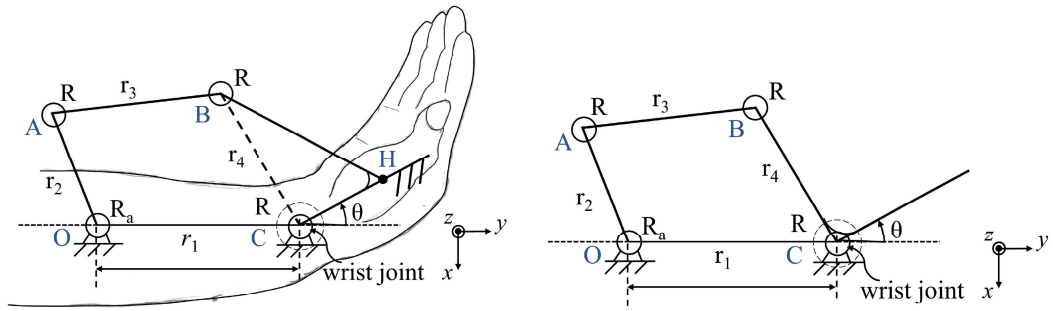

Figure 2.1: (a) Conceptual figure of RRRR four-bar linkage ; (b) Analytical model of RRRR four-bar linkage.

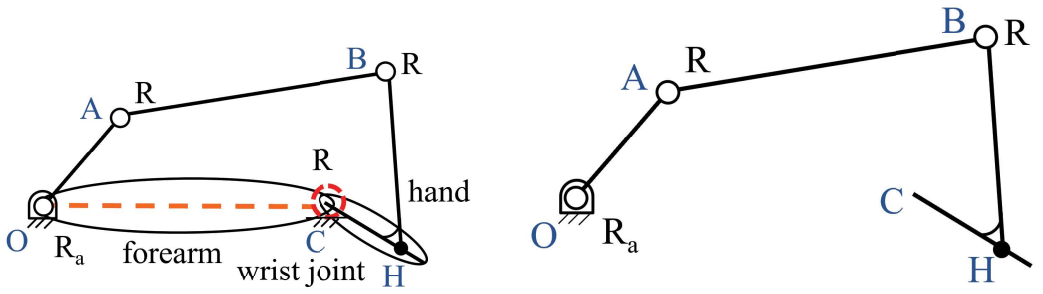

Figure 2.2: (a) Exoskeleton attached to the forearm; (b) exoskeleton detached from the forearm.

later in Subsection 2.4.1. Here, the rotation angle range, $\Delta\theta$, is given as 80 degrees ($-40°$ to $40°$) for wrist flexion-extension motion.

$$r_3 = \frac{r_1}{r_2}\sin\left(\frac{\Delta\theta}{2}\right) r_4,\ r_4 = \sqrt{\frac{{r_2}^2 - {r_1}^2}{1 - \frac{{r_1}^2}{{r_2}^2}\sin^2\left(\frac{\Delta\theta}{2}\right)}} \tag{2.2}$$

Here, the rotation angle range ($\Delta\theta$) for the output rocker link (r_4) is given as 80 degrees ($-40°$ to $40°$) for wrist flexion-extension movement.

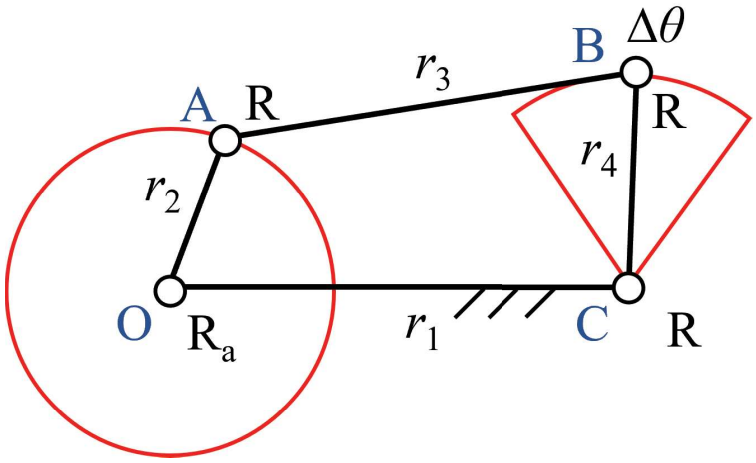

Figure 2.3: Geometric analysis of four-bar linkage.

2.3.2 Case 2: 3R+1P(with spring) model

Figure 2.4 shows a schematic illustration of a planar wrist rehabilitation robot. A coordinate system is defined, and its origin is fixed on the forearm located at the center of the human wrist joint, C-xyz. The wrist joint's considered rotation axis is parallel to the x-coordinate axis and the y-coordinate axis is aligned along the forearm and points in the direction of the hand. The user' s forearm is fastened by the braces to the forearm link (l_{f}). The human hand is also firmly attached to the holder. For the hand flexion/extension movement, the range of motion (ROM) of the wrist joint (θ) is set from $-40°$ to $40°$ according to the investigation provided by [66]. The wrist joint angle is set as $0°$ when the hand is in a neutral posture.

An analytical model of the robot mounted on the human forearm is shown in Figure 2.5. The points C and O marked in Figure 2.5a represent the rotation centers of the human wrist and the robot joint, respectively. k_{tot} is the total spring constant of the hand and holder. θ represents the rotation angle of the hand around the wrist joint,

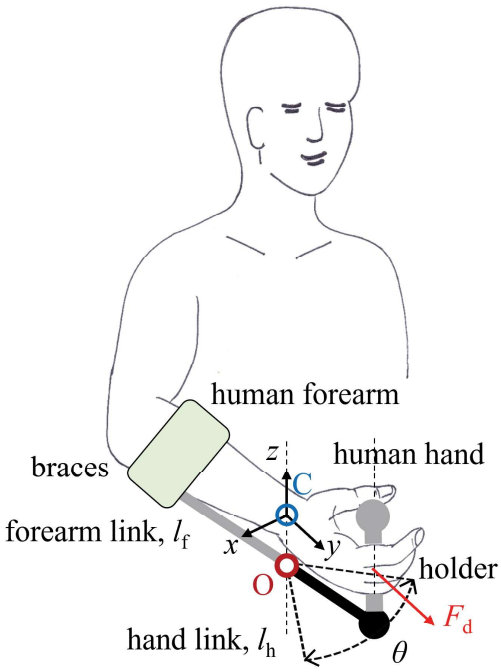

Figure 2.4: Sketch of a 1-DOF wrist rehabilitation robot.

which is defined as an angle between the positive y-axis and the line passing through the C and H. ϵ is the rotation angle of the output link of the robot, which is defined as an angle between the vertical line starting from the O with same direction of the positive y-axis and the line passing through the O and H. Between C and O, there are initial offsets x, y in x and y directions, respectively. l_{h} is the hand link length, and l_{begin} is the distance between C and the hand-attached point H at $\theta = 0$ and l_{end} is the distance at a specified hand rotation angle $\theta = \theta_{\mathrm{end}}$. Taking into consideration the characteristics of human hand soft tissue by applying the dynamic pair, the human hand is modeled as an element including a spring. The displacement (d_{tot}) between C and the hand-attached point H along with the hand varies throughout the rehabilitation motion. The unwanted force F_{d} runs alongside the hand by restricting the displacement in the same

direction.

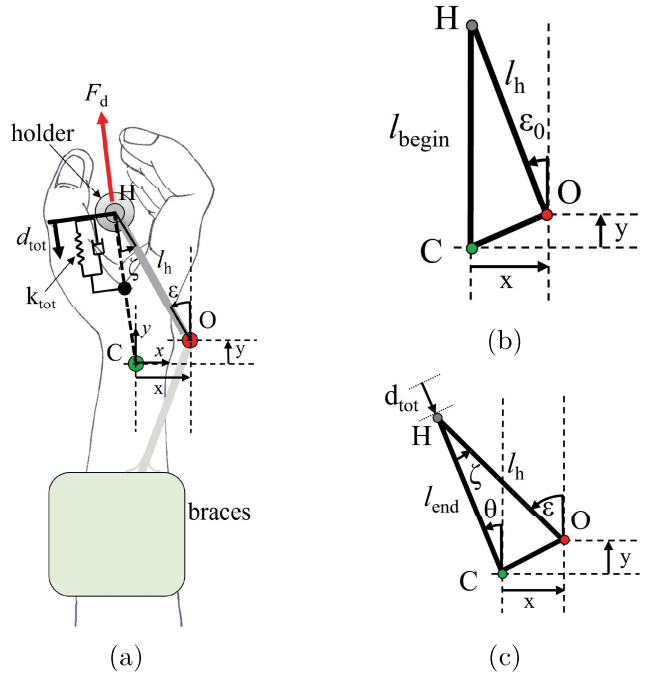

Figure 2.5: Analytical model of a robot with joint misalignment. (a) model of a robot with misalignment; (b) the beginning of the movement process, at $\theta = 0$; (c) the end of the movement process, at $\theta = \theta_{\text{end}}$.

Here, only the deformation of the hand is considered and the length of hand link, l_{h}, is set as 70 mm. An analytical model developed by [67] is adopted to determine the unwanted force caused by joint misalignment. The unwanted force F_d can be described as follows:

$$F_{\text{d}} = k_{\text{tot}} d_{\text{tot}}(\theta, l_h, x, y) \tag{2.3}$$

The beginning and the end of the movement are illustrated in Figure 2.5b and 2.5c. The total displacement can be calculated as follows:

$$d_{\text{tot}} = l_{\text{begin}} - l_{\text{end}} \tag{2.4}$$

$$l_{\text{begin}} = y + l_{\text{h}} \cos(\sin^{-1}(x/l_{\text{h}})) \tag{2.5}$$

$$\zeta = \sin^{-1}\left[\frac{\sqrt{x^2+y^2}\sin\{\theta + \tan^{-1}(x/y)\}}{l_{\mathrm{h}}}\right] \tag{2.6}$$

$$\begin{aligned} l_{\mathrm{end}} = &\Big[l_{\mathrm{h}}^2 + x^2 + y^2 - 2l_{\mathrm{h}}\sqrt{x^2+y^2} \\ &\cos\left\{\pi - \zeta - \theta_{\mathrm{end}} - \tan^{-1}(x/y)\right\}\Big]^{1/2} \end{aligned} \tag{2.7}$$

The displacement (d_{tot}) relies on the angle of rotation of the hand ($\Delta\theta$) and the offsets x and y. In addition, regarding the compliance of the human hand and holder, modeling these two parts as two springs is considered, which are connected in series with each other. If the displacement (d_{tot}) and the total spring constant (k_{tot}) are obtained, the unwanted force (F_{d}) can be calculated.

Here, For the hand flexion-extension movement, the range of motion (ROM) of the wrist joint is set from $-40°$ to $40°$, and when the hand is at a neutral position, the wrist joint angle is set as $0°$. In addition, the hand link length is set as 70 mm.

2.3.3 Case 3: 4R+1P (with spring) model

The 4R+1P model, with consideration of human tissue, is shown in Figure 2.6. d_{tot} represents the displacement of braces, which changes during the movement. The displacement of the human forearm soft tissue is considered only in the direction along the forearm that aligns with y-axis direction in this section. For simplicity, the linear displacement in other directions and the rotation of human soft tissue are ignored. Then, the position and force analysis are done to understand the impact of the human body's softness properties. The length of the fixed link (r_1) would become the following:

$$r_1^{'} = r_1 \pm d_{\mathrm{tot}} \tag{2.8}$$

The effects of human soft characteristics throughout rehabilitation

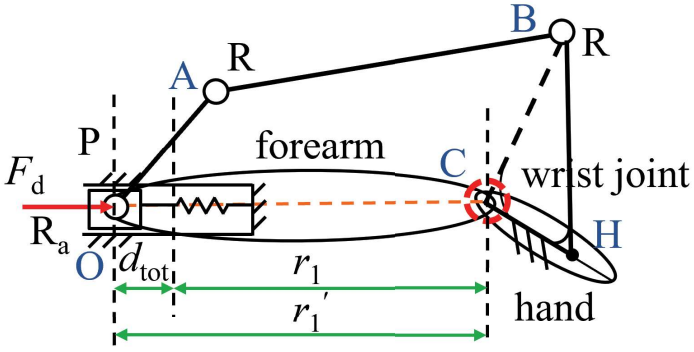

Figure 2.6: Model of 4R+1P with spring.

should be further considered. It's worth noting that the forearm's soft tissue will move during the movement due to its softness. Even if the braces are tightly fastened and attached to the forearm, the migration cannot be avoided due to the soft property of human tissue. Therefore, if the force is applied to the braces, it will cause the braces to move. In short, the distance between the braces and wrist is varied. Here, the maximum amount of forearm tissue expansion is assumed to be 10 mm. Therefore, if the force is applied to the braces, their displacement would be 10 mm. The spring constant of the forearm is set as 143 N/m, as found in the literature [53]. Even if only the maximum displacement (10 mm) is taken into account in this calculation and it cannot accurately predict the exact displacement of the braces' movement, which makes it impossible to forecast the attachment's exact displacement, the effect of the attachment's movement may now be discussed in a reasonable way.

2.3.4 Case 4: 3R+1P(with spring) model

The 3R+1P model is shown in Figure 2.7. The coordinate system is affixed to the human wrist joint, and its origin is located at the center

of the wrist joint. The y-axis points to the hand along the forearm, and the rotation axis of wrist joint is aligned with the x-axis. The links connected to the braces are fastened to the forearm. The human hand is firmly attached to the handle.

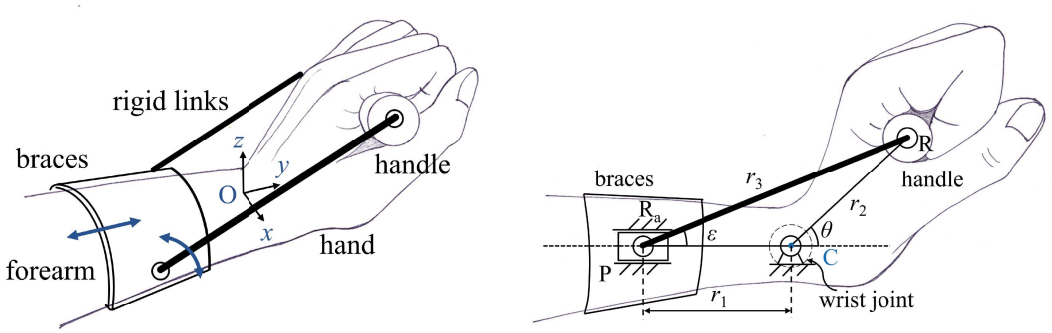

(a) (b)

Figure 2.7: (a) Sketch of a wrist rehabilitation robot; (b) Analytical model of a wrist rehabilitation robot.

The point C marked in Figure 2.7b is the rotation center of wrist joint. The length between the center of attachment and the center of wrist joint is r_1. Here, the value of r_1 changes during motion, which is related to the displacement of the human soft tissue. The distance from the wrist joint center of rotation to the center of handle is r_2. And r_3 represents the length of rigid links connecting the braces and the handle.

The forearm soft tissue is modeled as a passive prismatic joint with the spring. Three passive joints are shown in the closed-loop to form a planar RRPR four-bar slider-crank linkage, as shown in Figure 2.7b which is able to adapt for joint misalignment. This approach follows the previous study [68] by adding passive joints into the kinematic chain. P, R, and R_a denote prismatic, revolute, and active revolute joints, respectively.

Next, the initial distance r_1 between the braces and the wrist joint

can be determined, which is also regarded as a natural length, as shown in Figure 2.8a, and the length of rigid link r_3. Here, by changing the wrist rotation angle θ between θ_{min} and θ_{max}, only the wrist extension motion is considered. The human soft tissue displacements at both θ_{min} and θ_{max} is assumed to be the same value d_{tot}. Then, r_3 can be determined at $\theta = \theta_{min} = 0°$ with a given d_{tot} value as shown in Figure 2.8b. Also, by using the following Equation (2.9), r_1 can be obtained.

$$(r_1 + d_{\text{tot}} + r_2 \cos\theta)^2 + (r_2 \sin\theta)^2 = (r_1 - d_{\text{tot}} + r_2)^2 \tag{2.9}$$

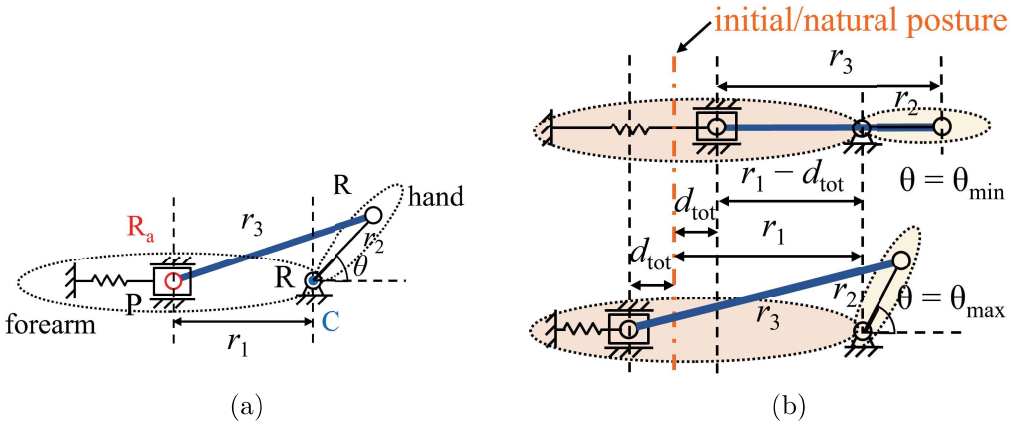

Figure 2.8: (a) Model of four-bar linkage; (b) Geometric analysis of four-bar linkage.

Here, for flexion-extension movement, the range of motion (ROM) is assigned from $-40°$ to $40°$, and the wrist joint angle is $0°$ when the hand is in a neutral posture. In addition, the distance from the wrist joint center of rotation to the center of handle (r_2) is given as 80 mm.

2.4 Kineto-Static Analysis

In this section, the kineto-static analysis for each case described in Section 2.3 is conducted.

2.4.1 Case 1: 4R model

For the four-bar linkage geometry displayed in Figure 2.9, a vector-loop equation is written as follows:

$$\overrightarrow{r_2} + \overrightarrow{r_3} = \overrightarrow{r_1} + \overrightarrow{r_4} \tag{2.10}$$

where each vector represents each link. Then, to express Equation (2.10) in polar form as follows:

$$r_2 e^{j\theta_2} + r_3 e^{j\theta_3} = r_1 e^{j\theta_1} + r_4 e^{j\theta_4} \tag{2.11}$$

By introducing complex numbers for each vector, Equation (2.11) can be written as follows:

$$\begin{aligned} & r_2(\cos\theta_2 + j\sin\theta_2) + r_3(\cos\theta_3 + j\sin\theta_3) \\ & = r_1(\cos\theta_1 + j\sin\theta_1) + r_4(\cos\theta_4 + j\sin\theta_4) \end{aligned} \tag{2.12}$$

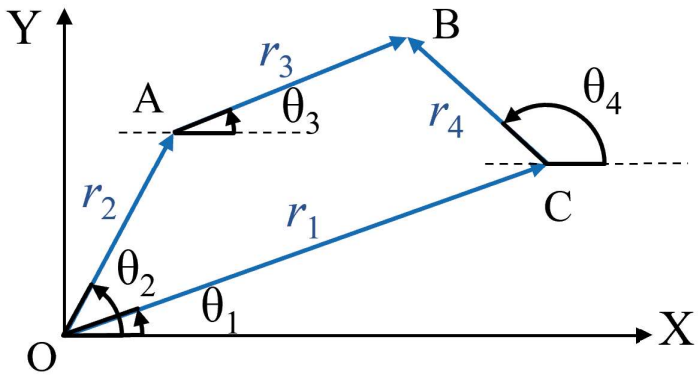

Figure 2.9: Vector loop of four-bar linkage.

Next, Equation (2.12) can be separated into its real and imaginary

components.

$$r_3 \cos\theta_3 = r_1 \cos\theta_1 + r_4 \cos\theta_4 - r_2 \cos\theta_2 \tag{2.13}$$

$$r_3 \sin\theta_3 = r_1 \sin\theta_1 + r_4 \sin\theta_4 - r_2 \sin\theta_2 \tag{2.14}$$

$$\begin{aligned} r_3^2 = r_1^2 + r_2^2 + r_4^2 &+ 2r_1 r_4(\cos\theta_1 \cos\theta_4 + \sin\theta_1 \sin\theta_4) \\ &- 2r_1 r_2(\cos\theta_1 \cos\theta_2 + \sin\theta_1 \sin\theta_2) \\ &- 2r_2 r_4(\cos\theta_2 \cos\theta_4 + \sin\theta_2 \sin\theta_4) \end{aligned} \tag{2.15}$$

To simplify the expression of Equation (2.15), the constants A, B, and C for a given value of θ_2 are defined as follows:

$$\begin{aligned} A &= 2r_1 r_4 \cos\theta_1 - 2r_2 r_4 \cos\theta_2 \\ B &= 2r_1 r_4 \sin\theta_1 - 2r_2 r_4 \sin\theta_2 \\ C &= r_1^2 + r_2^2 - r_3^2 + r_4^2 - 2r_1 r_2(\cos\theta_1 \cos\theta_2 + \sin\theta_1 \sin\theta_2) \end{aligned} \tag{2.16}$$

and Equation (2.15) becomes the following:

$$A \cos\theta_4 + B \sin\theta_4 + C = 0 \tag{2.17}$$

Then, θ_3 and θ_4 can be solved with the universal trigonometric substitution for given θ_2.

$$\theta_4 = 2\tan^{-1}\left(\frac{-B \pm (B^2 - C^2 + A^2)^{1/2}}{(C - A)}\right), -\pi \leq \theta_4 \leq \pi \tag{2.18}$$

$$\theta_3 = \tan^{-1}\left(\frac{r_1 \sin\theta_1 + r_4 \sin\theta_4 - r_2 \sin\theta_2}{r_1 \cos\theta_1 + r_4 \cos\theta_4 - r_2 \cos\theta_2}\right), -\frac{\pi}{2} \leq \theta_3 \leq \frac{\pi}{2} \tag{2.19}$$

Then, based on the aforementioned position analysis, static force analysis has been done in order to analyze the joint forces and required in-

put torque to achieve the desired motion under the wrist joint torque. The free body diagram of the linkage for this analysis is shown in Figure 2.10. According to several biomechanical studies of the activities of daily living, the maximum torque for hand flexion/extension motion is about 0.35 $\mathrm{N} \cdot \mathrm{m}$ [69, 70]. However, patients who require rehabilitation typically have joints that are more resistant to joint motions caused by injury, inflammation, and other conditions. Hence, the output torque (T_{out}) is set as 1.2 $\mathrm{N} \cdot \mathrm{m}$. Then, the equilibrium equations of each link can be put into an equation of using a matrix form as follows:

$$\begin{bmatrix} 1 & 0 & 1 & 0 & 0 & 0 & 0 & 0 & 0 \\ 0 & 1 & 0 & 1 & 0 & 0 & 0 & 0 & 0 \\ 0 & 0 & -a & b & 0 & 0 & 0 & 0 & 1 \\ 0 & 0 & -1 & 0 & 1 & 0 & 0 & 0 & 0 \\ 0 & 0 & 0 & -1 & 0 & 1 & 0 & 0 & 0 \\ 0 & 0 & 0 & 0 & -c & d & 0 & 0 & 0 \\ 0 & 0 & 0 & 0 & -1 & 0 & 1 & 0 & 0 \\ 0 & 0 & 0 & 0 & 0 & -1 & 0 & 1 & 0 \\ 0 & 0 & 0 & 0 & -e & f & 0 & 0 & 0 \end{bmatrix} \begin{bmatrix} F_{1x} \\ F_{1y} \\ F_{2x} \\ F_{2y} \\ F_{3x} \\ F_{3y} \\ F_{4x} \\ F_{4y} \\ T_{in} \end{bmatrix} = \begin{bmatrix} 0 \\ 0 \\ 0 \\ 0 \\ 0 \\ 0 \\ 0 \\ 0 \\ T_{out} \end{bmatrix} \tag{2.20}$$

The unknowns are kept on the left-hand side and the known output torque (T_{out}) is on the right-hand side. These nine unknowns can be solved by Equation (2.20).

Optimal Design

As mentioned earlier, determining the length of links would have a significant impact on the static analysis, the details are shown and discussed later. Here, the genetic algorithm (GA) proposed by Hol-

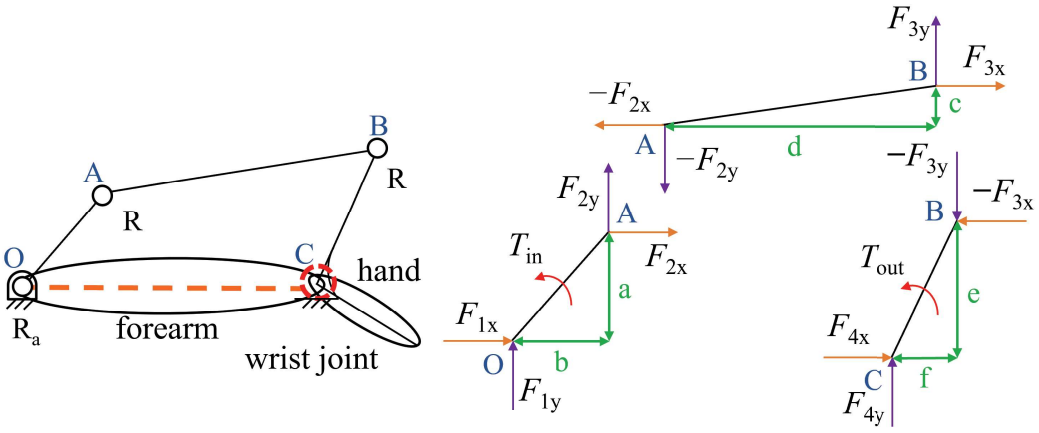

Figure 2.10: Free body diagram of four-bar linkage.

land et al. [71] is used for the optimization of the link length. The GA is an optimization method inspired by evolution for seeking the maximum or minimum value of a given objective function $f(x)$, where $x = x_i = 12, ..., N$. It is capable of producing solutions to prevent falling into local optimal solutions through processes including inheritance, selection, mutation, and crossover. In other words, it shows great promise in obtaining the global optimal solution. This feature is the main reason why this approach is chosen for optimization. For the objective function, the length of each link is determined when the minimum average force is applied on the wrist joint when the rotation of the wrist (θ) varies from $-40°$ to $40°$. In addition, considering the portability of the device, the size and weight of the rehabilitation robot are limited in order to be a light-weight robot. For this purpose, each link length is restricted to not exceeding the length of the r_1 link. The average length of the human forearm between the elbow and the wrist is 274.33 mm [72]. A certain distance between the location of braces and the elbow is reserved; therefore, the maximum link length constraint is set as 200 mm in the optimization. The optimization

problem is expressed in the following statement:

$$\begin{aligned} &minimize\, f(x) = \frac{1}{N}\sum_{i=1}^{N} F_{wrist,i}(x) \\ &subject\, to\, 0 < l_n \leq 200,\ n = 1, \ldots, 4 \end{aligned} \tag{2.21}$$

where N is the number of calculations and F_{wrist} is the force applied on the wrist obtained through each calculation. Since the number of variables used for optimization is two (r_1 and r_2), the population size is set as 70, which follows the rule for a general case that the population size is more than 10 times the of number of variables. Moreover, with the 40-bit length of one variable, the higher accuracy of solutions is ensured. Furthermore, the typical values of crossover rate are in the range 0.5–1.0, and the common values of mutation rate are in the range 0.005–0.05 [73]. Therefore, the crossover rate and mutation rate are set as 0.7 and 0.02, respectively. The flowchart of optimization process is seen in Figure 2.11, and the selected GA parameters are displayed in Table 2.1.

Table 2.1: Genetic algorithm (GA) parameters used in optimization.

Bit Length of One Variable	Population Size	Crossover Rate	Mutation Rate
40	70	0.7	0.02

After one thousand times of genetic generation, the optimal length of each link can be obtained. The optimal link lengths obtained and the constant values of parameters used in analysis are listed in Table 2.2.

2.4.2 Case 2: 3R+1P model (with spring)

With the consideration of the displacement of the hand-attached point, this moving part have been regarded as a prismatic joint con-

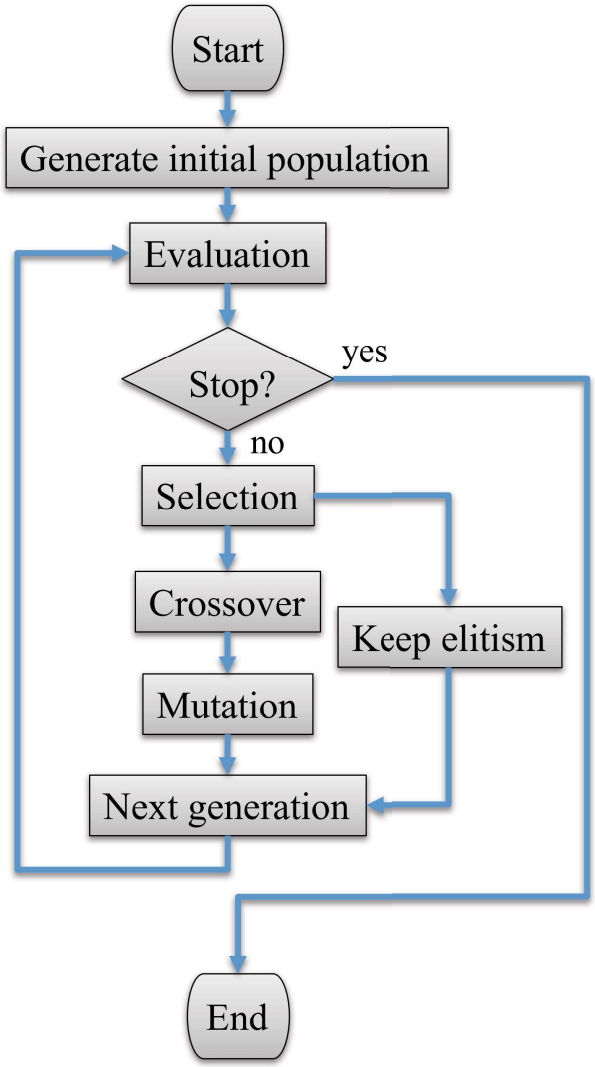

Figure 2.11: Flowchart of genetic algorithm (GA).

Table 2.2: The obtained optimal and constant values of parameters.

Description	Parameter	Value	Unit
Optimal distance between braces and wrist joint	r_1	138.0	mm
Optimal length of crank link	r_2	71.6	mm
Optimal length of coupler link	r_3	199.8	mm
Optimal length of rocker link	r_4	161.3	mm
Spring constant of forearm	k	143	N/m
Output torque	T_{out}	1.2	$\text{N} \cdot \text{m}$

nected to a spring. Therefore, the movement of the prismatic joint should be related to the spring constant of the hand. Owing to various measurement conditions, the spring constant of the human hand could be varied [74] and it is adopted as 172.5 N/m here. Based on the above presumptions, the mechanism with the wrist joint can form an RRPR planar four-bar linkage. Similarly, the free body diagram depicted in Figure 2.12 is applied to calculate the joint forces. Then, the equilibrium equations can be written in the matrix form as follows:

$$\begin{bmatrix} 1 & 0 & 1 & 0 & 0 & 0 & 0 & 0 & 0 \\ 0 & 1 & 0 & 1 & 0 & 0 & 0 & 0 & 0 \\ 0 & 0 & -a & b & 0 & 0 & 0 & 0 & 1 \\ 0 & 0 & -1 & 0 & \cos\theta & 0 & 0 & 0 & 0 \\ 0 & 0 & 0 & -1 & \sin\theta & 0 & 0 & 0 & 0 \\ 0 & 0 & 0 & 0 & 0 & 1 & 0 & 0 & 0 \\ 0 & 0 & 0 & 0 & -\cos\theta & 0 & 1 & 0 & 0 \\ 0 & 0 & 0 & 0 & -\sin\theta & 0 & 0 & 1 & 0 \\ 0 & 0 & 0 & 0 & -\sqrt{c^2+d^2} & -1 & 0 & 0 & 0 \end{bmatrix} \begin{bmatrix} F_{1x} \\ F_{1y} \\ F_{2x} \\ F_{2y} \\ F_3 \\ T_3 \\ F_{4x} \\ F_{4y} \\ T_{in} \end{bmatrix} = \begin{bmatrix} 0 \\ 0 \\ 0 \\ -F_d \sin\theta \\ -F_d \cos\theta \\ 0 \\ F_d \sin\theta \\ F_d \cos\theta \\ -T_{out} \end{bmatrix} \tag{2.22}$$

where F_{d} is a spring force in a direction opposite to the displacement of hand-attached point H along with the human hand.

2.4.3 Case 3: 4R+1P(with spring) model

For this model, the method of kineto-static analysis is similar to Case 1 (4R model). Although there is a prismatic joint with spring in this model, only the maximum displacement as 10 mm is considered, which means the value of r_1 is different from the 4R case. Also, with consideration of displacement, the spring force is considered. Therefore, from Equation (2.20), the results can be obtained by substituting

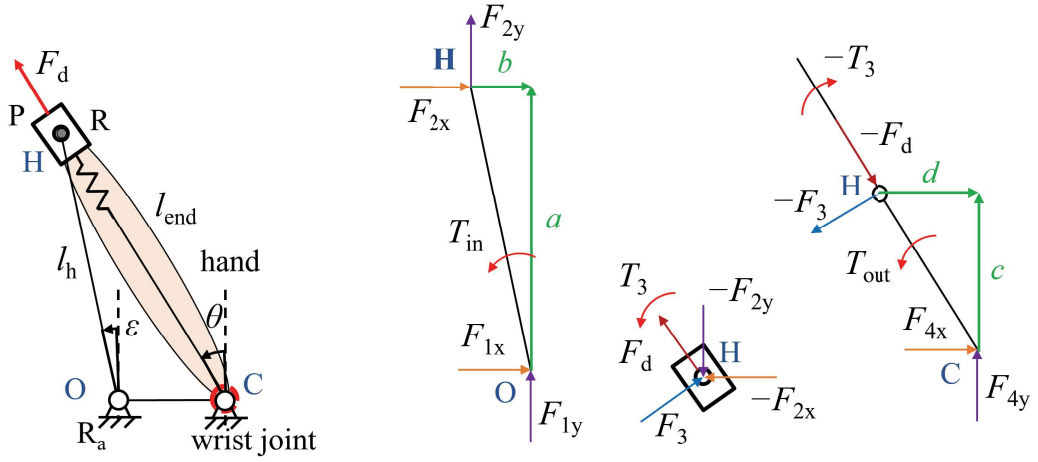

Figure 2.12: Free body diagram of the wrist robot.

different parameter values.

2.4.4 Case 4: 3R+1P(with spring) model

For the position analysis of the four-bar linkage from the geometry shown in Figure 2.13, by introducing complex number, a vector-loop equation can be written as

$$r_3 e^{j\theta_3} = r_1 + r_2 e^{j\theta_2} \tag{2.23}$$

Then, Equation (2.23) can be separated into its real and imaginary components, and r_1 and θ_3 can be solved with the quadratic formula and the trigonometric substitution,

$$r_1 = \frac{-2r_2\cos\theta_2 \pm \sqrt{(2r_2\cos\theta_2)^2 - 4(r_2^2 - r_3^2)}}{2} \tag{2.24}$$

$$\theta_3 = \tan^{-1}\left(\frac{r_2\sin\theta_2}{r_1 + r_2\cos\theta_2}\right), \; -\frac{\pi}{2} \le \theta_3 \le \frac{\pi}{2} \tag{2.25}$$

A static analysis was then carried out based on the aforementioned

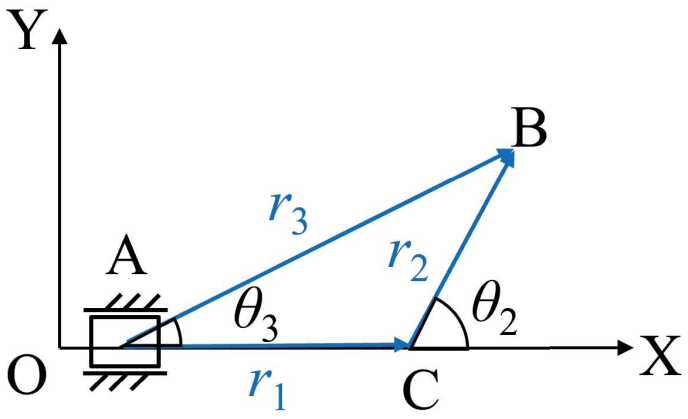

Figure 2.13: Vector-loop of four-bar linkage.

position analysis in order to determine the joint force and required input torque to achieve the desired movement under the wrist joint torque. The free body diagram of the linkage for this analysis is shown in Figure 2.14.

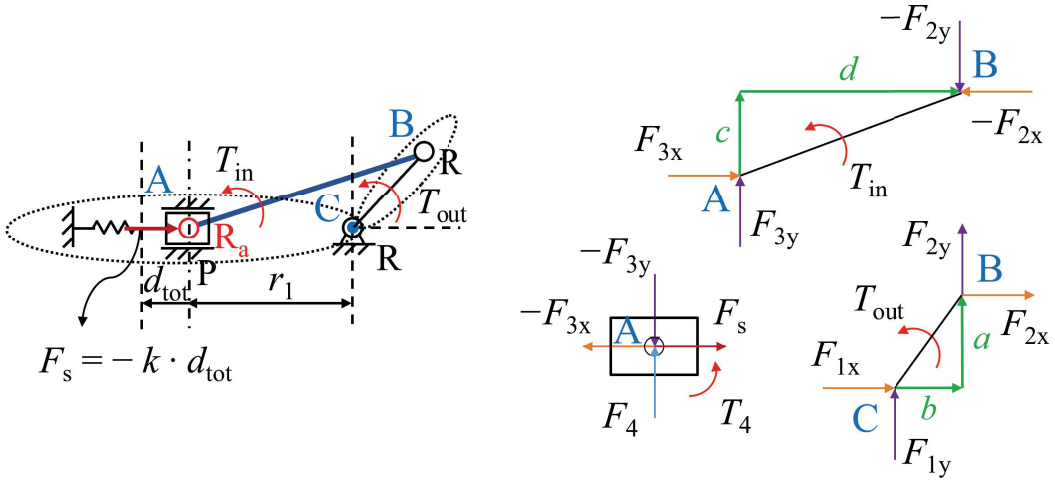

Figure 2.14: Free body diagram of four-bar linkage.

Furthermore, according to biomechanical analysis of daily life activities, the maximum torque of flexion/extension motion is 0.35 N · m

[69, 70]. However, due to surgery, inflammation, and other factors, patients who need rehabilitation typically have joints that are more resistant to movement, thus, the output torque used here is 1.2 $\mathrm{N} \cdot \mathrm{m}$. The spring constant of the forearm found in the literature could be varied due to different measurement environment and here it is set as 143 N/m [53]. The parameters used in analysis are shown in Table 2.3.

Table 2.3: The values of parameters used in analysis.

Description	Parameter	Value	Unit
Distance between brace and wrist joint	r_1	81.04	mm
Length of hand	r_2	80.0	mm
Length of coupler link	r_3	156.04	mm
Spring constant of forearm	k	143	N/m
Output torque	T_{out}	1.2	mm

2.5 Results and Discussions

In this section, the results of kineto-static analysis are discussed, and the forces applied on the wrist in different conditions are evaluated. Using the methods described previously, the outcomes are presented into three parts: (1) comparison between case 1, case 2, and case 3 with consideration of the effects of the forearm's softness during movement. (2) the effects of the offsets between human and robot joints and using the compliance for case 2. (3) comparison between different design parameters for a compact design for case 4.

2.5.1 Comparison Effects of Human Soft Tissue between Case 1, Case 2, and Case 3

The same output torque is applied for the cases of the addition of passive joints into the exoskeleton, and the soft characteristics of the

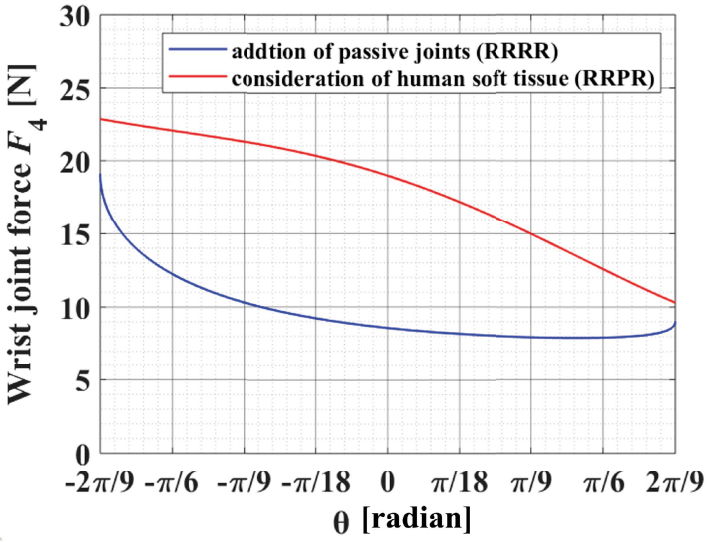

Figure 2.15: Wrist force comparisons with the addition of passive joints (RRRR) and consideration of human soft characteristics (RRPR).

human body are taken into account for joint misalignment compensation. The force acted on the wrist joint can be seen from Figure 2.15. While the average wrist force is less for the addition of the passive joint case, he difference between the maximum and minimum wrist forces is not obvious in both cases. The displacement caused by the softness of the hand can be regarded as an addition of a prismatic joint into the robot, which may be the reason of the results. Therefore, this seems to provide the first evidence that the human soft tissue may be modeled as one passive joint in robot design.

Secondly, the effectiveness of the characteristics of the human soft tissue on an exoskeleton during rehabilitation is verified. The Case 1 (4R model) is considered without any displacement of the brace. On the other hand, as mentioned, the displacement of braces exists for Case 3 (3R+1P model with spring); however, only the maximum displacement of the braces is considered. The results of two cases are

shown in Figure 2.16, if the braces is considered has the maximum displacement, the maximum wrist force decreases from 19.10 to 16.79 N. It may be reasonable to suppose that considering the characteristics of human soft tissue, the braces become equivalent to the addition of compliance, which results in a relatively small wrist force. In simpler terms, part of the force is absorbed by the soft human part. Moreover, the distance between braces and wrist changes due to the movement of the braces, so that the angle range of the wrist also changes from 80° to 73.75°. It is apparent that only one link length changes while the other rigid links remain unchanged. Moreover, the range of the output angle should change. Consequently, from the results, it is fair to say that the effects of human soft tissue cannot be ignored in robot design.

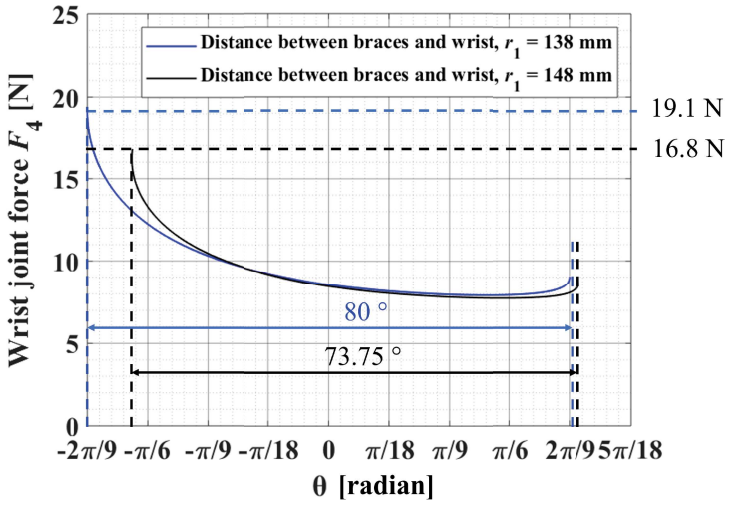

Figure 2.16: Wrist force comparisons with different distances between braces and wrist (Case 1 and Case 3).

2.5.2 The Effects of Offsets and Compliance for Case 2

The discussion of outcomes is addressed in two parts as follows: (a) offset influences; (b) compliance effects. Firstly, if the human joint and robot joint are not properly aligned, the offset may exist. It is important to know how these existing offsets can have potentially adverse effects on rehabilitation. For this propose, it is assumed that the mechanism has no compliant components; therefore, only the hand is regarded to comply with its spring constant as 172.5 N/m. Moreover, the offset shown in Figure 2.5 is assigned as 30 mm in six directions. More specifically, the offsets are set in the x-direction, y-direction and at an angle of 45 degrees to the x-direction with both the positive and negative directions. Figure 2.17a shows the results of each case and the comparisons of the results are seen in Figure 2.17b. According to the analysis of the unwanted force, the effect of the x-direction offset is greater than in other cases, however, the offset in the y-direction has only a slight impact. This implies that, when a larger x-direction offset exists, it generates a larger displacement of the attachment along with the human hand (d_{tot}), leading to a larger unwanted force. More thought should go into decreasing the x-direction offset in order to improve user comfort. Moreover, Figure 2.18a demonstrates the proportionality of the offset magnitude and unwanted force. In both the positive and negative directions of the x-axis, a clear trend can be found. In Figure 2.18b, the increasing of the initial offset results in a greater unwanted force. It is evident that a larger initial offset causes an increased displacement of the hand-attached point and producing a larger unwanted force. To avoid making patients uncomfortable during rehabilitation, the offset should be as small as possible, generating an undesired force only within the allowable range. The rotation angle

of the hand link (l_h) with the offsets is further examined in various magnitudes and directions. Figure 2.19 shows that that, despite the beginning and the end angles of the hand link have changed, the overall rotation angle is not influenced by the offset in the x-direction in all cases. However, as shown in Figure 2.20, a larger rotation angle range of the hand link results from a larger offset in the positive y-direction. A smaller motion range of the hand link, on the other hand, can be obtained due to a larger offset in the negative y-direction. These results indicate that if there is an offset in the y-direction, the range of motion of the hand link changing should be given more consideration.

From the perspective of the safety of the rehabilitation robot, there is a question that must be faced: how much offset is allowed to ensure that the user is safe when using the robot. Here, as mentioned in the Subsection 1.3.3, 5 N is set as the pain threshold value for human to ensure the safety. The results are discussed with the offsets along the x- and y-directions. For the offsets in the x-direction (the lateral direction), when the offset is 37.6 mm, the maximum force is 4.989 N. Therefore, the offset in the x-direction must be less than 37.6 mm to ensure that the force applied to the human limb does not exceed pain threshold of 5 N. In addition, in the y-direction, when the offset is 64.9 mm, the maximum force is 4.998 N. Therefore, the offset in the y-direction must be less than 64.9 mm to ensure the safety. On the other hand, the allowable offset in the y-direction is larger than the allowable offset in the x-direction, which agrees with the results shown in Figure 2.18b that the offsets in y-direction have smaller effects on the unwanted forces generation compared to the offsets in the x-direction.

Furthermore, the use of various spring constants of compliance elements combined with the human hand as a series spring set was

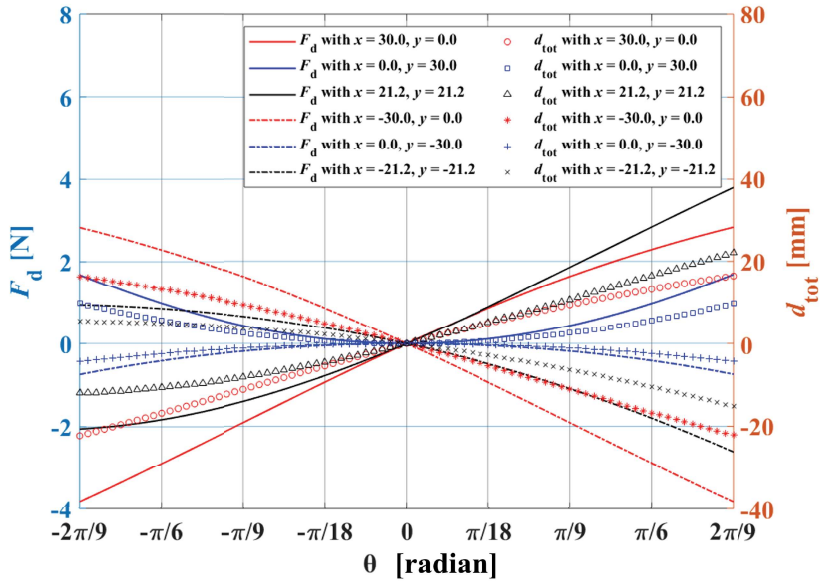

(a)

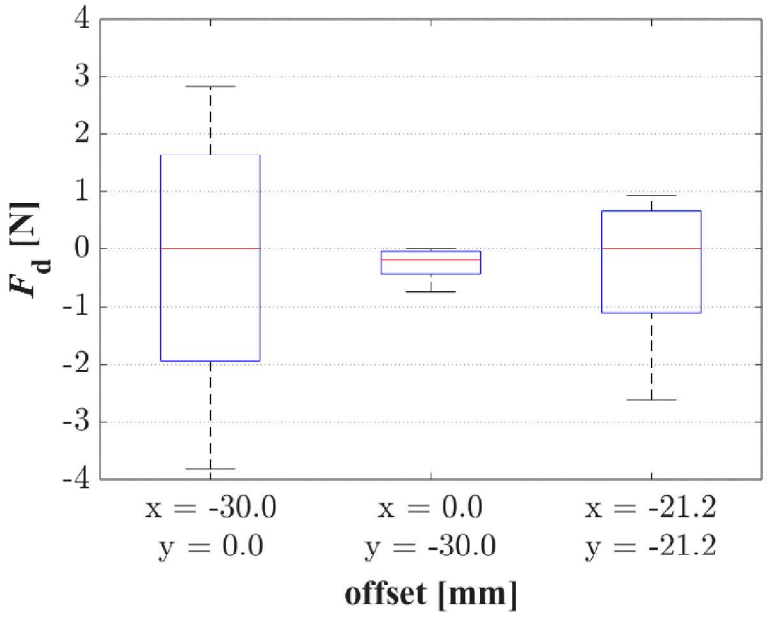

(b)

Figure 2.17: (a) Influences of the offset direction; (b) comparisons of offset direction.

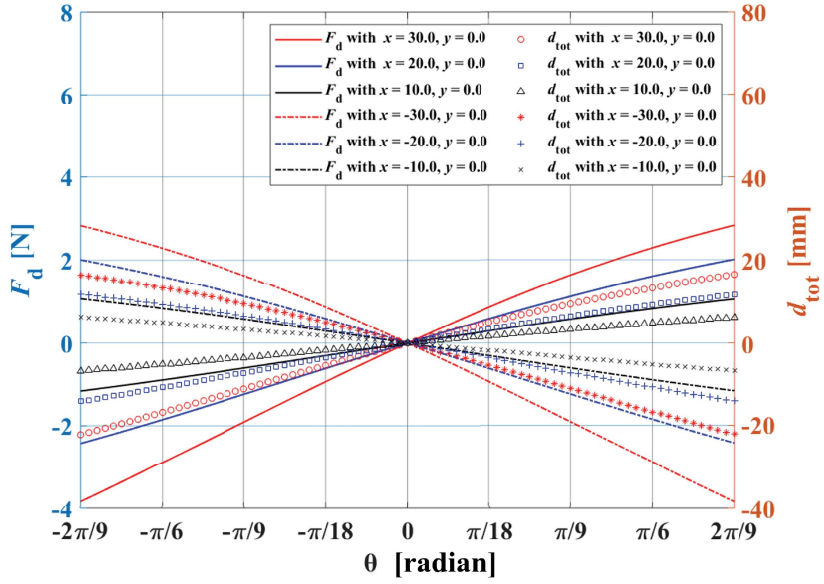

(a)

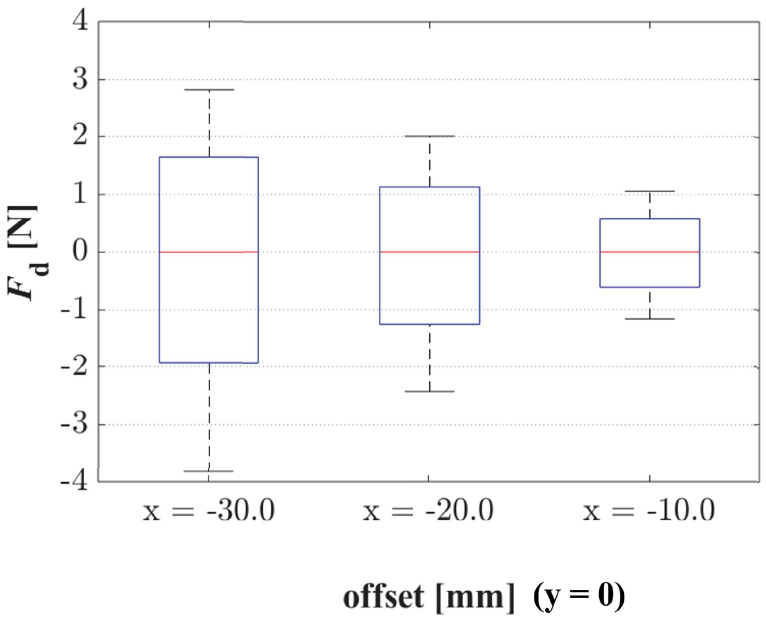

(b)

Figure 2.18: (a) Influences of the offset magnitude; (b) comparisons of offset magnitude.

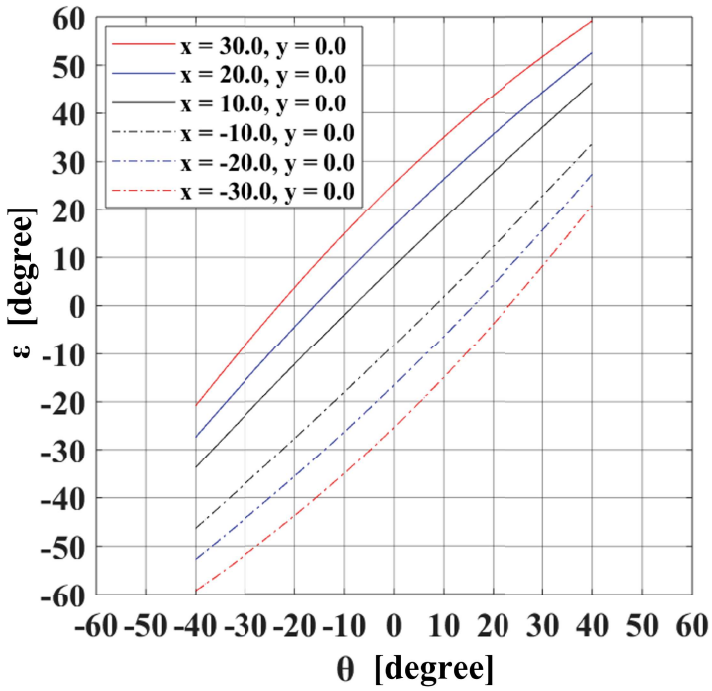

(a)

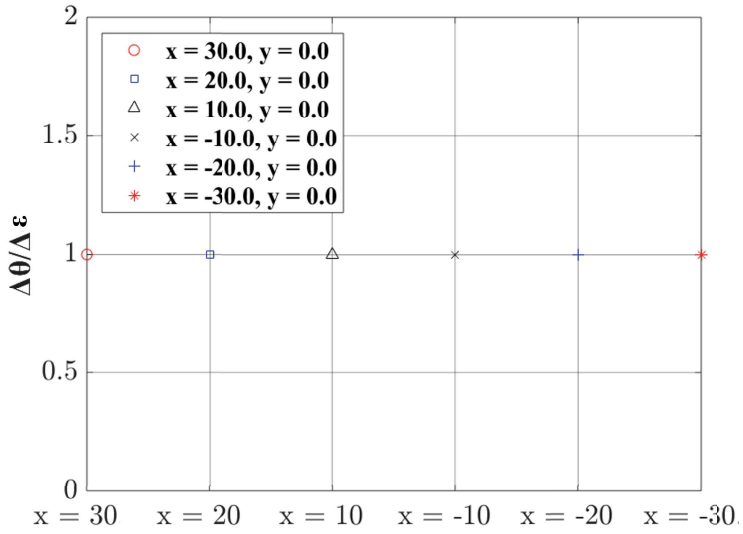

(b)

Figure 2.19: (a) Relationship of θ and ϵ with the x offset; (b) comparison of θ and ϵ with the x offset.

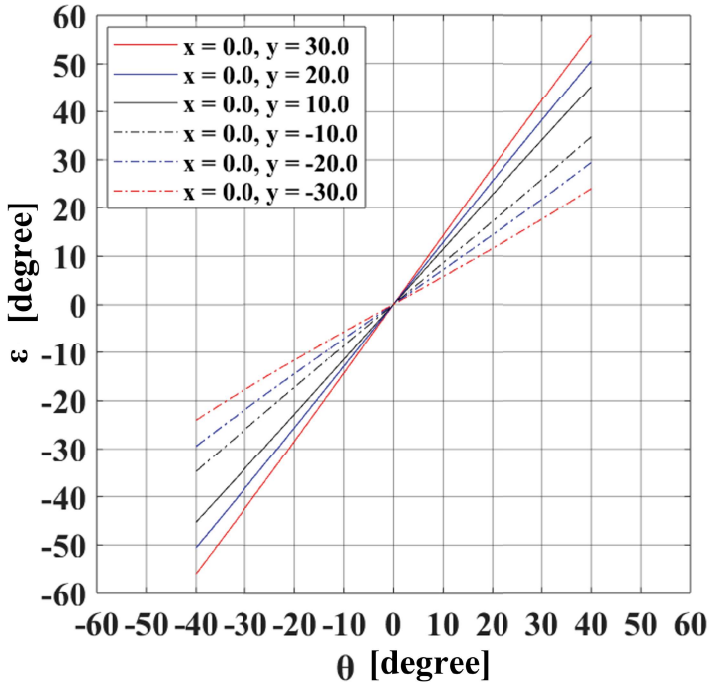

(a)

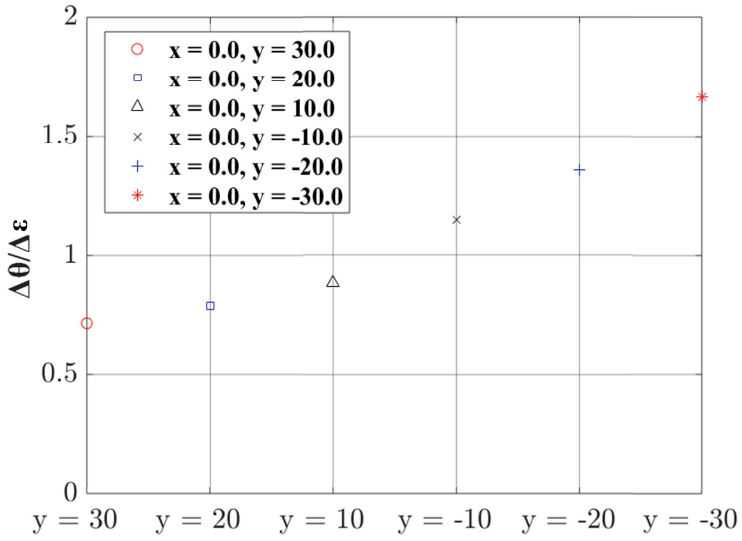

(b)

Figure 2.20: (a) Relationship of θ and ϵ with the y offset; (b) comparison of θ and ϵ with the y offset.

considered. Here, the stiffness of compliance elements are considered as 3 levels from hard, medium, and soft as 1800, 1080, 280 N/m, respectively. The results are given in Figure 2.21a, and the unwanted force varies depending on the total spring constant (k_{tot}) of the hand with compliance. From Figure 2.21a, the range of F_{d} is reduced from $2.8 \ -3.7$ to $1.7 \ -2.3$. The average force applied to the user's hand is reduced and furthermore, the difference between the maximum and minimum values is also reduced. This is expected to be beneficial for improving the comfortability. From Figure 2.21b, it can be observed that a larger spring constant causes a larger unwanted force. These results are in line with the expectation according to Equation (2.3) that the unwanted force increases with the total spring constant (k_{tot}). Compared to the case without compliance, the maximum unwanted force is reduced to 38% while the softest compliance ($k_{\mathrm{tot}} = 106.7$ N/m) is used.

2.5.3 Analysis and Design for Case 4

The soft tissue deformation makes it possible to consider of the forearm as a prismatic joint that moves along the limb. This concept makes it possible for the compact design of the robot with a lightweight structure, which is advantageous for portability. It is important to know that the stroke of the prismatic joint must be carefully determined. The selection of forearm soft tissue displacement does, in fact, have a significant impact on robot design. Human soft tissue is a complicated substance with individual variances in maximal expansion and contraction displacement. Within the preliminary observation range of maximum forearm soft tissue displacement, total soft tissue movement varied from 6 to 14 mm in this subsection. The wrist angle ranges from 0° to 40° for wrist extension, while the hand

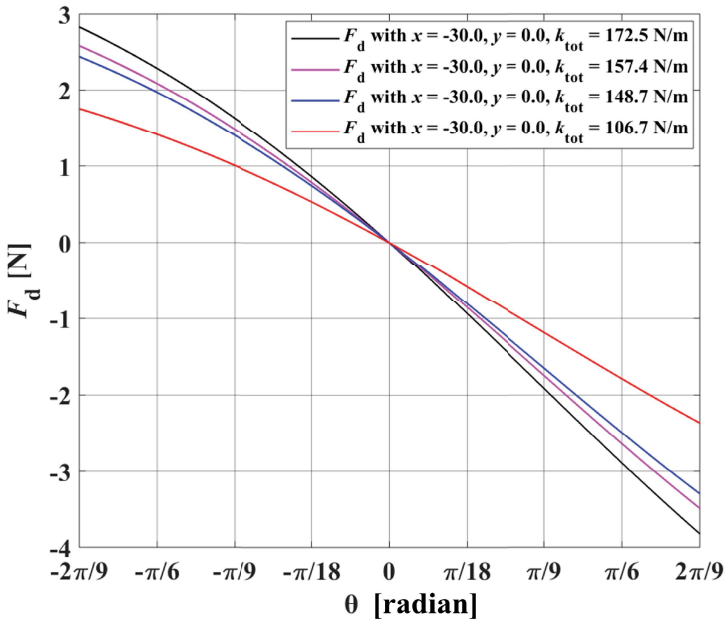

(a)

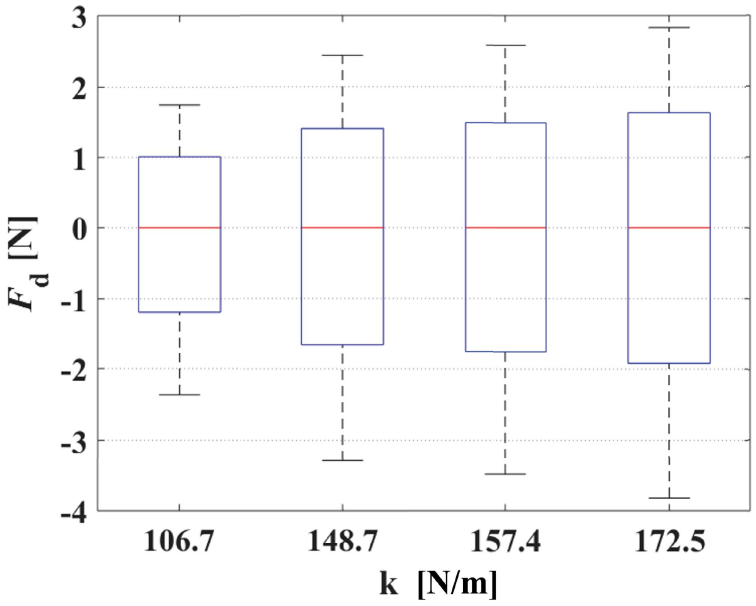

(b)

Figure 2.21: (a) Effects of compliance elements; (b) comparisons of compliance elements.

length is set at 80 mm. Equation (2.9) can be used to calculate the initial position of the braces r_1 and the length of the rigid link r_3. The calculation results of r_1 and r_3 for each selected displacement d_{tot} are shown in Figure 2.22. According to the results, a larger forearm displacement results in a longer link length and a farther position of the braces. First, the longer rigid link length makes the exoskeleton heavier and bulkier, which has a negative influence on portability. Taking these factors into account, it is required that the length of the rigid link does not to exceed 200 mm, which means that the cases of $2d_{\text{tot}}$=12 mm and 14 mm soft tissue displacement may not be appropriate. In addition, when the forearm displacement decreases, the braces' initial position moves closer to the wrist joint. The attachment should not be placed close to the wrist since it is commonly considered that the tissue there is hard and will affect the wearer's comfort. The location of the braces is expected to be more than 50 mm from the wrist. Then, the case of 6 mm and 8 mm soft tissue displacement may not be suitable. As a result, the soft tissue displacement of 10 mm can be selected, which is the most suitable design for a comfortable and portable design. It is true that the allowable range for human soft tissue is around 20 mm, and half of allowable range is 10 mm. It can ensure that human soft tissue moves smoothly.

Kinematic analysis of the robot designed above has been done by changing the wrist angle θ between 0° and 40°. Using the Equation (2.9), the robot angle ϵ and the slider position r_1 are obtained as shown in Figure 2.23. The dotted line indicates the initial position of the brace at 81 mm from the wrist joint. The movement of the forearm's soft tissue causes the distance between the center of the wrist joint and the center of the brace to change from 76 mm to 86 mm during wrist extension.

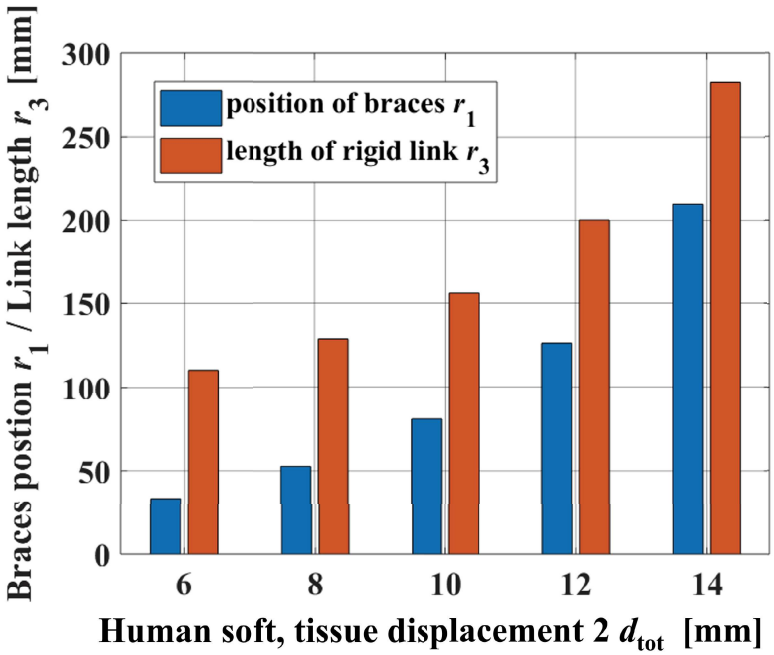

Figure 2.22: Effect of varying human soft tissue displacement.

The static analysis results are shown in Figure 2.24. As shown from Figure 2.24a, the resultant force applied on the wrist joint is within the maximum force 20 N. The force is larger in the y-axis direction than it is in the x-axis direction. In other words, during wrist extension motion, the exerted force is mainly applied in the direction of perpendicular to the forearm. The magnitude of this force increases as the wrist's rotation angle increases. Also, in Figure 2.24b, the input torque was obtained to generate the constant desired output torque. As a result, the input torque ranged from 2.34 to 2.94 $\mathrm{N} \cdot \mathrm{m}$, which is used to determine the motor design parameters.

2.6 A Human-Robot Model

To assess the forearm tissue deformation and further understand the impact of the deformation of the human body's soft tissue when

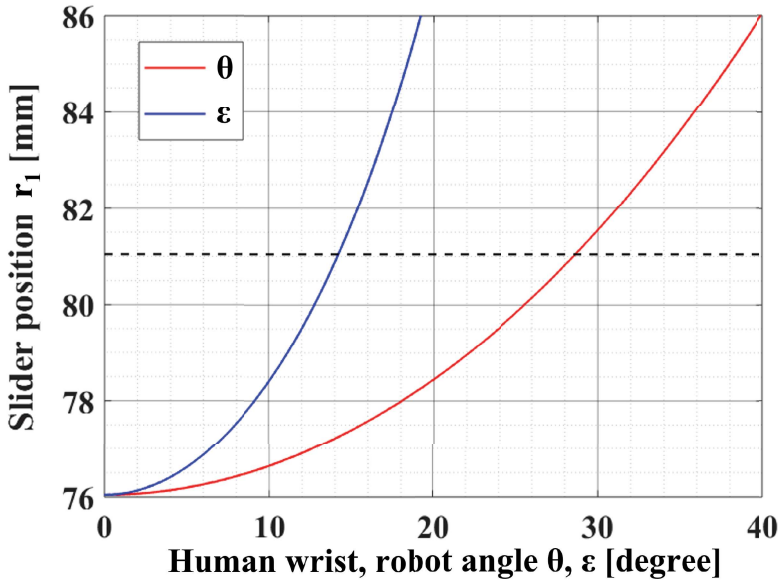

Figure 2.23: Results of kinematic analysis.

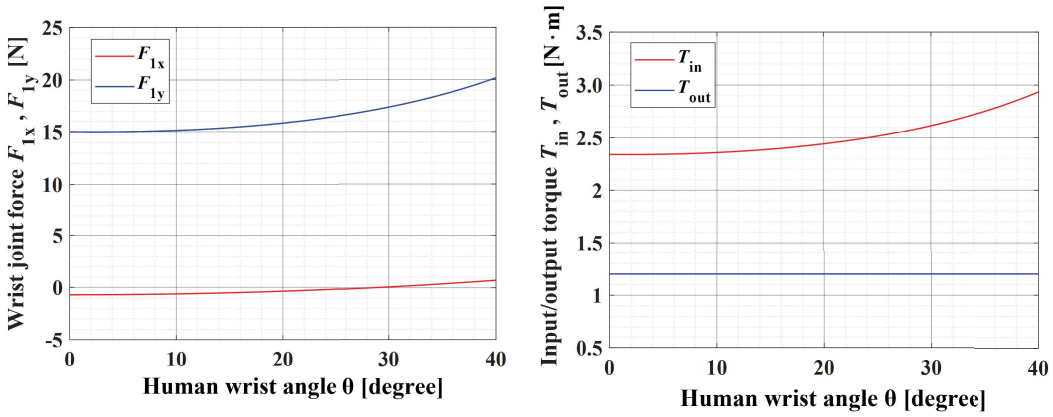

(a) (b)

Figure 2.24: Results of kineto-static analysis (a) Wrist joint force; (b) Input/output torque.

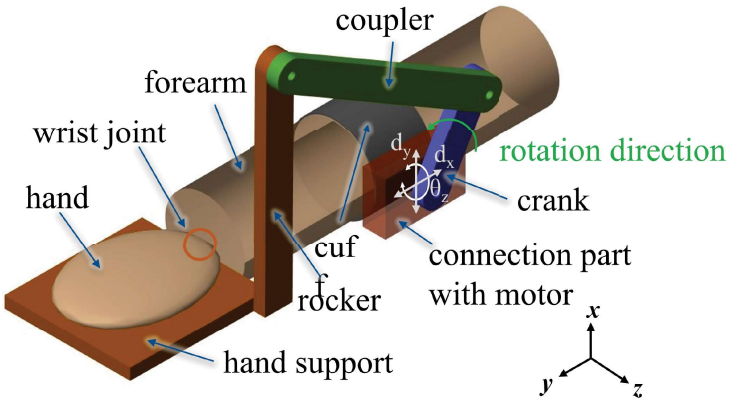

Figure 2.25: Model of the wrist rehabilitation robot with human forearm.

using a wearable rehabilitation robot, a human-robot model is developed. The target system is a 1-DOF wrist rehabilitation robot with the forearm depicted in Figure 2.25. The wearable robot is attached to the human forearm and hand through a cuff. First, without consideration of deformation of the connection part, the robot with the forearm including the wrist joint form a planar four-bar linkage (RRRR), which realizes the flexion and extension movements of wrist joint from $-40°$ to $40°$. Next, with consideration of the deformation of connection part, the detailed block diagram implemented in Simscape Multibody Environment (MathWorks, MA, USA) is shown in Figure 2.26.

The developed model of the target system is composed of two kinematic chains: a robot serial chain and a human serial chain, which are represented as the green and yellow areas depicted in Figure 2.26, respectively. To create of the simulation model, Matlab Simulink and Simscape Multibody library are used. The defined blocks from Simscape Multibody library, such as body elements, joints, frames, transforms and some customized blocks, are applied to build the model. The blocks can be inputted some parameters and connected to each other in the Matlab Simulink environment. For the proposed model,

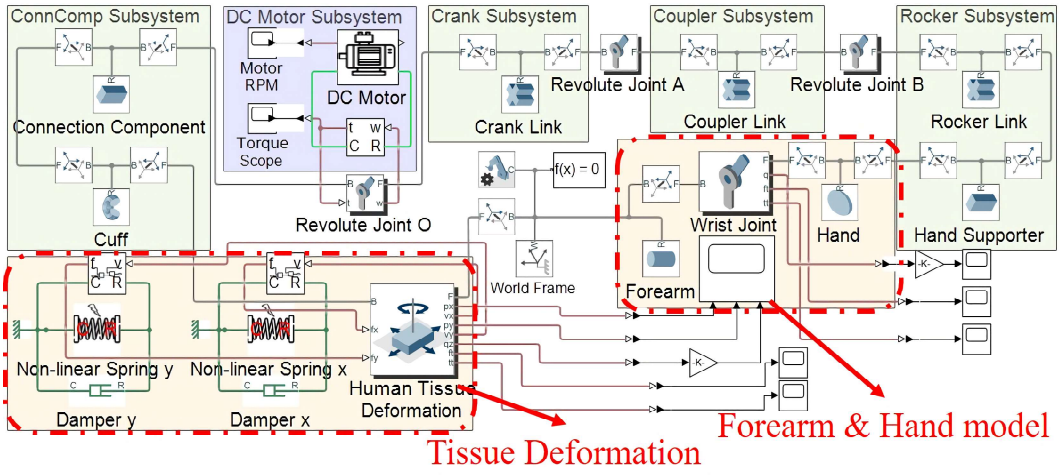

Figure 2.26: Block diagram of wearable robot system.

the robot and human chains are connected by the connection part and the hand. However, the hand effect is not considered in the model. With consideration of the soft property of human forearms, the forearm is regarded as an integral part including springs and dampers. Here, the soft tissues of the forearm have a nonlinear elastic behavior and are assumed to be similar to the skin [52].

In this model, the deformation of the forearm tissue is considered as: translational deformation in the x-direction, translational deformation in the y-direction, and rotational deformation around the z-axis. The ranges of deformations are set as -3 mm to 3 mm, -10 mm to 10 mm, and $-5°$ to $5°$, respectively. Through the combination of the planar joint and the forearm model, the model can realize these three deformations in simulation. Also, considering the highly nonlinear stiffness of human tissues, the stress-strain curve of the skin is used [52] to represent the nonlinear characteristics of the deformation of the forearm in the x and y directions. The custom nonlinear spring blocks are used in the model, thus the different spring coefficients

for deformations in x- and y-directions can be used. To obtain the correlation between displacement and forearm spring coefficient, which can be used to the model's custom nonlinear spring blocks. Here, by using the polynomial curve fitting method, the spring coefficients of the forearm, k_x and k_y (N/m) with the third-order polynomial fits are expressed as follows:

$$\begin{aligned} k_x &= 124 \cdot |x|^3 - 328 \cdot |x|^2 + 228 \cdot |x| + 1.2 \times 10^{-9} \\ k_y &= 3.3 \cdot |y|^3 - 29.1 \cdot |y|^2 + 67.2 \cdot |y| + 1.3 \times 10^{-9} \\ &|x| \leq 3,\ |y| \leq 10 \end{aligned} \tag{2.26}$$

A 12V, 3RPM, DC geared motor with a rated torque of 1.4 N $\cdot$ m is used as the actuation for this model, which drives the crank to rotate counterclockwise around the z-axis and is installed on the connection part. The link lengths and the values of parameters used in analysis are listed in Table 2.4. Among them, the link lengths used here are the same as the values shown in the Table 2.2.

In the case described in this Subsection, the revolute joint O shown in Figure 2.26 is actuated by the DC Motor with an input torque. Motions of the links and angles of the joints are obtained through simulation process [75], which starts with multibody kinematic analysis to find the numerical solutions for the designated time instant by using Newton-Raphson method. The kinematic conditions of the whole closed loop system are fully satisfied. Finally, the analysis of forces and torques of each element and joint are done which takes into consideration of the equilibrium on the external loads and the spring/-damper forces of the human soft tissue model are fully satisfied.

Table 2.4: The values of parameters used in analysis.

Parameter	Value	Unit
Distance between cuff and wrist joint	138.0	mm
Length of crank link	71.6	mm
Length of coupler link	199.8	mm
Length of rocker link	161.3	mm
Forearm, translational spring coefficient	Equation (2.26)	N/m
Forearm, rotational spring coefficient	0.60 [53]	$\mathrm{N \cdot m/rad}$
Forearm, translational damping coefficient	1.74 [53]	$\mathrm{N \cdot s/m}$
Forearm, rotational damping coefficient	0.10 [53]	$\mathrm{N \cdot m \cdot s/rad}$

2.6.1 Simulation Results

In this section, the discussion of the results is divided into two parts: 1) tissue deformation and applied forces; 2) range of motion (ROM) of wrist. The simulation of the developed dynamic model has been performed in 60 seconds for the motion. The results of the forearm deformations during rehabilitation are shown in Figure 2.27. It can be seen that, compared with the x-direction deformation, the y-direction deformation has not reached the limit of deformation. This is mainly due to the magnitude of the forces exerted on the forearm tissue in different directions. Also, the deformation pattern is asymmetric with respect to the zero point.

Moreover, the rotational deformation about the z-axis changes with the torque applied to the tissue. The rotational deformation first reaches the limit value of 5°, and then fluctuates to $-2.5°$, producing a trough at the circle marked in Figure 2.27. As a result, the reason for the result leads to the rotational displacement may be affected by the displacement in the y-direction. Hence, deformation in multiple directions are coupled and should be considered together.

The results of the range of motion of the wrist joint during the

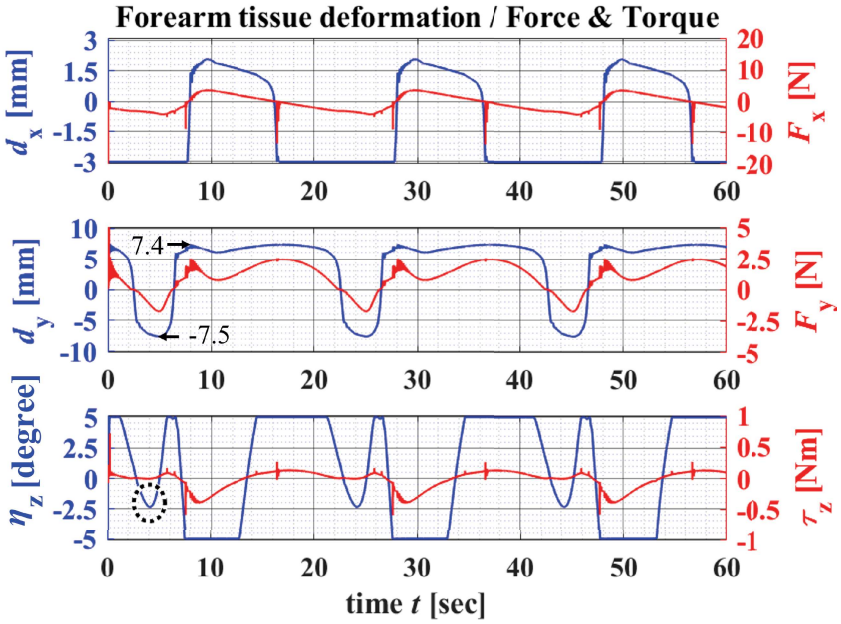

Figure 2.27: Forearm tissue deformations.

rehabilitation process are shown in Figure 2.28. The designed wrist rotation angle is from $-40°$ to $40°$ plotted with a blue line. Owing to the soft property of forearm tissue, the ROM of the wrist is changed from $-38.4°$ to $33.1°$ which is plotted with a red line. The ROM of the wrist is reduced, which can only achieve 89.4 % of the designed ROM. In addition, the influence of the reduced wrist ROM in the positive angle direction is greater than in the negative angle direction. Consequently, it can be said that the deformation of human soft tissues can affect the ROM of the wrist, which is expected to reduce the rehabilitation effect. Although the softness and deformability of the human tissue is inherent and difficult to be avoided. However, if the reduction of human joint's ROM due to human tissue deformation can be considered at the design stage, the reduction compensation can be done by design approaches, such as increasing the target ROM to compensate for the potential reduction of ROM.

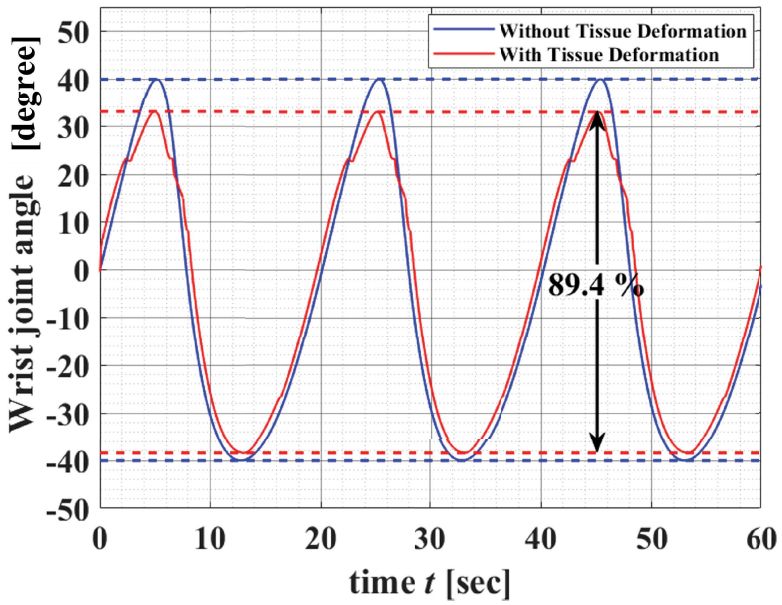

Figure 2.28: Range of motion (ROM) of the wrist.

2.7 Summary

Unlike many rehabilitation devices, which rely on manual adjustment for joint misalignment, the use of compliance and the addition of passive joints have been separately discussed in this chapter with simple planar motion cases. Kineto-static analysis on a planar wrist rehabilitation robot has been performed, providing valid and feasible ideas for designing a safer and comfortable rehabilitation robot.

(1) The effects of the offsets between human and robot joints in various directions and magnitudes are studied. The x-direction offset (in the lateral direction), which is in the direction as same as the rotation axis of the RUD movement, produces a larger unwanted force, while the y-direction offset, which is in the direction along the forearm, has influenced the angular range of the hand link. Allowable range for the offsets are proposed based on the human pain threshold. As for

the offset is less than the proposed value, it can ensure the safety of the user when using the wearable rehabilitation robot. In addition, compliance between the human and the robot is used to reduce an unwanted force.

(2) The addition of passive joints is applied to compensate for joint misalignment. The results show that if the soft nature of the human body is considered as a passive joint in the exoskeleton, the compensation for joint misalignment is similar to the addition of passive joints. Applying the soft and deformable characteristics of the human body as a passive joint can also be a solution to solve the misalignment compensation. By replacing the addition passive joints, the robot can be simpler and more lightweight.

(3) A concept of modeling human soft tissue as a passive prismatic joint is applied. Thanks to the deformation of human soft tissue, one prismatic joint in a slider-crank linkage can replace the soft tissue effect. This approach, when compared to other existing devices, provides an effective design in terms of compactness and portability. Furthermore, the magnitude of human soft tissue displacement is compared in order to reduce the size of the exoskeleton without compromising user comfort. Finally, the kineto-static analysis is conducted to show the feasibility of the current design. Due to its portability and ability to compensate for joint misalignment, the proposed design is expected that can be used for portable and safer in-home rehabilitation.

(4) A human-robot model is established to assess the forearm tissue deformation. The deformations of human soft tissues are considered as two translational and one rotational deformations. In addition, the non-linear spring coefficients of the human tissues are considered. From the simulation results, the deformations in multiple directions

may be coupled and have effect on each other. Therefore, the deformations of human soft tissue in multiple directions should be considered. Also, the results show that the tissue deformation can affect the performance of the robot, specifically, to reduce the ROM of human joint. And this effect should not be ignored in the design of wearable rehabilitation robots, which it may reduce the rehabilitation outcomes.

Chapter 3

Kineto-Static Analysis and Design of a 3-DOF Wrist Rehabilitation Robot

In this chapter, a parallel robot (3-R$\underline{P}$S) is used for performing wrist FE and RUD movements for wrist rehabilitation. The analysis of the 3-R$\underline{P}$S robot is presented with consideration of soft characteristics of human limb. First, the human upper-limb model, which is composed of a serial chain and joint stiffness model, and its inverse kinematic analysis is presented. Second, a static analysis is conducted to obtain the force and torque acting on the human limb based on the proposed model. Then, the optimal design parameters of the 3-R$\underline{P}$S robot are obtained by generic optimal algorithm through kineto-static analysis. Two factors are taken into account that may have an impact on the forces and torques applied to the human limb. The first is the parasitic motions of the 3-RPS robot which is defined as the undesired motions in the constrained DOF. They are considered to lower the accuracy of the robot and are not easily to avoid. The second is the initial offsets between the centers of the wrist and the moving platform. The main reason for taking offsets into account is that it is difficult to achieve

a perfect adjustment to guarantee that the center of the wrist and the center of the MP are consistent when the robot is attached to the user's limb. Also, to identify the center of the wrist is particularly challenging due to the inherent complicated structure of the wrist joint. The influence of the parasitic motion of the 3-RPS robot and the initial offset between the wrist and the moving platform of the robot are analyzed and presented.

3.1 Kineto-Static Analysis and Design Optimization

3.1.1 Position Analysis of a Wrist Rehabilitation Robot

The spatial 3-R$\underline{\text{P}}$S parallel robot used for wrist rehabilitation, in which underlined joint represents actuated joint, is illustrated in Figure 3.1. The robot consists of a moving platform (MP), a fixed base platform (BP) and three identical limbs connecting MP and BP. As illustrated in Figure 3.1a, each limb is composed of a revolute joint (R), a prismatic joint (P), and a spherical joint (S) in sequence from BP to MP, and the joints of BP and MP are placed at the vertices of the triangular platforms. A linear actuator drives the prismatic joint, while the other joints are passive. The 3-R$\underline{\text{P}}$S robot is a lower-mobility parallel robot with 3 DOFs, which can perform two rotations and one translation. Three parasitic motions occur during the movement in the constrained DOFs, including one rotation around the z-axis and two translations in xy plane. The robot is used for wrist rehabilitation to achieve hand flexion/extension movement and ulnar/radial deviation. To achieve the requirement, only two rotational DOFs of the robot are used. Although the translational DOF in the z-axis may be beneficial for adapting the different user limb lengths, here the fixed

initial distance between BP and MP is considered for the analysis. A lower-mobility parallel robot can be used for in-home rehabilitation because it has fewer linkages and actuators, which reduces the cost and weight of the robot. The range of motion (ROM) of the wrist joint is defined as between $-50°$ and $50°$ for the flexion/extension movement and between $-30°$ and $30°$ for the ulnar/radial deviation of the hand. Among them, the ROM of FE movement is increased from the value used in Chapter 2 to better meet the rehabilitation needs. As shown in Figure 3.2, the coordinate is attached to the center of the wrist and the z-axis is along the forearm. The wrist joint is modeled as a simple universal joint with two DOFs as rotating about x and y axes at a center of the wrist C. The displacement of C according to the movement which causing misalignment, is considered in this chapter.

The coordinate system of the fixed BP is represented by O-xyz at the centroid of the platform $A_1A_2A_3$. $A_{i=1\sim3}$ represents the location of the R joint of the BP, while $B_{i=1\sim3}$ represents the location of the S joint on the MP. The x-axis lies in the BP plane and points to point A_1. Correspondingly, the MP frame is denoted by P-$uv\omega$ at the centroid of the platform $B_1B_2B_3$. The u-, v- axes lie in the MP plane and the u- axis passes through point B_1. The radii of the triangular circumscribed circles of the BP and MP are a and b, respectively. The angles between $OA_1(PB_1)$ and $OA_2(PB_2)$, $OA_1(PB_1)$ and $OA_3(PB_3)$ are denoted by α_1 and α_2, respectively, as shown in Figure 3.1b. The axes of the revolute joints are coplanar with BP and the direction of the ith revolute joint axis is perpendicular to OA_i. Also, the ith prismatic joint axis is perpendicular to the direction of revolute joint axis. In the corresponding coordinate system, the position vectors of the vertices of BP and MP with reference to each local coordinate

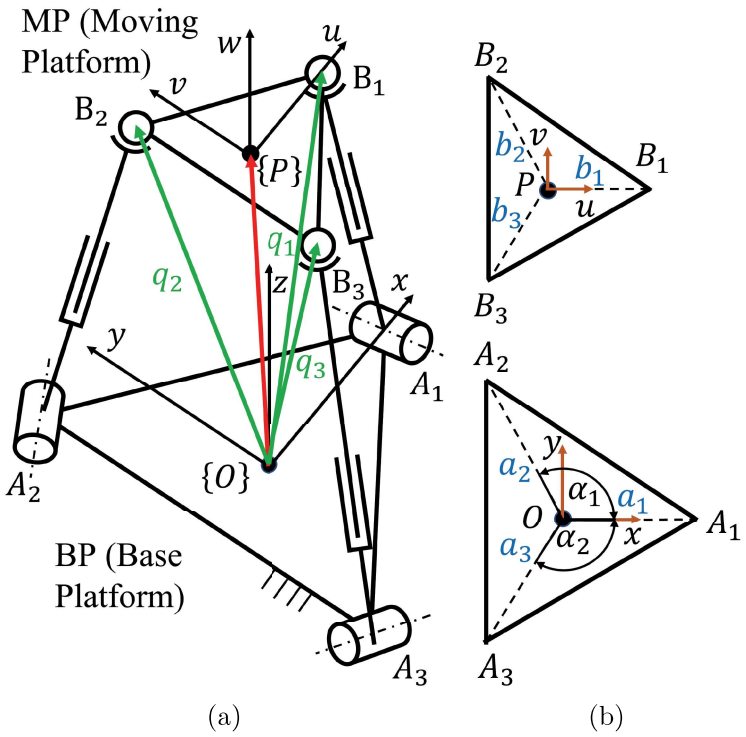

(a) (b)

Figure 3.1: The kinematic diagram of the 3-RPS parallel robot: (a) analytical model of 3-RPS; (b) analytical model of BP and MP.

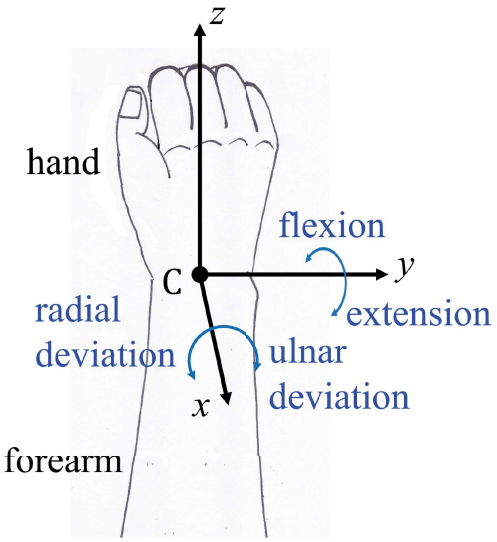

Figure 3.2: The target movement of wrist: FE and RUD movements.

system can be expressed as follows:

$$\begin{aligned}
\overrightarrow{a_1}^{xyz} &= \begin{bmatrix} a & 0 & 0 \end{bmatrix}^T \\
\overrightarrow{a_2}^{xyz} &= \begin{bmatrix} a\cos\alpha_1 & a\sin\alpha_1 & 0 \end{bmatrix}^T \\
\overrightarrow{a_3}^{xyz} &= \begin{bmatrix} a\cos\alpha_2 & a\sin\alpha_2 & 0 \end{bmatrix}^T
\end{aligned} \tag{3.1}$$

$$\begin{aligned}
\overrightarrow{b_1}^{uv\omega} &= \begin{bmatrix} b & 0 & 0 \end{bmatrix}^T \\
\overrightarrow{b_2}^{uv\omega} &= \begin{bmatrix} b\cos\alpha_1 & b\sin\alpha_1 & 0 \end{bmatrix}^T \\
\overrightarrow{b_3}^{uv\omega} &= \begin{bmatrix} b\cos\alpha_2 & b\sin\alpha_2 & 0 \end{bmatrix}^T
\end{aligned} \tag{3.2}$$

The orientation of the MP can be described by using a Z-X-Y type Euler angle (ψ, θ, ϕ) with respect to the fixed coordinate system, and the rotation matrix is

$$\begin{aligned}
R_P^O &= Rot(y,\theta) \cdot Rot(x,\psi) \cdot Rot(z,\phi) \\
&= \begin{bmatrix} c\theta c\phi + s\psi s\theta s\phi & -c\theta s\phi + s\psi s\theta c\phi & c\psi s\theta \\ c\psi s\phi & c\psi c\phi & -s\psi \\ -s\theta c\phi + s\psi c\theta s\phi & s\theta s\phi + s\psi c\theta c\psi & c\psi c\theta \end{bmatrix} = \begin{bmatrix} u_x & \upsilon_x & \omega_x \\ u_y & \upsilon_y & \omega_y \\ u_z & \upsilon_z & \omega_z \end{bmatrix}
\end{aligned} \tag{3.3}$$

where s and c correspond to sine and cosine functions, respectively.

As depicted in Figure 3.1, the position vectors of the MP vertices with respect to the BP coordinate can be written as

$$\overrightarrow{OB_i} = \overrightarrow{OP} + \overrightarrow{PB_i},\ i = 1, 2, 3. \tag{3.4}$$

Then, Equation (3.4) can be written as

$$\overrightarrow{q_i} = \begin{bmatrix} P_x & P_y & P_z \end{bmatrix}^T + R_P^O \ \overrightarrow{b_i}^{uv\omega}, \ i = 1, 2, 3. \tag{3.5}$$

Substituting Equations (3.2) and (3.3) into Equations (3.5) yields

$$\begin{aligned}
\overrightarrow{q_1} &= \begin{bmatrix} q_{x,1} \\ q_{y,1} \\ q_{z,1} \end{bmatrix} = \begin{bmatrix} P_x + bu_x \\ P_y + bu_y \\ P_z + bu_z \end{bmatrix} \\
\overrightarrow{q_2} &= \begin{bmatrix} q_{x,2} \\ q_{y,2} \\ q_{z,2} \end{bmatrix} = \begin{bmatrix} P_x + bu_x \cos\alpha_1 + bv_x \sin\alpha_1 \\ P_y + bu_y \cos\alpha_1 + bv_y \sin\alpha_1 \\ P_z + bu_z \cos\alpha_1 + bv_z \sin\alpha_1 \end{bmatrix} \\
\overrightarrow{q_3} &= \begin{bmatrix} q_{x,3} \\ q_{y,3} \\ q_{z,3} \end{bmatrix} = \begin{bmatrix} P_x + bu_x \cos\alpha_2 + bv_x \sin\alpha_2 \\ P_y + bu_y \cos\alpha_2 + bv_y \sin\alpha_2 \\ P_z + bu_z \cos\alpha_2 + bv_z \sin\alpha_2 \end{bmatrix}
\end{aligned} \tag{3.6}$$

Due to the constraint of the revolute joint, the limb can move only in the limb plane. The following constraint equations can be obtained:

$$\begin{aligned}
q_{y,1} &= 0 \\
q_{y,2} &= \frac{\sin\alpha_1}{\cos\alpha_1} \, q_{x,2} \\
q_{y,3} &= \frac{\sin\alpha_2}{\cos\alpha_2} \, q_{x,3}
\end{aligned} \tag{3.7}$$

Here, to simplify the problem, the angles for the arrangement of R joints are set as $|\alpha_1| = |\alpha_2| = \alpha$. The output motions of 3-R$\underline{\text{P}}$S, are defined including the rotations about the x- and y-axes, ψ and θ, and translation along the z-axis, P_z, as output motion parameters. The parasitic motions of the lower-mobility parallel robot are the unwanted motions in the constrained DOF of the robot, which is considered to be

detrimental to many applications, and its impacts cannot be ignored. The parasitic motions of 3-R$\underline{\text{P}}$S, which are the coupled motions with the independent output motion parameters, the components including one rotation about the z-axis and two translations along the x- and y-axes, can be obtained by using Equations (3.3), (3.6), and (3.7). The parasitic motions of 3-R$\underline{\text{P}}$S are described by the following Equation (3.8).

$$\begin{aligned} \mathrm{P}_x &= -b\cos\alpha(c\theta c\phi + s\psi s\theta s\phi - c\psi c\phi) \\ \mathrm{P}_y &= -bc\psi s\phi \\ \phi &= \tan^{-1}\left(\frac{s\psi s\theta}{c\psi + c\theta}\right) \end{aligned} \tag{3.8}$$

3.1.2 Inverse Kinematic Analysis of the Human Limb

The conceptual diagram of the human limb with the 3-R$\underline{\text{P}}$S robot can be seen in Figure 3.3. The proximal end of the forearm is attached to the BP of the 3-R$\underline{\text{P}}$S robot by the cuff and the hand is firmly fixed to the handle. The handle height and the distance from the fixed origin O to the center of the cuff are denoted as l_{h} and l_{a}, respectively. Because the human tissue is soft and deformable, the cuff can have up to 6 DOFs, including 3 degrees of rotational freedom and 3 degrees of translational freedom. In order to simplify the problem, here the attachment part is described as a complex joint [76] with 4 DOFs consisting of three prismatic joints and one revolute joint, as illustrated in Figure 3.4. Specifically, this complex joint is considered having 3P+1R motions. The point E is at the end of the forearm and is regarded as a fixed point. The analysis conducted in this chapter is in the case that the point O and the point E are in the same position.

Based on these assumptions, the human limb model is comprised

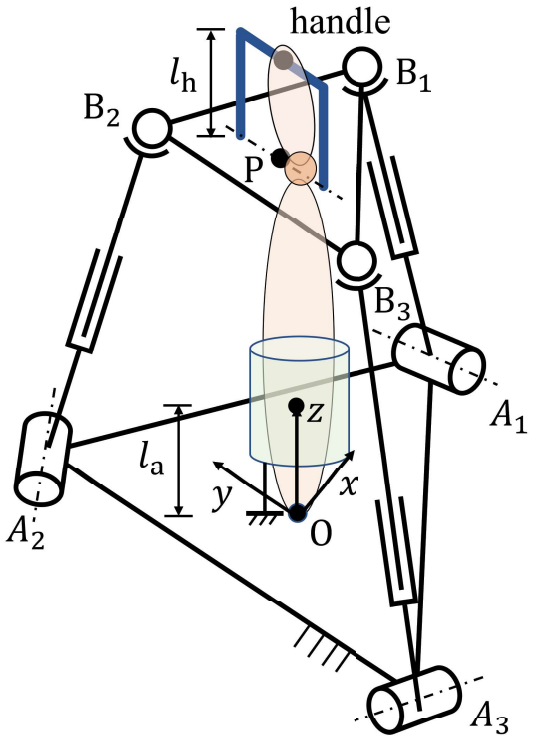

Figure 3.3: The sketch of a wrist rehabilitation robot and human limb.

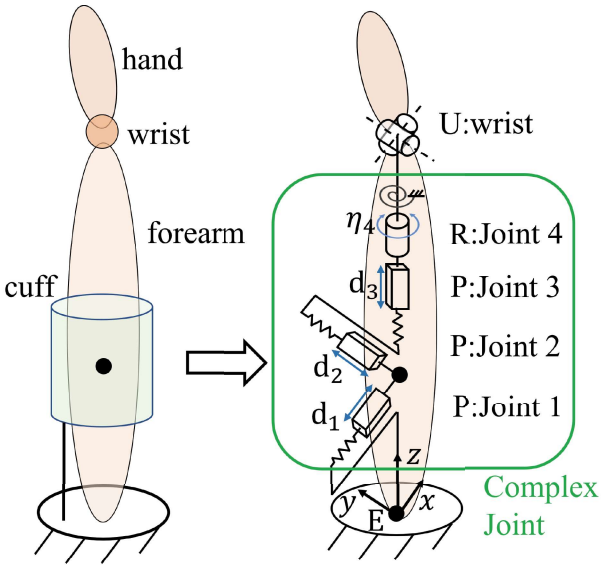

Figure 3.4: The model of human limb.

of three prismatic joins, one revolute joint, and one universal joint, as shown in Figure 3.4. It is worth mentioning that the hand is considered to be firmly attached to the handle of the MP, so that the distance between the center of the wrist and the MP is assumed to be unchanged. Therefore, if the pose of the 3-R$\underline{\text{P}}$S is determined, the three angular parameters and three position parameters of the MP are known. Then, the position of the center of the wrist joint and the orientation of the hand can be simply derived. As a result, this problem can be considered as solving the inverse kinematics of an open chain (PPPRRR) with six degrees of freedom (DOFs), which is the defined human limb model.

Inverse kinematic problems can be solved numerically using a variety of procedures. To calculate the inverse kinematics,the iterative Newton–Raphson method conducted in [77, 78] is used. To begin, the product of exponentials (PoE) formula for forward kinematics is as follows:

$$T_{sb}(\theta) = e^{[S_1]\theta_1} e^{[S_2]\theta_2} e^{[S_3]\theta_3} e^{[S_4]\theta_4} e^{[S_5]\theta_5} e^{[S_6]\theta_6} \mathcal{M} \tag{3.9}$$

where T_{sb} is homogeneous transformation matrix, s and b represent the fixed base frame and end-effector frame, respectively. $\mathcal{S}_n = (\omega_j, \upsilon_j)$ represents the screw axis along joint j, θ_j denotes the joint j variables, and $\mathcal{M}$ is the position and orientation of the end-effector at the home position of the limb. Then, the twist in the end-effector frame $\mathcal{V}_b$ can be represented by using the matrix logarithm algorithm in the form of $[\mathcal{V}_b]$:

$$[\mathcal{V}_b] = \log\left({T_{sb}}^{-1}(\theta_i) T_{sd}\right) \tag{3.10}$$

where T_{sd} is a desired end-effector configuration respect to the fixed base frame, s. In addition, the twist in the fixed frame $\mathcal{V}_s$ can be

obtained by adjoint representation $[Ad_T]$:

$$[\mathcal{V}_s] = [Ad_{T_{sb}}]\mathcal{V}_b \tag{3.11}$$

When a desired end-effector configuration T_{sd} and an initial guess $\theta_0 \in \mathbb{R}^6$, the iteration form can be expressed as follows:

$$\theta_{n+1} = \theta_n + J_s(\theta_n)\mathcal{V}_s \tag{3.12}$$

where n denotes the number of iterations and J_s denotes the Jacobian matrix. The iteration algorithm tries to find the joint variables until it reaches the target configuration with a small tolerance for the position and orientation of the end-effector, which are set as 10×10^{-4} m and 10×10^{-3} rad, respectively. Then, the approximate solution can be obtained that is closest to the initial guess.

3.1.3 Analysis of Unwanted Forces at the Mechanical Interface between the Human and Robot

The connection parts between the human and robot are modeled with the specified type of movement and mechanical properties. Considering the human body' s deformability and softness, the forearm tissue can be considered as having a spring-like behavior. The forces and the torque are expected to be applied since the forearm tissues are modeled as a complex joint (CJ_{3T1R}) composed of three prismatic joints and one revolute joint. It is vital to note that the spring coefficients of the forearm may change as a non-linear spring element and will rise dramatically when approaching the limit of the deformation range. In this chapter, only the smooth motions of the soft tissue are considered and assumed that it satisfies the linear relationship between the applied force/torque and the amount of deformation. The

translational and rotational spring coefficients of the forearm reported in the literature could vary due to varied measurement conditions and here they are set as 143 N/m and 0.6 N $\cdot$ m/rad, respectively [53]. Then, the force and torque can be calculated as follows:

$$\begin{aligned} F_x &= -k_{\mathrm{t}} \cdot d_1 \\ F_y &= -k_{\mathrm{t}} \cdot d_2 \\ F_z &= -k_{\mathrm{t}} \cdot d_3 \\ M_z &= -k_{\mathrm{r}} \cdot \eta_4 \end{aligned} \tag{3.13}$$

where d represents the displacement of the prismatic joint, η represents the angle of the revolute joint, k_{t} and k_{r} denote the translational and rotational spring constants, namely $k_{\mathrm{t}} = 143$ N/m and $k_{\mathrm{r}} = 0.6$ N $\cdot$ m/rad, respectively.

3.1.4 Static Analysis of the Human Limb with the 3-RPS Robot

In the above analysis, only a kinematic analysis on the robot with the human limb is presented. In other words, no external forces are considered. Here, in order to have a better understanding of the interaction between the robot and the human limb during the rehabilitation process, a static analysis of the robot with the human limb is conducted. First, according to the assumptions, the elbow of the human limb is attached to the table, and the hand is firmly fixed to the handle of the MP. Therefore, the human limb can be regarded as an open chain, while the external force is applied to the hand by the robot. Although the maximum torque for hand FE and RUD motions in daily living is about 0.35 N $\cdot$ m according to several studies [69, 70], for patients who need rehabilitation, their joints usually

have more resistance to joint movement due to injury, inflammation, and so on. Therefore, the external torque (T_{out}) is set as 1.2 N $\cdot$ m in this dissertation.

Then, considering an external wrench $\mathcal{F}$ as the applied load to the human hand with the condition that the human limb is in a static equilibrium, the following equation can be used:

$$\tau = J^T(\theta)\mathcal{F} \tag{3.14}$$

where τ is the joint force/torques, and J is the Jacobian matrix. When an external wrench $-\mathcal{F}$ is applied to the human hand by the robot and keeping the human limb at an equilibrium state, Equation (3.14) can be used to calculate the joint force/torque of the human limb model to create an opposing wrench $\mathcal{F}$. The obtained force/torque of the human limb, which needs to be minimized, is related to the comfort and safety of the user.

3.1.5 Multi-Objective Optimization

As stated in the previous subsection, the analyzed joint forces/-torques of the human limb are expected to be minimized in order to ensure the comfort and safety of the user. In this subsection, the genetic algorithm (GA) proposed by Holland et al. [71] is applied to determine the value of the design variables. According to the analysis results, the parasitic motions of the 3-R$\underline{\text{P}}$S robot lead to the generation of force/torque. Therefore, from Equations (3.7) and (3.8), the design parameters related to the parasitic motion including the radius of MP, b, and the arrangement of the revolute joints, which are governed by the angles α_1 and α_2, can be chosen. As mentioned above, here, the angle for the arrangement of R joints is set as $|\alpha_1| = |\alpha_2| = |\alpha|$ for

simplicity. Since multiple objective functions such as the maximum absolute value of joint forces and torques should be considered in this design and there should be a tradeoff between them. GA is applied to the determination of b and α and Pareto optimal solutions, which is a set of solutions between certain objectives that conflict to each other, is considered. The multi-objective optimization functions are expressed in the following equations:

$$\begin{aligned} &P(X) = [f_1(X), f_2(X)] \\ &f_1(X) = \sum_{i=1}^{n} \max\{|F_j| \ : j = 1, \ldots, m\} \\ &f_2(X) = \sum_{i=1}^{n} \max\{|\tau_j| \ : j = 1, \ldots, m\} \\ &\textit{minimize } P(X) \\ &\textit{subject to } 0.05 \leq b \leq 0.15, \ 90^\circ \leq \alpha \leq 170^\circ \end{aligned} \tag{3.15}$$

where X is the vector of design parameters to be optimized. In this case, the radius of MP, b, is selected in a range from 0.05 m to 0.15 m, taking into account the acceptable size of the rehabilitation robot. Also, the angle α is set in the range from 90° to 170°. Obviously, the angle a close to 180° is an unreasonable arrangement. For the objective functions, n is the number of data sets and m is the number of analyzed data, and $f_1(X)$, $f_2(X)$ represent the sum of the maximum absolute value of the joint forces and joint torques, respectively. Here, the number of analyzed data, m, is the total number of calculations per degree in the angular range of the target movement. And the number of data sets, n, is the number of sets of calculation with the chosen initial offsets with magnitude and direction. The reason for choosing the absolute maximum value is that the values of forces and

torques acting on the human limb should be relatively small and avoid a peak of force or torque during the rehabilitation, which is directly related to causing discomfort or may even causing injury to the user. It is worthy to know that the singularity and motion transmissibility are not evaluated in the optimization design. The selected GA parameters are shown in Table 3.1. The optimization process is calculated by the multi-objective functions provided in the MATLAB optimization toolbox. The flowchart of the analysis procedure is presented in Figure 3.5.

Table 3.1: GA parameters used in optimization.

Population Size	Crossover Rate	Mutation Rate
50	0.8	0.01

3.2 Results and Discussion

3.2.1 Kineto-Static Analysis and Optimal Design

In this section, the results of kineto-static analysis and the optimal design is presented. Two factors are considered that may affect the force and torque exerted on the human limb. The first is the parasitic motion of the 3-R$\underline{P}$S robot, and the second is the initial offset between the wrist joint and the center of the MP. The parasitic motion of 3-R$\underline{P}$S is relatively intuitive and can be obtained by using Equation (3.8). The FE and RUD movements are the main subjects of the analysis. In an ideal situation, only θ changes and ψ remains zero during FE movement, and similarly, only ψ changes and θ remains zero during the RUD movement. However, in the actual use, it is not easy to keep the angle to remain zero, so the existence of angle errors are considered

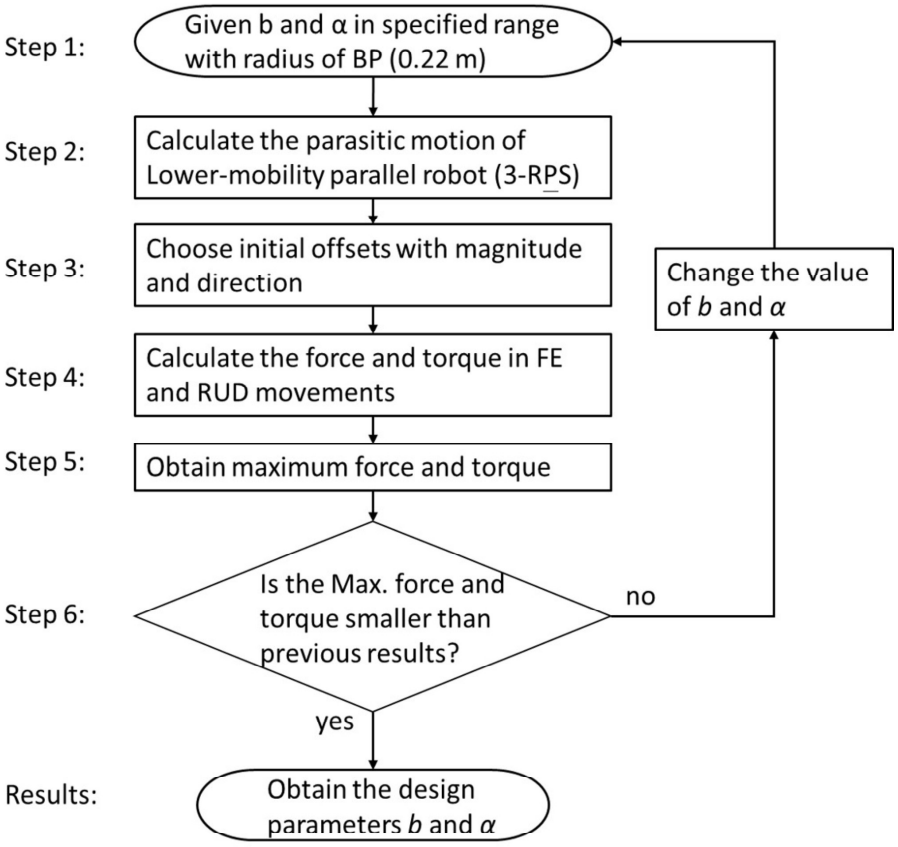

Figure 3.5: Flowchart of optimization.

from $-3°$ to $3°$. Here, the scope of the analysis is set as the following two ranges: (1) $\theta = -50°$ to $50°$ and $\psi = -3°$ to $3°$ for FE movement and (2) $\psi = -30°$ to $30°$ and $\theta = -3°$ to $3°$ for RUD movement. For the initial offsets, translational offsets as 5 mm are considered along the x-, y-, and z-axis in both positive and negative directions. There are a total of seven sets of calculations for each movement since there are six cases with offsets in six directions and one example without an offset. The Pareto optimal solutions with the corresponding objective function values are shown in Table 3.2, and the results have also been verified through the equilibrium equations mentioned in Section 3.1.

Table 3.2: Pareto optimal solutions with two objective functions.

b [m]	α [degree]	$f_1(X)$ [N]	$f_2(X)$ [N $\cdot$ m]
0.0502	90.1497	3.1945	0.1026
0.0503	90.1514	3.1957	0.1026
0.0504	90.1514	3.1961	0.1026
0.0512	90.1707	3.2032	0.1026
0.0565	90.0000	3.9313	0.0038
0.0571	90.0000	3.9482	0.0038
0.0574	90.0000	3.9574	0.0038
0.0586	90.0000	3.9910	0.0038
0.0597	90.0000	4.0246	0.0038
0.0683	90.0000	4.3412	0.0038
0.0780	90.0000	4.8647	0.0038
0.0850	90.0000	5.2978	0.0038

It can be seen from the results that the optimal solutions of the radius of the MP change within a specific range, that is, $b \in [0.050, 0.085]$ [m], while all the values of the optimized angle α are close to 90°. These optimization results show that the arrangement of revolute joints is suitable for 90° to fulfill the objective goal of reducing the maximum force and torque applied to the human limb. Here, although the maximum absolute torque is relatively large, the candidate is chosen with a structural parameter set, $X = [0.05$ m, $90.15°]$, which has the smallest maximum absolute force. The findings of the analysis are discussed in the next section.

3.2.2 Kineto-Static Analysis of the Candidate Design

In this subsection, the candidate design parameters obtained from previous subsection is used for the 3-R$\underline{\text{P}}$S parallel robot. The force and torque applied to the forearm is estimated under two conditions. First,

only the parasitic motion of the 3-R$\underline{P}$S is considered. Second, the specified value of initial offsets in different directions are considered. The influence of these two conditions on the maximum applied forces and torques are evaluated. The structural parameters of the 3-R$\underline{P}$S robot are shown in Table 3.3. It is worth noting that the radius of BP does not affect the value of the parasitic motion of 3-R$\underline{P}$S from Equation (3.8). However, the radius of BP will have other impacts on the design. For example, large radius of the BP may improve the stiffness of the robot, but also increase the size and weight of the robot, which is not desirable. Here, the radius of the BP is set as 0.22 m for the analysis, which is referred to the design parameters of a wrist rehabilitation robot designed by Liang et al. [79]. With consideration of having a relatively larger base but not increasing the size and weight of the robot too much. Moreover, the initial distance between the BP and MP is set as 0.25 m, which corresponds to the average length of the human forearm between the elbow and wrist joint [72].

Table 3.3: The structural parameters of the 3-R$\underline{P}$S robot.

Description	Value	Unit
Radius of moving platform (MP), b	0.05	m
Arrangement angle of the revolute joints, α	90.15	degree
Radius of base platform (BP)	0.22	m
Initial distance between BP and MP	0.25	m

The results of the parasitic motion analysis are shown in Figure 3.6. It can be seen that the parasitic motion in the x-direction is close to zero, and the parasitic motions in the y-direction and around the z-axis are changed according to the angle θ and ψ. In this section, the FE and RUD movements are focused with a certain angular error in the range of $\theta = -50°$ to $50°$ and $\psi = -3°$ to $3°$ for FE movement and in

the range of $\psi = -30°$ to $30°$ and $\theta = -3°$ to $3°$ for RUD movement.

First, only the influence of the parasitic motions of 3-R$\underline{P}$S is considered, assuming that the center of the wrist joint coincides with the center of the MP. The analysis results for FE and RUD movements are shown in Figures 3.7 and 3.8, respectively. From the results, the forces of joints 1 and 3 for both FE and RUD movements are relatively small, while the force of joint 2 is the primary force for both FE and RUD movements. The average of the absolute value of force for FE movement (0.049 N) is almost double that of the average of the absolute value of force for RUD movement (0.025 N). Therefore, when using this rehabilitation robot, priority should be given to ensuring that the user does not experience discomfort during FE movement. The torque for joint 4 in both FE and RUD motions, on the other hand, is relatively small. In addition, the relation between the parasitic motions and the force/torque of joints for FE and RUD movements are shown in Figures 3.9 and 3.10, respectively. Here, three conditions are set as $\psi = -3°$, $0°$, and $3°$ in the range of $\theta = -50°$ to $50°$ for FE movement, and three conditions as $\theta = -3°$, $0°$, and $3°$ in the range of $\psi = -30°$ to $30°$ for RUD movement. From Figures 3.9 and 3.10, for both FE and RUD movements, the larger the absolute value of the parasitic motion along the y-axis, P_y, the larger the force of joint 2. However, the parasitic motion, P_y has a minor influence on the relatively small force of joints 1 and 3. Moreover, a clear tendency can be found that the parasitic motion about the z-axis, ϕ, has a proportional relationship on the torque of joint 4.

Second, to investigate the influence of the existing offsets in different directions, an initial offset of 5 mm is given and its direction is assigned along the x-, y-, and z-axis in both positive and negative directions which is total six directions. Here, analyzing the maximum

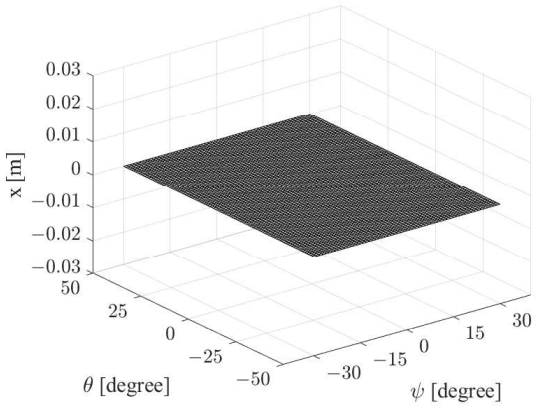

(a)

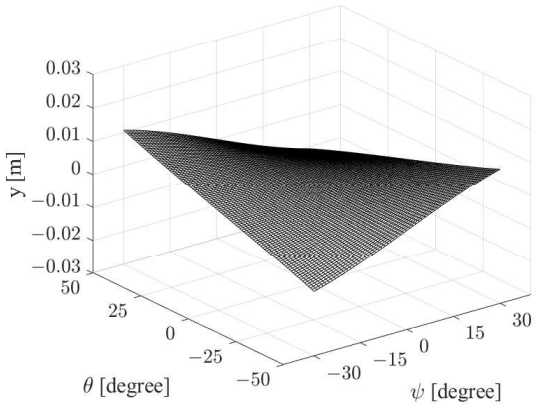

(b)

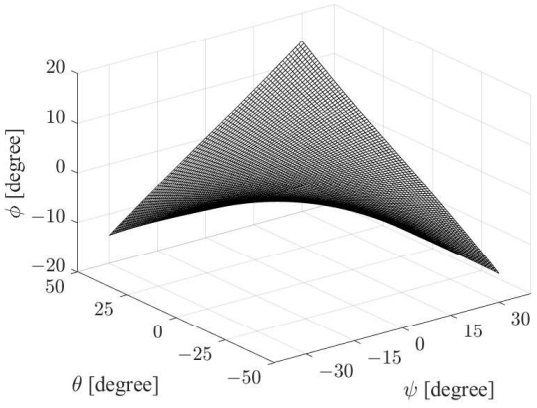

(c)

Figure 3.6: Parasitic motion of the 3-RPS robot. (a) x; (b) y; (c) ϕ

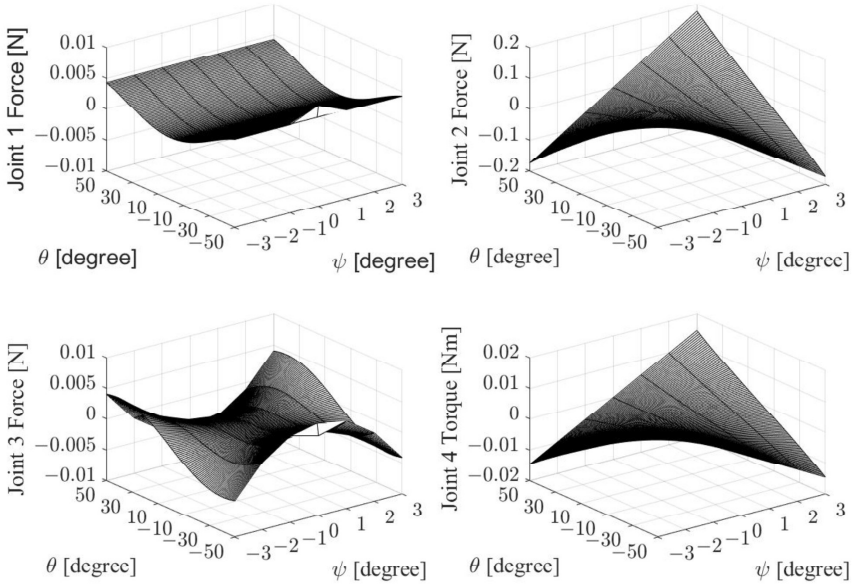

Figure 3.7: Force and torque caused by parasitic motions for FE movement.

value of force and torque within the target range of motion is focused, which is in the range of $\theta = -50°$ to $50°$ and $\psi = -3°$ to $3°$ for FE movement and in the range of $\psi = -30°$ to $30°$ and $\theta = -3°$ to $3°$ for RUD movement. The maximum force and torque under different initial offset conditions as (d_x, d_y, d_z), which is defined as displacement between center of the wrist and center of the MP in different directions, are displayed in Table 3.4. As shown in Table 3.4, the initial offset, however, has no influence on the torque. As a result, The initial offset will cause the force to increase. Therefore, reducing the initial offset aids in alleviating the user's discomfort.

Additionally, it will be addressed if the initial offset in various directions will affect the maximum force's magnitude. First, in the case of the FE movement, if the initial offset exists along the x-axis, namely, the lateral direction, and the z-axis, namely, the longitudinal direc-

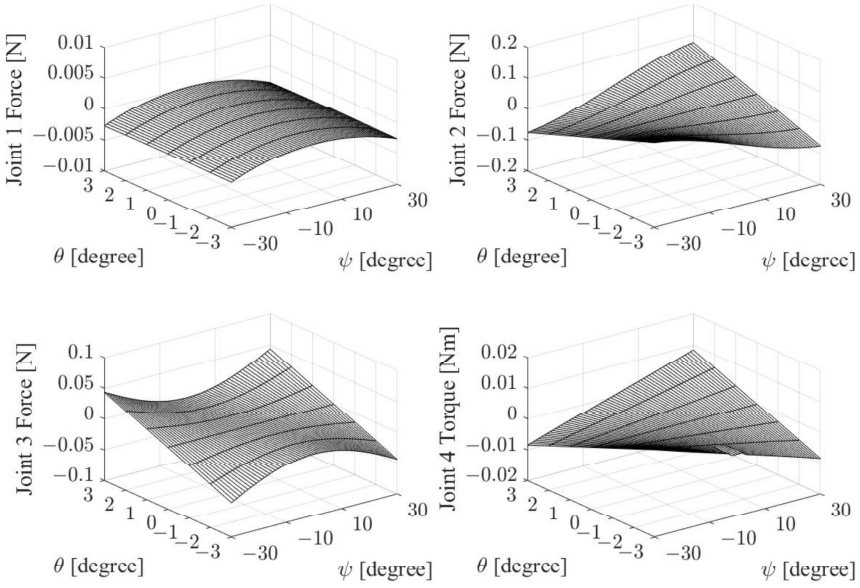

Figure 3.8: Force and torque caused by parasitic motions for RUD movement.

tion, the maximum force will increase significantly, while the offset along the y-axis, namely, the anterior direction, has little effect on increasing the value of maximum force. Therefore, for the FE movement, special attention must be paid to the initial offset in the x-direction, and z-direction to avoid a larger maximum force. Next, regarding the RUD movement, the initial offset along the y-axis and the z-axis causes the maximum force to increase; however, the offset along the x-axis has minimal influence on the results. As a result, in the case of RUD movement, special attention must be given to reducing the initial offset in the y-direction, and z-direction.

3.3 Summary

In this chapter, the 3-RPS parallel robot for wrist rehabilitation with consideration of the soft characteristic of the human limb is an-

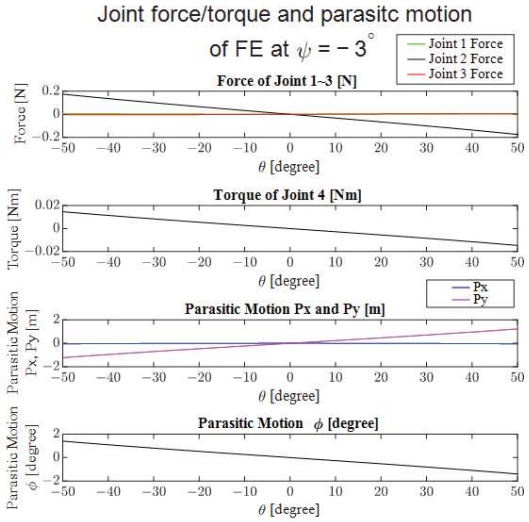

(a) $\psi = -3°$

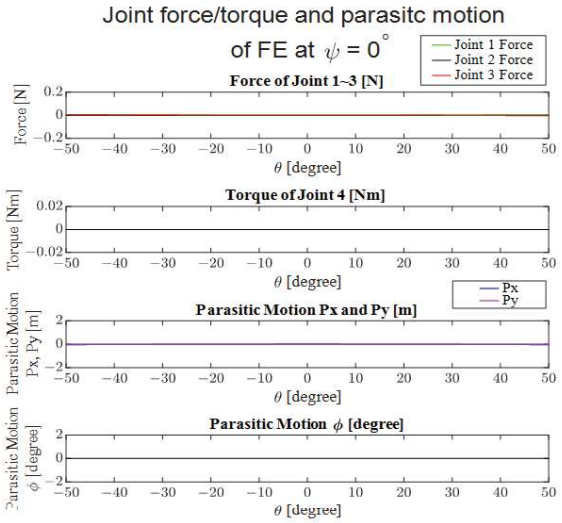

(b) $\psi = 0°$

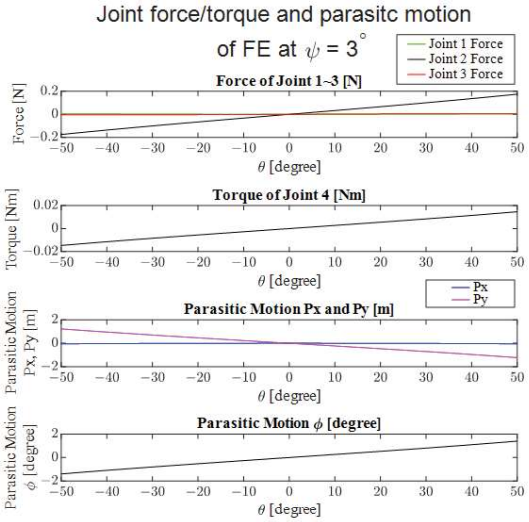

(c) $\psi = 3°$

Figure 3.9: Relation between parasitic motions of the 3-RPS robot and the force/-torque of the joints 1-4 for FE movement.

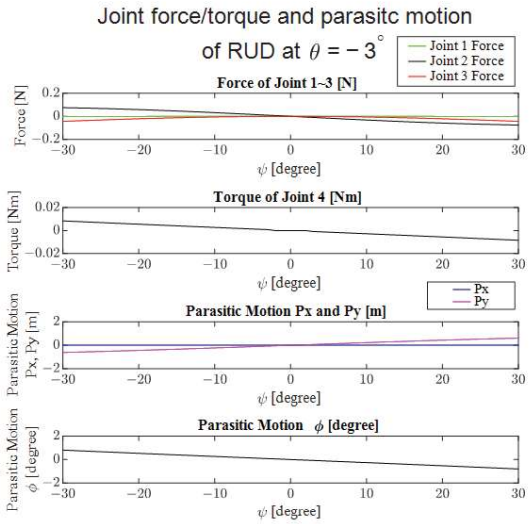

(a) $\theta = -3°$

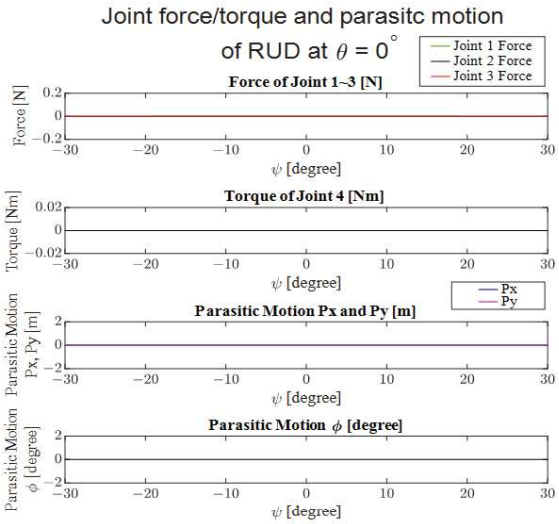

(b) $\theta = 0°$

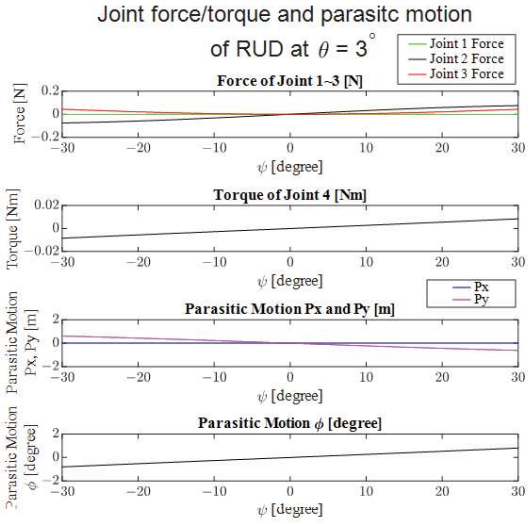

(c) $\theta = 3°$

Figure 3.10: Relation between parasitic motions of the 3-RPS robot and the force/-torque of the joints 1-4 for RUD movement.

Table 3.4: Maximum force and torque under different initial offset conditions.

FE Movement					RUD Movement				
(d_x,d_y,d_z)	$\|F_x\|_{max}$	$\|F_y\|_{max}$	$\|F_z\|_{max}$	$\|M_z\|_{max}$	(d_x,d_y,d_z)	$\|F_x\|_{max}$	$\|F_y\|_{max}$	$\|F_z\|_{max}$	$\|M_z\|_{max}$
(0, 0, 0)	0.006	0.175	0.005	0.015	(0, 0, 0)	0.003	0.075	0.044	0.008
(5, 0, 0)	0.588	0.126	0.267	0.015	(5, 0, 0)	0.003	0.042	0.067	0.008
(−5, 0, 0)	0.580	0.226	0.266	0.015	(−5, 0, 0)	0.005	0.109	0.037	0.008
(0, 5, 0)	0.027	0.177	0.038	0.015	(0, 5, 0)	0.018	0.337	0.305	0.008
(0, −5, 0)	0.027	0.177	0.038	0.015	(0, −5, 0)	0.018	0.337	0.305	0.008
(0, 0, 5)	0.266	0.175	0.589	0.015	(0, 0, 5)	0.037	0.336	0.307	0.008
(0, 0, −5)	0.266	0.178	0.589	0.015	(0, 0, −5)	0.037	0.336	0.308	0.008

Offset unit: mm; force unit: N; torque unit: N · m .

alyzed. The architecture optimization for a 3-R$\underline{P}$S parallel rehabilitation robot was performed, and the optimization goal was ensuring the safety and comfort of users. In addition, the estimation of the force and torque applied to the interface between the human and robot for the optimized design was discussed. Taking into account the softness of the human body, the proposed human limb model was applied to estimate the forces and torques exerted on the human limb. The main findings are summarized as follows:

(1) The influence of the parasitic motion of 3-R$\underline{P}$S on the maximum force and torque was analyzed. The maximum forces and torques of the FE movement are greater than those of the RUD movement. Therefore, from a design perspective, it is crucial to consider about how to ensure users do not feel discomfort during FE movement.

(2) The effect of the initial offset between the center of the wrist joint and the MP in different directions was investigated. Firstly, a larger initial offset will result in a larger maximum force and torque, thereby raising the potential risk that that users would experience discomfort. Secondly, for the FE movement, the initial offsets in the x-direction (the lateral direction) and z-direction (the longitudinal direction) generate a larger maximum force. Moreover, for RUD movement, the ini-

tial offsets in the y-direction (the anterior direction) and z-direction can cause a relatively large maximum force. Based on the findings of the analysis results, including the human limb in the design process will be required in order to generate useful ideas for designing a more comfortable and safer rehabilitation robot.

(3) The multi-objective optimization was done to obtain the architecture optimization design of 3-R$\underline{\text{P}}$S robot. The design can achieve reduced applied forces/torques to the human limb, which is considered to be beneficial for safety and comfort.

Chapter 4

Design of a Wearable Hybrid Robot for Wrist and Forearm Rehabilitation

In this chapter, a wearable hybrid robot is proposed for forearm and wrist rehabilitation. Specifically, the 3-R$\underline{P}$S parallel module is aimed at flexion/extension (FE) and radial/ulnar deviation (RUD) movements of the wrist and the serial module targets pronation and supination (PS) movements of the forearm, as depicted in Figure 1.5a. The optimal design of the 3-R$\underline{P}$S parallel module has been carried out while considering the comfort and safety of the users. Furthermore, the design of the novel mechanisms into the serial module is proposed to compensate for joint misalignment between human and robot.

4.1 Mechanism Design

4.1.1 Conceptual Design

As mentioned earlier in Subsection 1.3.3, the applications of robot-aided therapy includes providing rehabilitation functions and the ability to support some ADLs. Based on this requirement, a wearable

device is proposed which is capable of performing FE and RUD movements of the wrist and PS movement of the forearm. In addition, for most of basic ADLs, elbow movement is necessary, therefore the FE movement of the elbow is also considered. The target movements of the upper-limb are depicted in Figure 1.5b. There are many studies on the ROM of the joints of the human upper limb and the available range to perform ADLs [66, 80–83]. Although the range of results varies slightly among the studies because different sets of ADL tasks are tested, the Table 4.1 summarizes the ROM of each joint and the maximum required range of joints for performing some basic ADLs.

Table 4.1: ROM of human joins and required ROM for ADLs.

Movements	ROM [degree]	Required range for ADLs [degree]
Wrist Flexion/Extension	150 (80F, 70E)	70 (40F, 30E)
Wrist Radial/Ulnar Deviation	45 (15R, 30U)	40 (10R, 30U)
Forearm Pronation/Supination	160 (75P, 85S)	100 (50P, 50S)
Elbow Flexion/Extension	145 (145F, 0E)	130 (130F, 0E)

Abbreviations: F: flexion, E: extension, R: radial deviation, U: ulnar deviation, P: pronation, S: supination

Here, the 3-R$\underline{P}$S parallel robot proposed in Chapter 3, is used for performing the wrist FE and RUD movements. However, the size and weight of the robot should not be too large since it is attached to user's upper limb, and the weight of the robot is only carried by the user. Therefore, the design parameters of the robot are adjusted considering the wearability of the robot. The main reason of the use of the parallel robot here is that this type of robot is considered to have relatively small configuration changes according to the movement, which is benefit for user's safety. Also, as a lower mobility parallel mechanism, which has less than 6 DOFs, therefore reducing the linkages and actuators required for performing target movements. Furthermore, due to its simpler structure, the weight and cost of the robot can be reduced.

About PS movement, it is a challenge to use the parallel robot to

achieve the rotation about the z-axis due to the ROM of PS movement is relatively large ($-50°$ - $50°$). It needs to consider the problem of interference between the robot limbs and human arm. Another solution is achieved by rotating the rigid links or attachments which are fixed to the forearm and rotated around the rotation axis of robot. Here, by using an actuator to rotate the BP of the 3-R$\underline{\text{P}}$S robot. The user's forearm and the 3-R$\underline{\text{P}}$S robot are rotated together for performing the PS movement. However, the PS movement is a complex movement, and the axis of rotation is slightly migrated during the movement [59]. Therefore, joint misalignment may easily occur and need to be solved.

For the FE movement of the elbow, it is not focused on actuating the elbow joint, therefore, the elbow FE movement is considered as a passive movement in the design. However, it is necessary to consider the joint misalignment problem since if the misalignment exists, it will generate the unwanted forces to make the user feel uncomfortable. Therefore, a novel design is added to compensate for joint misalignment which will be discussed later.

The desired ROM and torques of the robot are shown in Table 4.2, and the required torques are according to the values given in [84] and the calculations of the current design. Base on the design methodology described in Chapter 1.6, the, the proposed design is expected to have improved safety and comfort. In addition, other requirements such as light weight, low cost and smaller size of the robot are also considered.

Table 4.2: Range of motion and required torques of the hybrid robot.

Movements	Range of motion [degree]	Required Max continuous torque [N · m]
Wrist Flexion/Extension	80 (50F, 30E)	1.5
Wrist Radial/Ulnar Deviation	60 (30R, 30U)	1.5
Forearm Pronation/Supination	100 (50P, 50S)	2.0
Elbow Flexion/Extension	90 (90F, 0E)	0.0

Abbreviations: F: flexion, E: extension, R: radial deviation, U: ulnar deviation, P: pronation, S: supination

4.1.2 Details of Mechanical Design

The wearable hybrid robot is designed using a computer-aided design tool, and its components are manufactured using 3D printing in onyx material reinforced with carbon fiber, which has the desirable properties of being lightweight and high strength. The 3D CAD model of the device is shown in Figure 4.1a and the schematic diagram is depicted in Figure 4.1b. Velcro straps with cuffs are used to attach the robot to the user's upper arm and forearm, and the end-effector is fixed to the user's palm. The overall weight of the robot, including the actuators, is around 1.05 kg, making it portable and appropriate for in-home rehabilitation. The proposed robotic system has two major parts: a parallel module and a serial module.

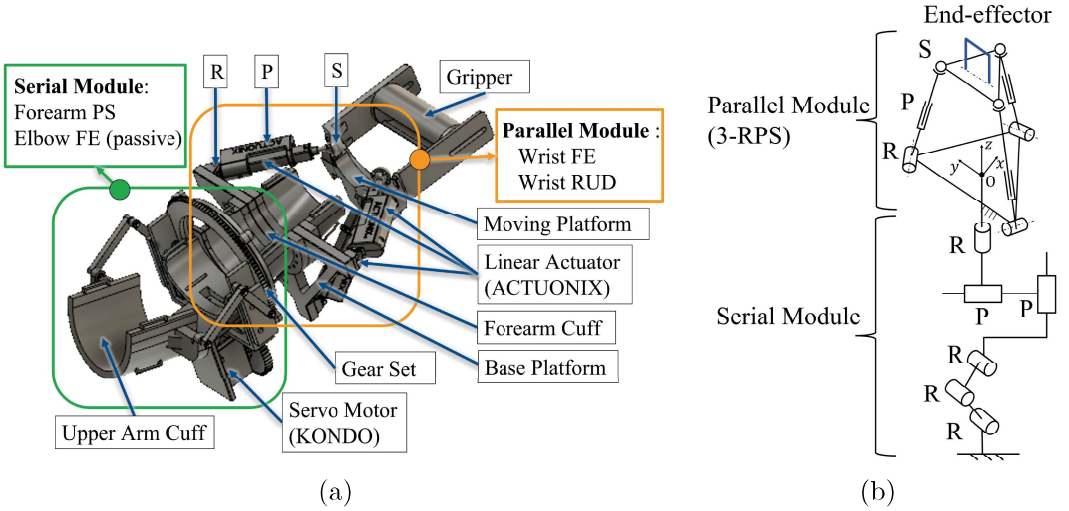

Figure 4.1: (a) 3D CAD model of the hybrid robot; (b) Schematic diagram of the hybrid robot.

The parallel module is a 3-RPS robot which is capable of performing two independent rotations and one translation. Two rotational degrees of freedom are used to implement FE and RUD movements of the wrist and the translational degree of freedom may be beneficial for adapting

to different upper limb lengths. The Actuonix P16-50-22-12-P linear electric motor drives the prismatic joint, which is controlled by an Actuonix Linear Actuator Control Board (LAC) and connected to an Arduino Mega board. In this chapter, the design of the 3-R$\underline{P}$S robot is based on the design proposed in Chapter 3, however, the design parameters have been adjusted to take into account the wearability, size and weight of the robot, which are shown in Table 4.3.

Table 4.3: The structural parameters of the parallel module.

Description	Value	Unit
Radius of moving platform (MP)	40	mm
Radius of base platform (BP)	110	mm
Initial distance between BP and MP	110	mm
Arrangement angle of the revolute joints	90	degree

The serial module is attached to the user forearm and upper arm through the forearm cuff and upper arm cuff, respectively, which is connected to the BP of the 3-R$\underline{P}$S. It performs PS movements of the forearm through a bayonet mount composed of a cylindrical forearm cover with an external gear and a drive pinion gear (gear ratio 1:2.5) directly connected to a servo motor KONDO-KRS-2542R2HV-ICS. The forearm cuff connected with the cylindrical forearm cover and the fixed upper arm cuff are assembled through a bearing and the user's forearm can insert through the hole of a cylindrical forearm cover. By rotating the cylindrical forearm cover, the forearm can be rotated with respect to the fixed upper arm cuff. In addition, mounting the robot on the upper arm by cuffs has the benefit of distributing the reaction forces throughout the user's body to prevent any harm or uncomfortable feelings. Moreover, because the wearable device includes the elbow, it has the potential to provide elbow assistance.

4.1.3 Design of Mechanisms for Joint Compensation

Although the size and weight of the wearable robot may increase, based on the results of Chapter 2 that adding passive joints to the robot is an effective solution to compensate for the misalignment of human–robot joints. Here, two joint misalignments require to be compensated for. The first is about the forearm rotation axis and the other is about the elbow joint. Here, similar to the method described in Chapter 2, each misalignment is compensated by adding passive joints to form a four-bar linkage. Therefore, these misalignments are compensated by the proposed novel design which is composed of RRPP and RRRR linkages. The detail will be discussed separately in the following.

Misalignment Compensation Mechanism (RRPP) for Rotation Axis of Forearm

The robot relies on the rotation of the attached cuff to rotate the forearm and due to the complex anatomy of the forearm mentioned in Subsection 1.3.3, it is difficult to have a good alignment between the rotation axis of the cuff and the forearm, as shown in Figure 4.2a. Here, $\mathbb{R}$ and $\mathbb{H}$ represent the robot and human rotation axis, respectively. And a maximum misalignment (δ) between robot and human rotation axis is considered as 10 mm. The mechanism is aligned within the transverse plane of the forearm which is in $X-Y$ plane, and the location of the transverse plane is set as 110 mm from the wrist joint. The red point and the blue point marked in Figure 4.2b(b) represent the rotation centers of the forearm and of the robot joint, respectively. The forearm rotation is regarded as a rotation around a virtual revolute joint and form a four-bar linkage as RRPP with the actuated revolute joint and the added two prismatic joints shown in Figure 4.3.

Through Gruebler's equation, the DOF of the mechanism can be obtained to be 1. This means that regardless of the dimensions of each link, the PS movement of the forearm can be achieved by one active revolute joint as an actuator of this mechanism. Hence, the proposed mechanism can be adapted to the position of the rotation axis of the forearm within allowable range.

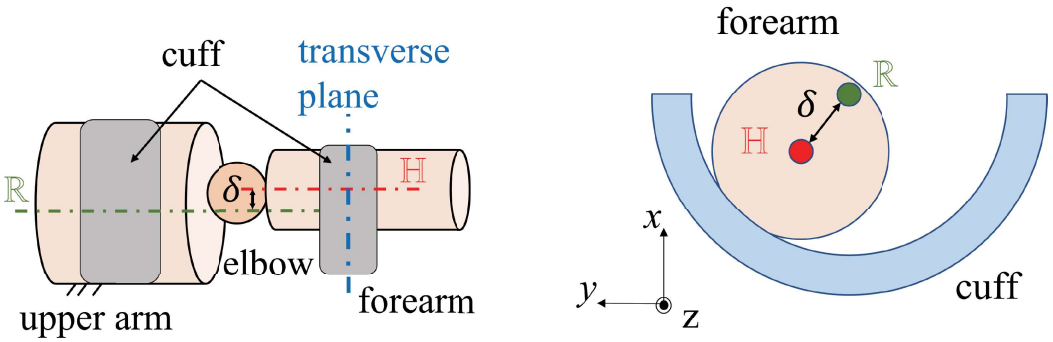

(a) (b)

Figure 4.2: (a) Conceptual model of the axis misalignment; (b) Transverse plane model of the upper limb with the cuff.

Next, about kinematic analysis of RRPP mechanism, its geometry is shown in Figure 4.3, and the displacements of two prismatic joints can be solved, s_1 and s_2, by using a vector-loop method for given δ, and variable ξ. The solutions are as follows:

$$s_1 = \delta \cos \xi, \quad s_2 = \delta \sin \xi \tag{4.1}$$

From above equations, the maximum displacement change of the prismatic joints can be obtained as 20 mm, which is twice the maximum allowable value of axis misalignment. The prismatic joint used here has a 30 mm stroke, therefore 10 mm of the axis misalignment can be fully compensated.

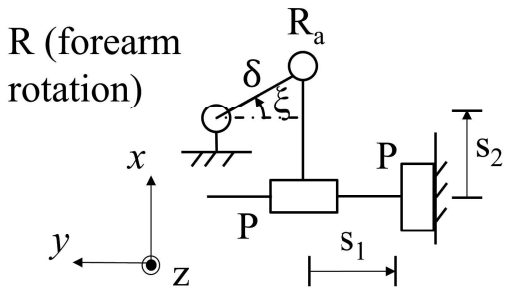

Figure 4.3: Analytical model of RRPP mechanism.

Misalignment Compensation Mechanism (RRRR) for Elbow Joint

The elbow joint is modeled as a virtual revolute joint similar to the approach described in Chapter 2. Three passive physical revolute joints are added including the elbow joint to form a four-bar mechanism, RRRR, shown in Figure 4.4a. The links l_1 and l_2 are connected to the forearm and the upper arm by the cuffs, respectively. set The locations of the cuffs for the forearm and the upper-arm are set to be 40 mm from the elbow joint in order to have a relatively smaller volume of the mechanism. Although the elbow is not actuated by the actuator in the present prototype depicted in Figure 4.4b and is considered as a passive joint during the movement, it is possible to add an actuator at point A to rotate the elbow for the next prototype. The link lengths of l_1 and l_2 are set as 60 mm and 55 mm, respectively.

4.2 Evaluation and Experimental Study of the Proposed Design

4.2.1 Evaluation of Range of Motion of the Robot

In this section, the evaluation of the proposed hybrid robot by setting different configurations of the prototype is done, as shown in

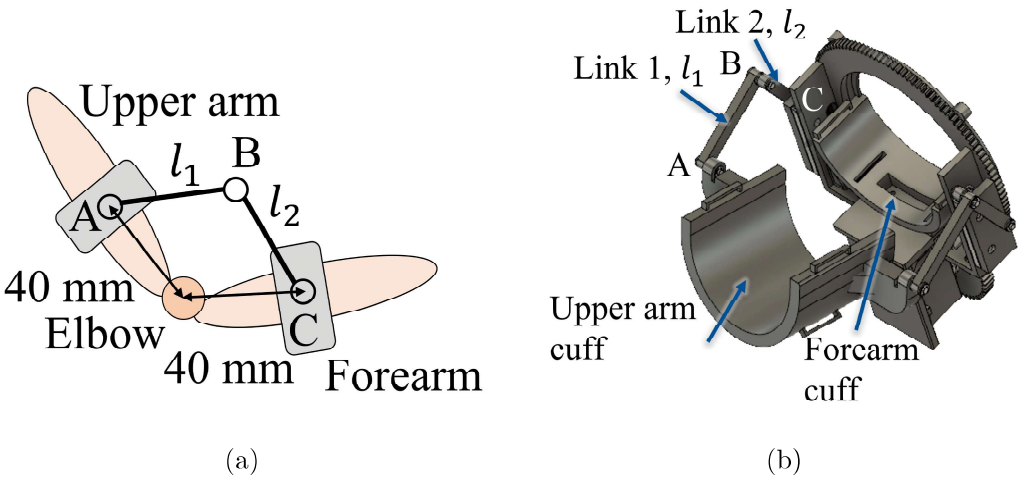

(a) (b)

Figure 4.4: (a) Analytical model of the RRRR mechanism; (b) 3D CAD model of the RRRR mechanism.

Figure 4.5. ACL500 (Biometrics Ltd.) wireless accelerometer is used to simultaneously measure the rotation angles of the moving platform of the 3-RPS in three planes. The FE, RUD and PS movements are measured independently, and 100 measurement data are recorded for every 10 degrees interval within the range of motion of each movement. From the results shown in Table 4.4, the robot can achieve the desired range of motion of FE, RUD and PS movements, with only a small angular error of less than 3 degrees. Therefore, the proposed robot design satisfies the specified requirements.

4.2.2 Experimental Study

In this experimental study, the proposed hybrid robot will be attached on the subject to perform the wrist flexion/extension (FE) and radial /ulnar deviation (RUD) movements, and forearm pronation/-supination (PS) movement. The desired range of motion of the wrist and forearm is shown in Table 4.2. The purpose of this study is to evaluate the effectiveness and comfort of the proposed rehabilitation robot.

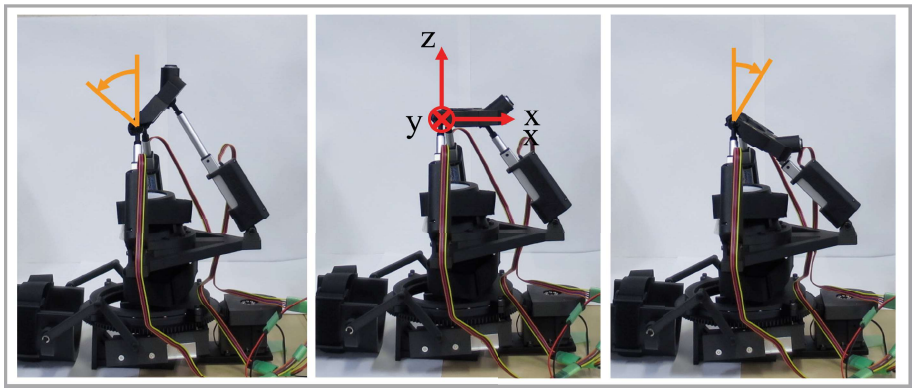

(a)

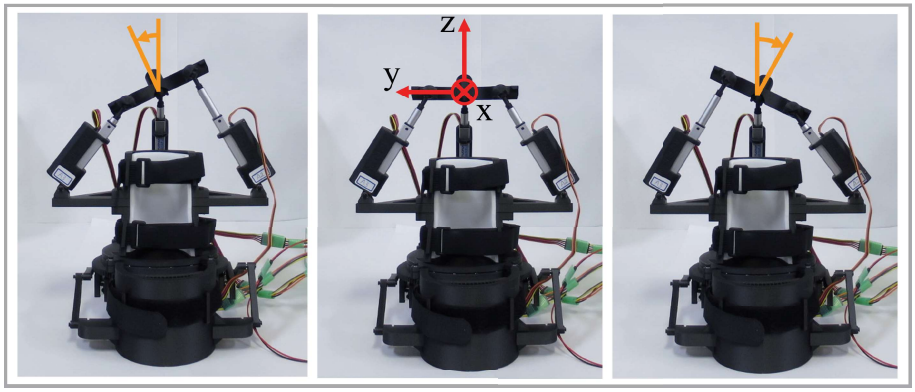

(b)

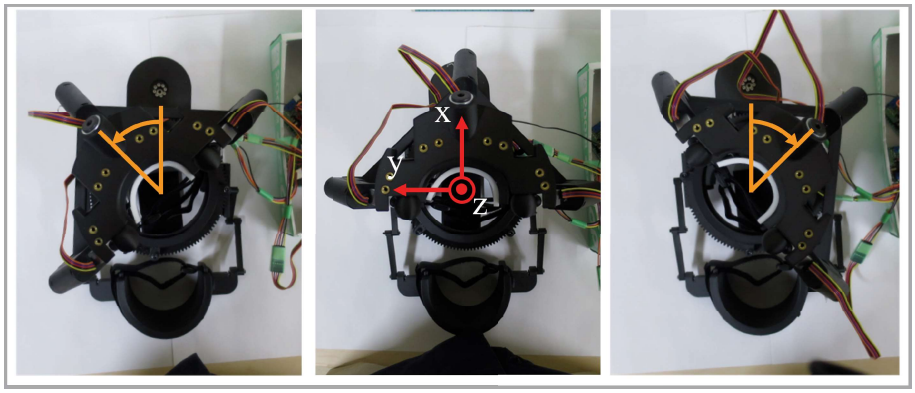

(c)

Figure 4.5: Movements evaluation for: (a) FE (b) RUD (c) PS movements.

Target angle [degree]	-50	-40	-30	-20	-10	0	10	20	30
Measured average angle	-51.938	-39.866	-30.835	-22.084	-10.183	0.557	8.792	18.225	28.700
Angular error	-1.938	0.134	-0.835	-2.084	-0.183	0.557	-1.208	-1.775	-1.300

(a)

Target angle [degree]	-30	-20	-10	0	10	20	30
Measured average angle	-32.363	-17.598	-8.176	0.455	10.780	20.212	30.783
Angular error	-2.363	2.402	1.824	0.455	0.780	0.212	0.783

(b)

Target angle [degree]	-50	-40	-30	-20	-10	0	10	20	30	40	50
Measured average angle	-50.290	-40.522	-31.514	-19.844	-11.533	0.576	8.373	20.846	29.104	40.155	49.184
Angular error	-0.290	-0.522	-1.514	0.156	-1.533	0.576	-1.627	0.846	-0.896	0.155	-0.816

(c)

Table 4.4: Results of movements evaluation for: (a) FE (b) RUD (c) PS movements.

The experiment targets healthy participants as the research subjects. Five subjects participated the experiment during the recruitment period from May 9, 2022, to May 20, 2022. The subjects are healthy individuals with ages ranging from 22 to 35 years. None had any previous experience using the proposed rehabilitation robot. First, subjects sit in front of a table and attach the wearable robot. Then, the robot performs target rehabilitation movements while measuring their limb motion through motion capture system (MoCap). The measurements are used for evaluating the effectiveness of the robot. After the measurement, the subjects will fill out the questionnaire customized based on System Usability Scale (SUS) to evaluate the usability and comfort of the proposed design. By these evaluations, the proposed design is validated, and further improvement points will be clarified, prototyped and tested. Details will be described in the following parts.

Experimental Protocol

Human Subjects Research Ethics Committee at Tokyo Institute of Technology approved the experiment protocol of the experimental study (NO. 2022037). All participants have been well informed about the objective, procedure and risks of the experiment and they have

signed the consent form before the experiment. The detailed steps of the experiment are described in Table 4.5. The proposed prototype is shown in Figure 4.7.

Table 4.5: Description of the experimental procedure.

Step No.	Step	Description	Time [min]
1	Introduction	Introduce the experiment purpose, method and possible risks in detail, and sign the consent form.	10
2	Warm up	Perform wrist and forearm relaxation exercises.	5
3	Pre-experiment	The subject put on the rehabilitation robot (see Figure 4.1a) without feeling discomfort. At the start of the experiment, the subject is seated comfortably on the chair and the subject's elbow joint is supported by the table (see Figure 4.6). After that, the marks are attached at specific locations to the subject and robot firmly.	10
4	Measurement	The measurement of position of subject's limb and the robot will be tested for 20 cycles for wrist FE and RUD movements and forearm PS movement with the specific range of motion through motion caption system. (see Figure 1.5a).	15
5	Post-experiment	Participants answer the questionnaire.	10
		Total	50

Motion Capture System

The movements of the wearable robot and user's upper-limb is measured by the marker-based motion capture system. A total of 13 markers are used, 6 for the robot and 7 for the human upper limb, and the placement of markers are shown in Figure 4.8. For the robot, there are 6 markers, BP1 BP3 and MP1 MP3, for the MP and BP, which are placed at the three vertices of them. And for the human limb, there is one marker, SLD, placed at shoulder joint. Two markers, ELR and ELL, for Elbow joint. Two markers, WRR and WRL, for wrist joint. And two markers are placed on the back of the hand as named

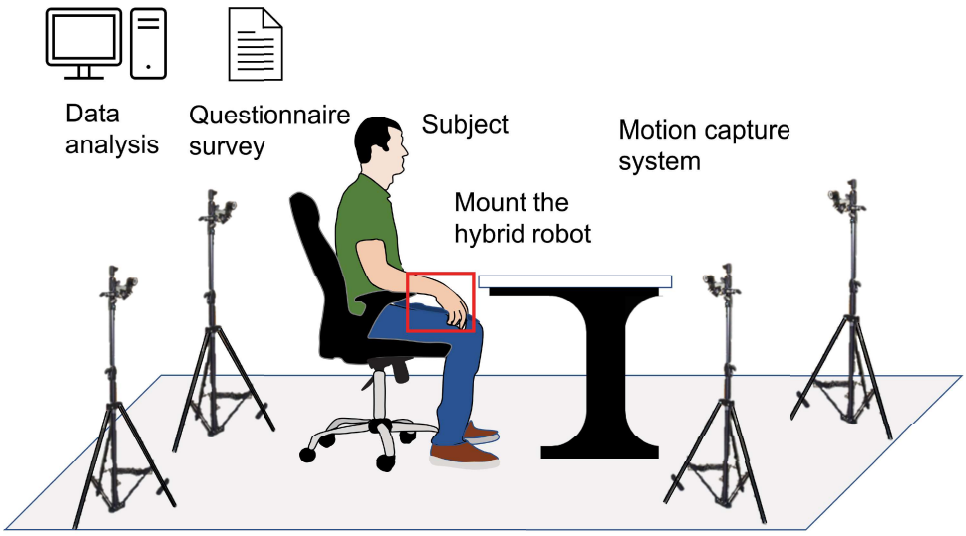

Figure 4.6: Sketch of the experiment.

HDR and HDL, which are near the second and the fifth metacarpophalangeal joints, respectively. In order to avoid the robot's MP from touching or blocking the markers during the movement, the locations of the wrist markers (WRL and WRR) are adjusted. However, the line connects the two markers, WRR and WRL, approximately pass through the center of the wrist.

There are 6 infrared light cameras used in the experiment to detect the reflective markers pasted on the human limb and robot. These cameras are placed as a circle, targeting at the robot and the subject in the center of the circle. The setup of the experiment is shown in Figure 4.9. Then the trajectory of the rehabilitation movements can be obtained to further calculate the rotation angles of human joints and the robot.

Calculation of Rotation Angles

In this subsection, the calculation of the rotation angles of the robot and human joints is described. First of all, the MP center (MPCP)

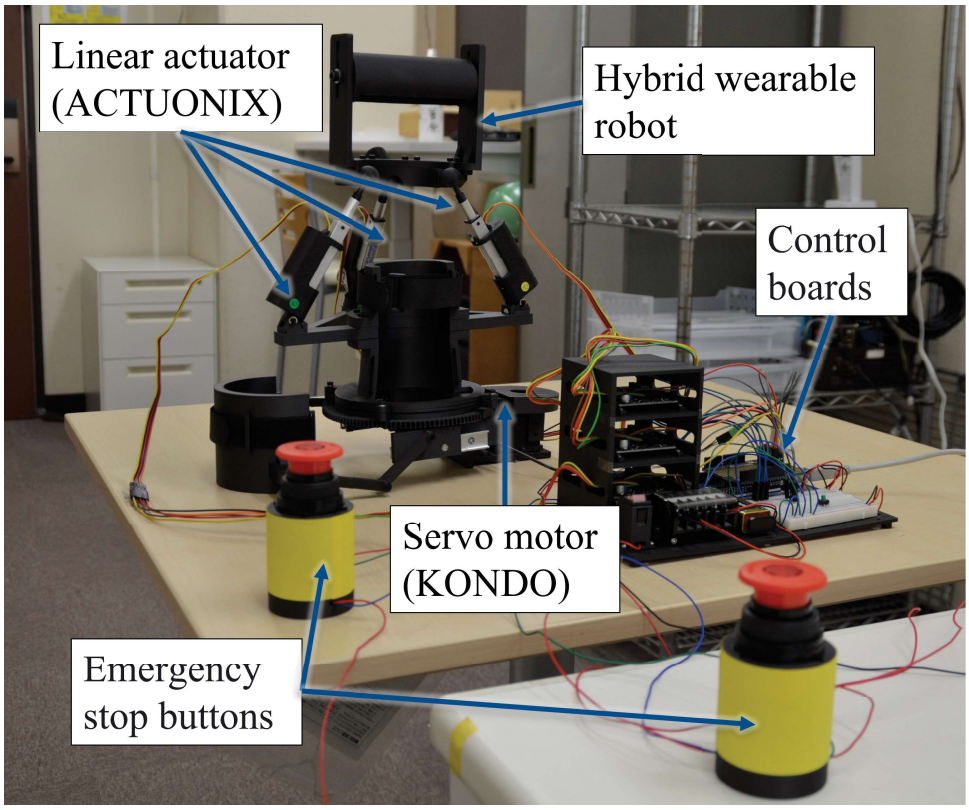

Figure 4.7: The proposed wearable hybrid robot.

is the midpoint of MP1 and MP2. And the BP center (BPCP) is the midpoint of BP1 and BP2 as shown in Figure 4.10. The initial position of the robot is used to define the reference planes before the robot starts to move . The normal vector of the coronal plane is defined as $BP2_0 - BP1_0$. Then, the normal vector of the sagittal plane is defined as the cross product of $BPCP_0 - MPCP_0$ and $BP2_0 - BP1_0$. Finally, the normal vector of the transverse plane is determined by cross product of the normal vector of the sagittal and coronal planes. Next, the rotation angles of robot and human limb are calculated based on the initial angle of the robot and human joints. The detailed calculations of the robot and human angles for each movement are described as follows.

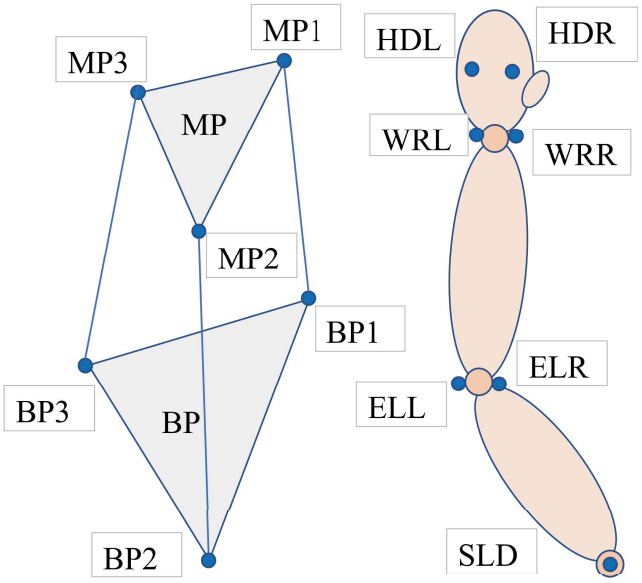

Figure 4.8: Locations of the markers

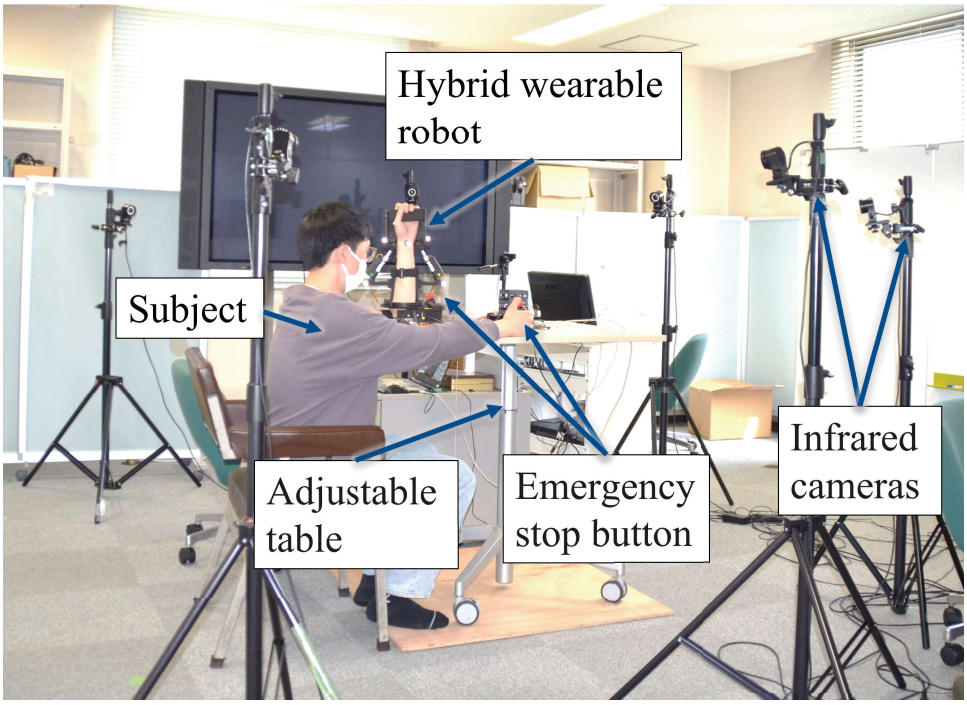

Figure 4.9: Setup of the experiment.

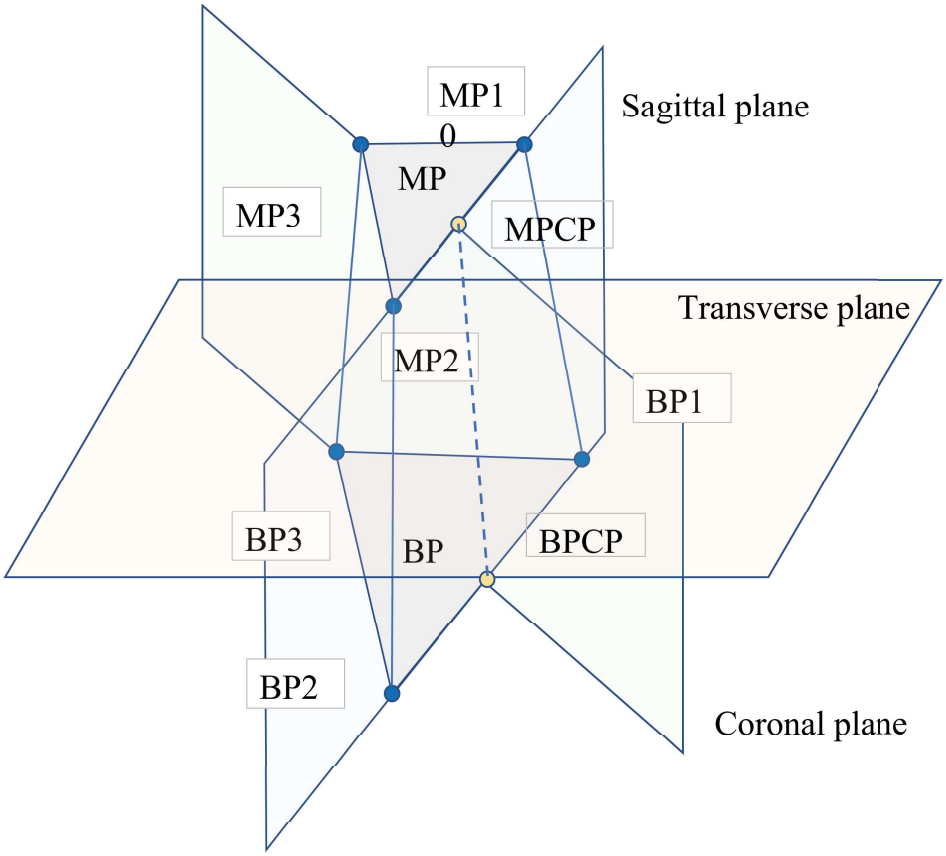

Figure 4.10: The projected planes for angle calculation.

For the FE movement, the rotation angle of the MP is obtained by calculating the angle between MP3, MPCP, and BPCP, projected to the coronal plane, to form the angle *theta*. For the RUD movement, the rotation angle of the MP is obtained by calculating the angle between MP2, MPCP and BPCP, projected to the sagittal plane, to form the angle *psi*. For the PS movement, the rotation angle of robot (MP and BP are rotated together) is obtained by calculating the angle between the negative direction of the normal vector of the sagittal plane and the vector of MP1 and MP2 projected to the transverse plane, to form the angle *phi*.

Next, for the calculation of human joints, the HDP represents the midpoint of HDL and HDR. The WCP represents the midpoint of WRL and WRR. It is worth knowing that the markers of the elbow joint should have been used. However, in some cases, the height of the experimental table is adjusted to make the subjects more comfortable, causing the ELL and ELR to be out of the detection range and resulting in too much data loss about the ELL and ELR markers. Instead, the BPCP is used for the calculation. For the FE movement, the rotation angle of the wrist is obtained by calculating the angle between HDP, WCP and BPCP projected to the coronal plane, to form the angle $theta_{wrist}$. For the RUD movement, the rotation angle of the wrist is obtained by calculating the angle between HDP, WCP and BPCP projected to the sagittal plane, to form the angle psi_{wrist}. For the PS movement, the rotation angle of the forearm is obtained by calculating the angle between negative direction of the normal vector of the coronal plane and the vector of WRL and WRR projected to the transverse plane, to form the angle $phi_{forearm}$

Questionnaires

The questionnaire is designed to evaluate two things: the first is the robot's usability, and the second is the comfort and safety during the use of the robot. The first part is a customized System Usability Scale (SUS), which is a reliable tool used for evaluating usability [85]; the second part is composed of some questions that the subjects can leave in their feedback of using the rehabilitation robot. The customized SUS questionnaire consists of 10 questions, and the odd number of questions are positive, while the even number of questions is negative. Each question has 5-point scales numbered from 1 (strongly disagree) to 5 (strongly agree). Positive questions are scored by the evaluation scale minus 1, while negative questions are scored by 5 minus the evaluation scale. Then, we can get the overall SUS score by multiplying the sum of the score by 2.5. Therefore, SUS scores vary from 0 to 100.

The second part has seven questions related to comfort and safety, and the questionnaires can collect the feedback of subjects on the use of the robot. The questions were written in both Japanese and English. Please see appendix for the Questionnaire questions.

4.3 Results and Discussions

4.3.1 Usability Assessment

The scores of the SUS questionnaire are ranged from 60 to 87.5, with an average score of 70, indicating usability between "Fair" to "Good" (Fair for scores at 51 and Good for scores at 71) [86]. This means that the subjects are generally satisfied with the proposed robot. The average score for each item ranges from 2 to 3.2, as shown in Table 4.6. Item Q2 and Q3 have the highest score, while item Q4 has the lowest score.

For reliability analysis, the reliability is identical to the calculation of Cronbach's alpha, which is widely used for an estimate of reliability. The calculation result shows that Cronbach' s alpha value is 0.724 for the SUS scores, indicating an acceptable degree of internal consistency [87]. In addition, compared with the score to the average SUS score obtained by Sauro et al. [88], who used about 500 different products in the market to obtain the average SUS score of 68, the results indicate that the usability of the proposed design is above average. Although several issues still need to be addressed, the proposed design reach considerable usability compared to the products already in the market.

Table 4.6: Score for each system usability scale item.

Item	Content	Average Score
Q1	I think I would like to use this rehabilitation robot frequently.	2.6
Q2	I think the rehabilitation robot is complex and difficult to use.	3.2
Q3	I think the rehabilitation robot is easy to use.	3.2
Q4	I think that I would need the technical assistance to be able to use this rehabilitation robot.	2.0
Q5	I think the various functions in this rehabilitation robot are well integrated.	2.8
Q6	I think the functionality of this rehabilitation robot are not organized.	3.0
Q7	I would imagine that most people would learn to use this rehabilitation robot very quickly.	2.8
Q8	I think most of users will have difficulties to learn how to use the rehabilitation robot.	2.6
Q9	I felt very confident when using the rehabilitation robot.	2.8
Q10	I may need to learn a lot of things before I am able to use this rehabilitation robot.	3.0

4.3.2 Comfort and Safety Assessment

Based on the questionnaire feedback of the subjects, most subjects did not feel any discomfort when wearing the robot before the testing. However, about during the rehabilitation process, three of the five subjects reported discomfort from their wrist contact with the robot. In addition, one subject reported that when performing PS movements, the forearm would get a little bit stuck with the cuff, causing discomfort. One main reason the small radius of the MP, which results in

a small space between the wrist and the robot. As a result, the area near the wrist is in contact with the robot, causing discomfort to the user. As the problem reported for the PS movement, one possible reason is that the the cuff is not able to adapt to the thicker forearm, so the cuff is too small for the subject, and leads to the forearm tissue is squeezed out of the cuff, causing a little stuck of the PS movement. This is truly an issue for current prototype since one subject was unable to perform the PS movement testing due to his forearm was too thick to fit the cuff. After testing, one subject reported a feeling of pressure on the forearm and wrist. Another subject reported a discomfort of the wrist. Although when wearing the robot, attention was paid to make the strap not too tight and to ensure that it would not cause discomfort. However, since the prototype do not have a corresponding design for weight balance, the subject may feel heavier weight on the left side of the upper-arm due to the unbalanced weight of the robot. It may cause the user to feel the pressure on the forearm in contact with the strap and the cuff.

Although there are several feedback from subjects about feeling discomfort during the use of the robot, the major reason is because of some parts of the prototype are designed too small. While such a design may allow the robot to have a smaller overall size and fit more tightly to the human body, it eventually makes the robot less adaptable. This requires to be modified in the next version of the prototype. From these feedback, there is no discomfort according to some force or torques applied to the subject's limb.

Regarding the weight of the robot, all subjects do not feel the robot is heavy, which means they are satisfied and can accept the weight of the robot. On the other hand, all subjects did not report any potential hazards or limitations of the robot. A simplified version of

the feedback from the subject is summarized in Table 4.7. Further improvements are needed for the proposed design according to the feedback from the experiment subjects.

Table 4.7: Results of the questionnaire for comfort and safety.

Questions	Subject 1	Subject 2	Subject 3	Subject 4	Subject 5
Discomfort before testing?	No discomfort	No discomfort	No discomfort	No discomfort	No discomfort
Discomfort during testing?	Feeling discomfort on the right side of the wrist	Feeling discomfort on the area near the wrist where it contacts the robot	Feeling discomfort on the area near wrist where it touches the spherical joint of the robot	During PS movement, the forearm is a bit stuck in contact with the robot	No discomfort
Discomfort after testing?	A feeling of pressure on the forearm and wrist	The area near the wrist where it touches the robot is uncomfortable	No discomfort	No discomfort	No discomfort
Robot's weight	Normal	Normal	Normal	Light weight	Normal
Potential dangers?	No	No	No	No	No
Limitations?	No	No	No	No	No
Comments	None	Feel fatigue	None	None	Did not do PS movement

4.3.3 Movements Assessment

Although the rotation angle of the proposed robot has been evaluated and it satisfies the requirements in the Subsection 4.2.1. However, it is necessary to actually put the rehabilitation robot on the subject to further understand the actual performance of the rehabilitation robot. Therefore, the main purpose of the movement assessment is to measure the rotation angles both of the robot and human joints, to understand whether the robot is able to achieve the ROM of the specified rehabilitation movements and to compare the difference in rotation angles between the robot and human joints.

As discussed in the previous section, it is true that the different limb shapes of the subject have a difference on the measurement results due some parts of the robot are designed too small. Subjects with thinner limb are expected to be suitable to use the proposed robot without obstacles to achieve rehabilitation movements. Figure 4.11 - 4.13 shows the measurement data of one of the subjects with approximately 10

cycles per movement and the maximum and minimum angular values of each cycle are indicated. The measurement results of the other four subjects are shown in the appendix. Among them, one of them did not complete the PS movement measurement.

For the FE movement, as shown in Figure 4.11, the measurement results are in general accordance with expectations, although there are some differences between each cycle of movements. The range of human joint rotation angle is slightly smaller than that of the robot, and there is a positive relationship between the robot and human joint rotation angle.

For the RUD movements, as discussed in the previous subsection, because of there are some obstacles caused by the contact between the robot and human, subject with different size of limbs may result in different measurement results. Figure 4.12 shows that the range of motion of both the robot and human joints are reduced largely. For some subjects, the measurement data shows a significant reduction in range of both human and robot angle for some cycles, resulting in fluctuations of the ROM. The reason for the results may be caused by the contact between the robot and the human hand during the movement. These results show that the robot needs to be modified to reduce the obstacles occur. Finally, for the PS movement, it can be seen that although there is still a positive relationship between the range of rotation angles of the robot and the human joint, there are some differences between each cycle. The possible reason for this is that the contact between the subject's forearm and the robot hinders the PS movement. For the cases of some subjects, there is a significant reduction in the rotational angle range. The results also indicate that the design of the robot needs to be modified to better fit the human forearm and avoid obstacles.

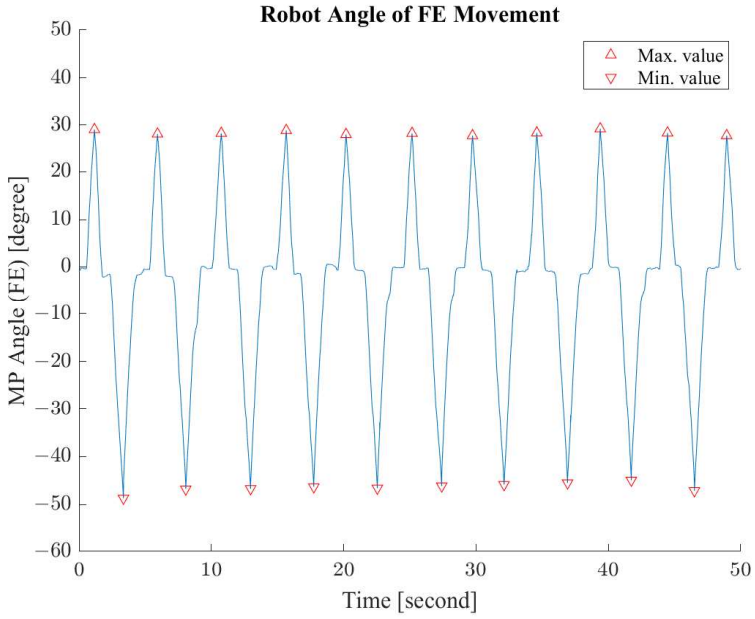

(a) Robot angle of FE movement

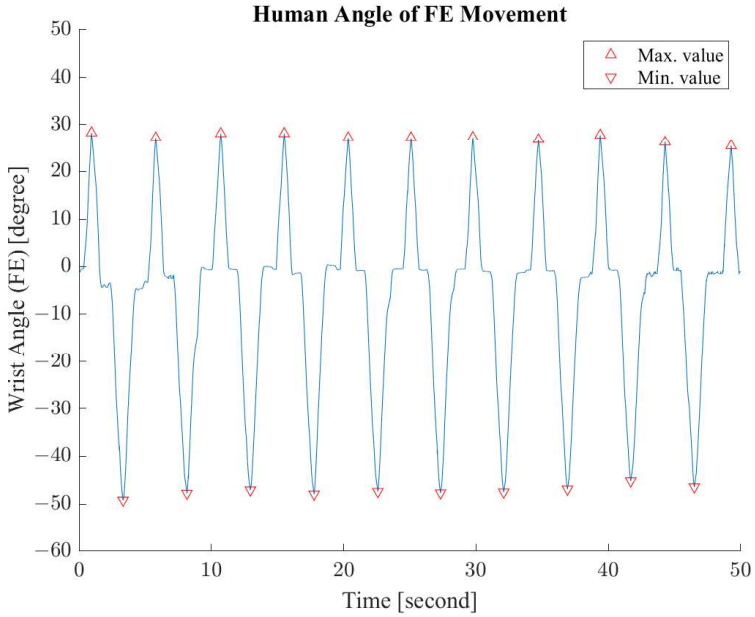

(b) Human angle of FE movement

Figure 4.11: Experimental results of FE movement (Subject 1)

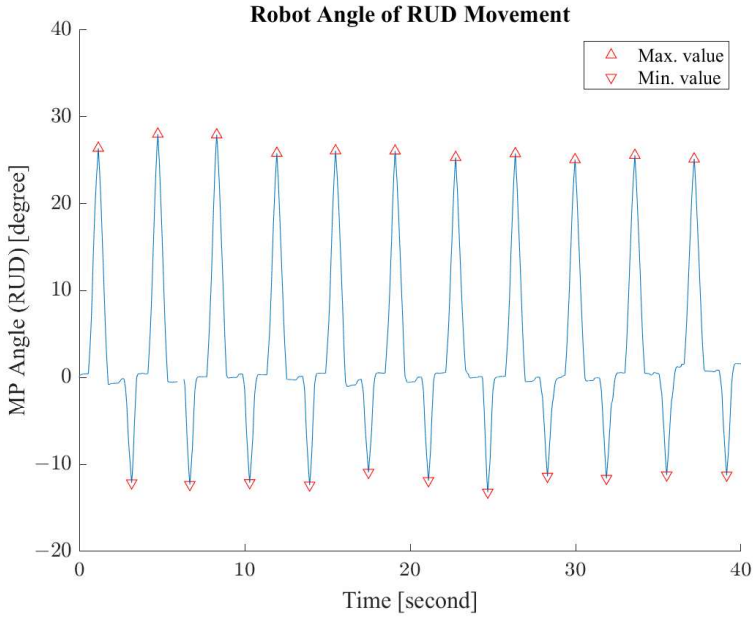

(a) Robot angle of RUD movement

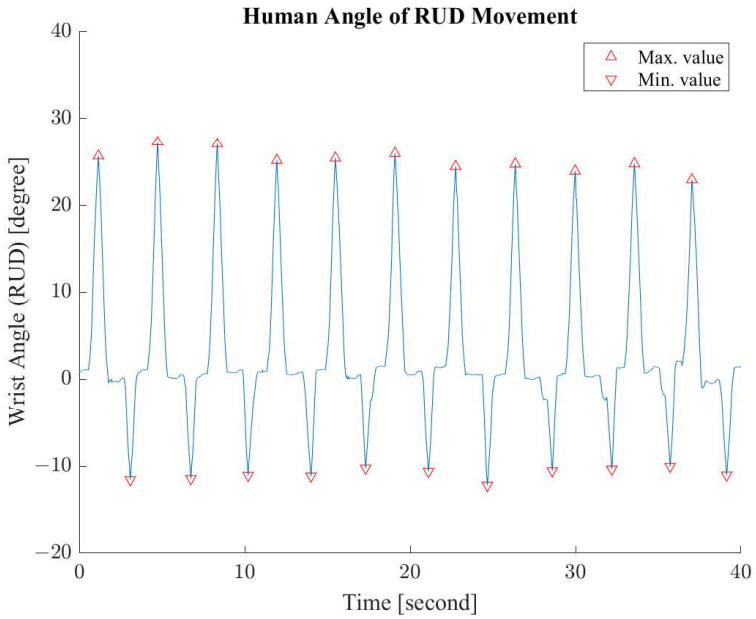

(b) Human angle of RUD movement

Figure 4.12: Experimental results of RUD movement (Subject 1)

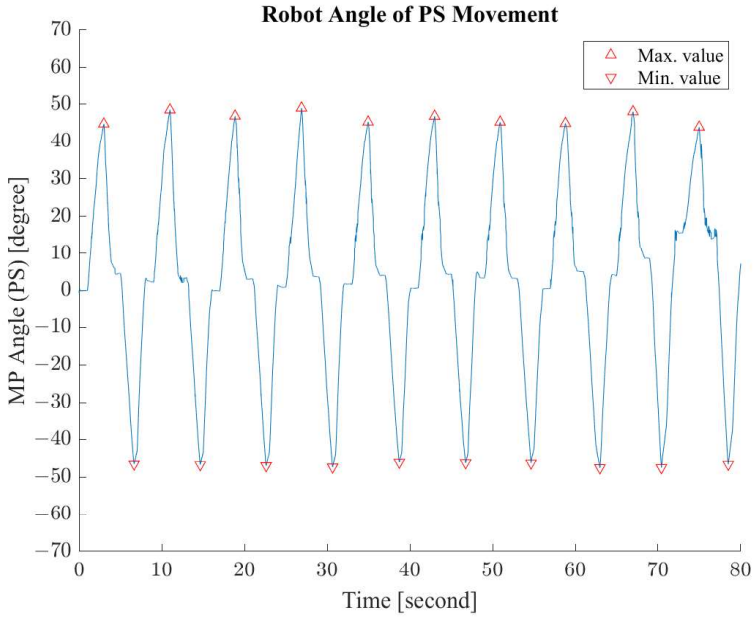

(a) Robot angle of PS movement

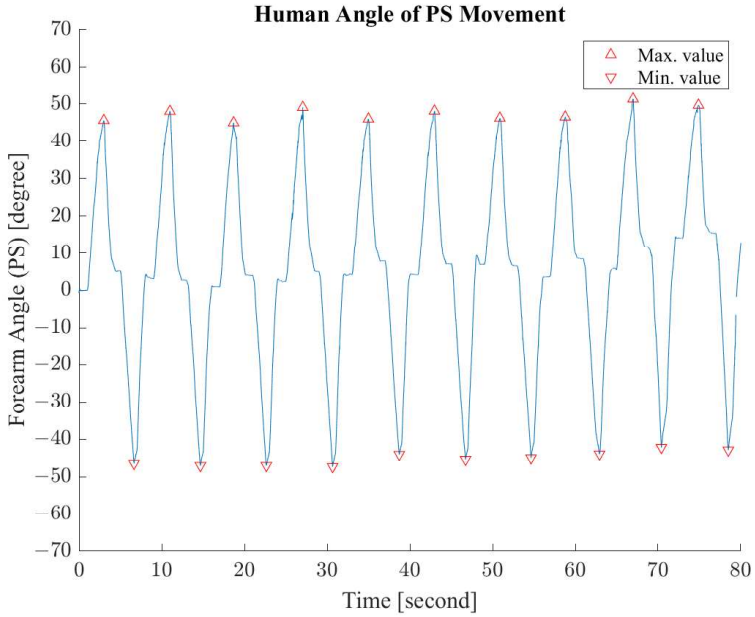

(b) Human angle of PS movement

Figure 4.13: Experimental results of PS movement (Subject 1)

4.3.4 Discussion

From the measurement results, the proposed rehabilitation robot cannot achieve expected range of motion. For the FE movement, the robot satisfies the requirement rotation angles with minor reduction. However, for RUD and PS movements, the ROM is smaller than expectation. These results may be mainly due to the several reasons addressed below. First, the robot movement is limited by the obstacles between the robot and human. For FE and RUD movement, the small radius of MP results in the small space between robot and human wrist. Therefore, during the movement, the spherical joints of MP may contact the area near the human wrist to hinder the movements of robot. In addition, for PS movement, the forearm cuff is designed too small to adapt the different width of the forearm and it may cause obstacles with the soft tissue of the forearm when the robot is rotated. As a result, the ROM of robot is reduced which requires further design changes for improvement.

Second, the performance of the robot should be considered which can affect the movements of the robot. There are several indices which are used for calculations of the parallel robots' performance for optimal design [89]. Here, the method presented by Liang et al. [65, 90] is applied to calculate the transmission index (TI) of the parallel robot. The TI is based on the pressure angle [91], which can be defined in a kinematically equivalent structure (KEM) of the prototype. The TI of the proposed design is shown in Figure 4.14. According to [91], $TI \geq 0.5$ is regarded as a condition which represents a good performance of the parallel robot. From the results shown in Figure 4.14, for both FE and RUD movements, there are some parts of ROM of the robots with TI less than 0.5 as shown as dashed lines in the figure. This means

that the robot needs design changes to increase the TI and improve the movements of the robot.

Third, the effects of human may influence the ROM. Here the effects of human include the effects of soft property of human limb as mentioned, however, how the subject grasps the handle of MP may also have effects on ROM. For instance, how much force is used to hold the handle by the subject. Since when the subject grasps the handle and applies strength from the arm muscle, it may become difficult to rotate the wrist compared with the relaxed status, which may affect the ROM. On the other hand, from observations, since the subject's elbow is simply placed on the designated position point on the table during the experiment. The subjects are asked to keep the forearm as vertical with the upper arm, however, during the experiment, due to the unbalanced weight of the robot and the applied force on the user's limb, the user's forearm would have a small swing according to the robot's movement. For example, the FE movement, the maximum horizontal displacement of the center of the subject's wrist joint is about 20 mm. Although such a condition does not affect the measurement results in this section, because the measurement of the rotation angle is based on the initial position. However, in order to make the subject's forearm more stable during the experiment, additional supporter for the user's forearm should be made in the next experiment in the future.

According to the experimental results, the proposed robot can be designed to performing the specification as for FE movement: $-45°$ to $20°$; RUD movement: $-10°$ to $20°$; PS movement: $-45°$ to $45°$. This design includes the effect of the human soft tissue, driving torque of human wrist joint, allowable comfort of the user as well as the mechanical motion transmission characteristics of the mechanism. In

addition, some allowance in the motion range should be considered in the specification of ROM of the robot and the allowable transmission index. The modification of the prototype will be discussed in the next Subsection.

4.3.5 Improvement of the Proposed Design

Based on the feedback from subjects, several modifications of the prototype should be made. There are two obvious improvements that can immediately improve the design of the prototype. First, the radius of MP can be larger to have more space between the wrist and the MP. Second, to increase the size of the forearm cuff, so that the robot can adapt to users with thicker forearm.

Regarding the first point, taking into account the width of the human wrist [72] and some space for the spherical joints, the radius of MP is increased from previous 40 mm to 55 mm. Through the analysis, some candidates of design parameters, such as the radius of the BP and the initial distance between BP and MP, can be obtained. In addition, the actuators of the prismatic joints are replaced by an Actuonix P16-100-64-12-P linear electric motor with stroke of 100 mm. About the second point, the width of the human forearm [92] and the space for adding soft materials are also considered. Therefore, the width of the forearm cuff will be increased by 15 mm.

In addition, to improve the performance of the modified prototype, The TI of the robot is calculated, and the results are shown in Figure 4.15. The TI of the modified design for both FE and RUD movements are larger than 0.5 in the full range of the specified ROM, which indicates that the modified design has a good performance, and it is expected to improve the movements and ROM of the robot.

4.4 Summary

A wearable parallel-serial hybrid robot for wrist and forearm rehabilitation with novel RRPP and RRRR mechanisms for joint misalignment compensation to improve the comfort and safety of the user is proposed. The robot is lightweight and portable, which is suitable for in-home rehabilitation. In addition, the robot ROM of the FE, RUD and PS movements are evaluated. It is shown that the proposed robot meets the requirement of rehabilitation of the wrist and forearm.

An experimental investigation to evaluate the effectiveness of the proposed design is done. Due to the size of some parts of the robot are designed too small such as the radius of MP and the forearm cuff, there exists contact between the human and the robot, causing obstacles in the movement. The ROM of the RUD and PS movements are smaller than expected. Moreover, through questionnaire surveys, the comfortability of the proposed robot is evaluated. The usability of the proposed robot is acceptable, however, some robot parts are designed too small as mentioned, which indeed cause discomfort to the user.

Based on user feedback, an improved version of the design is proposed to solve the problem of obstacles caused by robot contact with the human. In addition, the performance (TI) of the robot is evaluated and it is expected to improve the movements and ROM of the robot. With the features of lightweight, portable and safer design, the proposed wearable robot is expected to be suitable for in-home rehabilitation.

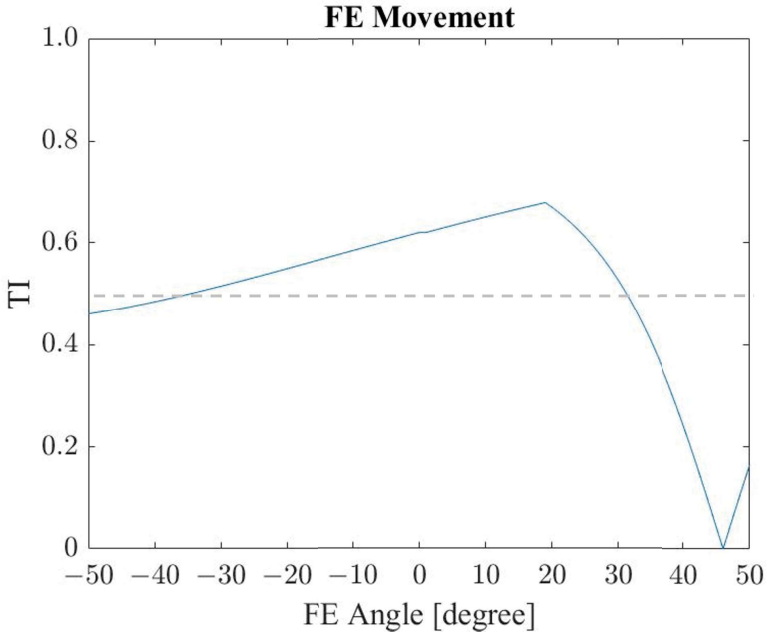

(a) Transmission Index of the original design of FE movement

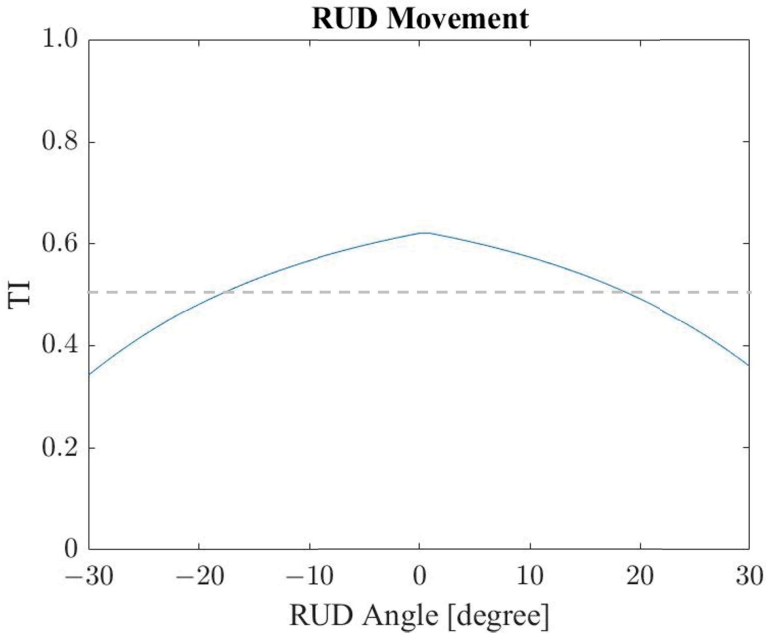

(b) Transmission Index of the original design of RUD movement

Figure 4.14: Transmission Index (TI) of the original design

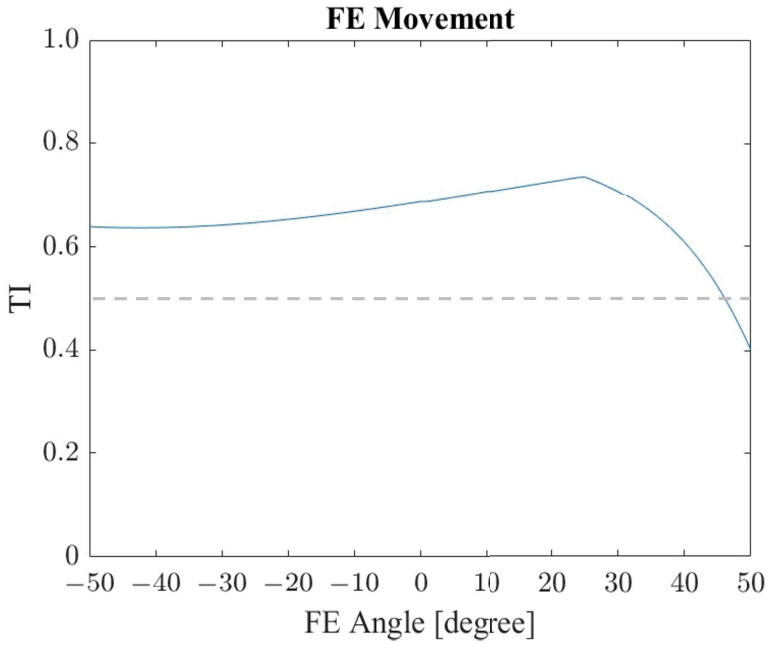

(a) Transmission Index of the modified design of FE movement

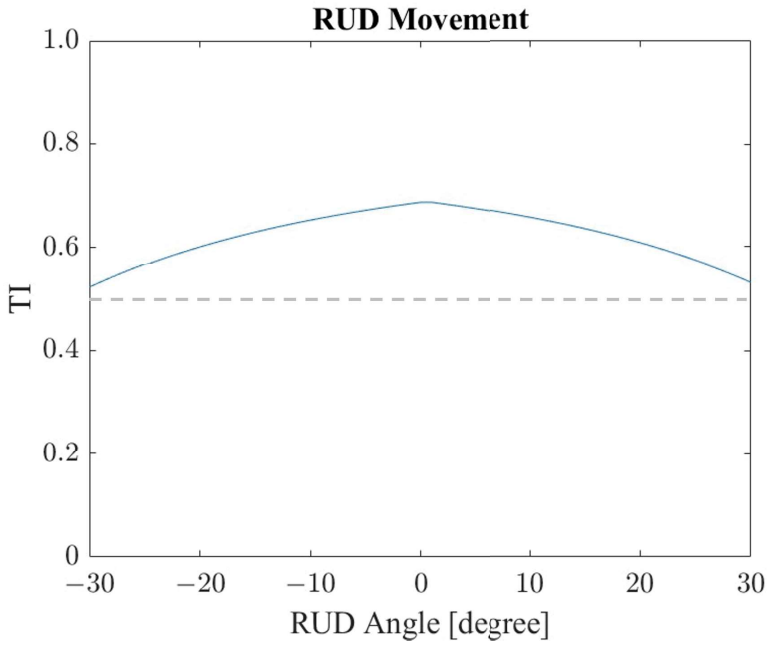

(b) Transmission Index of the modified design of RUD movement

Figure 4.15: Transmission Index (TI) of the modified design

Chapter 5

Conclusions

5.1 Conclusions

This dissertation focuses on kineto-static analysis and design of a wearable hybrid robot for wrist and forearm rehabilitation. The design requirements of the proposed robot are not only to achieve the required rehabilitation functions, but also to improve the safety and comfort of users. To achieve this goal, a design methodology that integrates the human and the robot as a whole system in the design process is proposed. Designer can follow the proposed design methodology to analyze both the human and the robot together and obtain a better design consideration of reduced interaction forces/torques between the human and robot. The proposed wearable hybrid robot is developed based on the design methodology and an experimental study is conducted to evaluate its performance and comfortability.

The requirement and challenges for current wearable rehabilitation robots is established through literature review presented in Chapter 1. To address these difficulties and needs, the design methodology is presented. This design methodology considers the effect of human limb with the robot at the early stage of design, and can achieve a

design with improved safety and comfort. In Chapter 2, starting from a simple planar 1-DOF wrist rehabilitation robot, kineto-static analysis of the robot is conducted. The effects of the initial offset and the use of compliant components are investigated. From the results of the analysis, the initial offsets along the lateral direction increase the force applied to the human body, so special attention should be paid to reducing it. From perspective of safety, allowable range of the offsets are proposed based on the human pain threshold. With the offsets less than the proposed value, the safety of the user can be ensured when using the wearable rehabilitation robot. In addition, the use of compliant elements with less stiffness can reduce the force applied to the human body. Then for joint misalignment compensation, the addition of passive joints is applied to form a RRRR four-bar linkage for wrist rehabilitation. Also, the utilization of soft nature of human tissues, and modeling human soft tissues as added passive joints for misalignment compensation is investigated. Through kineto-static analysis, the results show that regarding the soft and deformable characteristics of human tissue as a passive joint can compensate joint misalignment. Furthermore, the compact design of the robot which applies modeling soft human tissues as a passive joint is proposed. The robot has desirable features of lightweight which reduced the added passive joints and the ability for misalignment compensation. Moreover, the deformations of human soft tissues with nonlinear stiffness behavior and deformations in 2 translations and 1 rotation are addressed. Through the simulation results, the ROM may reduce due to the effect of human tissues and it should not be ignored in the design.

In Chapter 3, the lower-mobility parallel robots have some appealing features for rehabilitation, therefore, in order to support more wrist rehabilitation movements, the 3-R$\underline{P}$S parallel robot is designed

as a wrist rehabilitation robot. The parasitic motions of the 3-R$\underline{P}$S are analyzed and the effects of parasitic motion and initial offsets are investigated. Through the analysis results and with consideration of safety and comfort of the users, an optimization for the design of the 3-R$\underline{P}$S parallel rehabilitation robot is performed. The proposed design has reduced forces/torques applied to the human limb, which can improve the safety and comfort of the user.

In Chapter 4, a wearable parallel-serial hybrid robot for wrist and forearm rehabilitation is proposed. The robot can perform the FE and RUD movements of the wrist and the PS movement of the forearm. For the FE and RUD movement, based on the results obtained from Chapter 3, the 3-R$\underline{P}$S is proposed with the consideration of reducing applied forces/torques to the human limb. Furthermore, based on the investigation of misalignment compensation from Chapter 2, the novel RRPP and RRRR mechanisms are applied for joint misalignment compensation to improve the comfort and safety of the user. By applying the proposed design methodology, the robot has improved safety and comfort. In addition, it is lightweight and portable due to most of the parts are manufactured by 3D printing in onyx material reinforced with carbon fiber, therefore the robot is suitable for in-home rehabilitation. Moreover, an experimental study to evaluate the robot's performance by using motion capture system and assess comfortability by questionnaires. The results of the experimental study show that the proposed design methodology is effectiveness for designing and the usability of the proposed robot is acceptable. However, some modifications of proposed robot are needed to improve the ROM and comfort of the use. In addition, based on the feedback of the subjects, the improved version of the design is proposed to solve some problems reflected by the subjects. Furthermore, the TI of the modified design is

evaluated, and it shows that the performance of the modified design is improved. With the features of lightweight, portable and safer design, the proposed wearable robot is expected to be suitable for in-home rehabilitation.

5.2 Future Work

Some related research topics are not included in this research but are still important and interesting. They are address below:

This methodology can not only apply to the cases described in this dissertation, but also can be applied to other wearable rehabilitation robots.

The optimal design is based on minimum applied forces/torques, however, the acceptable limit of human tolerance of force and torque should be carefully investigated to avoid harmful effects on the users. Therefore, it is necessary to conduct experiments to obtain human tolerance through measurement to ensure that the users are under a comfortable and safe condition when using the wearable robot.

The design methodology should include more design needs, not only considering functionality and safety, but also lightweight, low cost, easy to put on and take off, weight balance, and other needs should be taken into account.

To improve our proposed wearable rehabilitation robot, more comprehensive testing should be conducted. Also, for the subject, not just for healthy subject, but also the therapists and patients should participate the testing and to give more comprehensive feedback.

Appendix A

Questionnaires

A.1 Questionnaires for Experimental Study

A.2 Measurement Results for Experimental Study

"Experimental Study of a Wearable Robot for Wrist and Forearm Rehabilitation"
Questionnaire

Mechanical Systems Design Laboratory,
Mechanical Engineering Department,
Tokyo Institute of Technology
Principal Investigator: Prof. Yukio Takeda
Representative Researcher: Ying-Chi Liu

Thank you for participating in the experiment today. We appreciate your participation and contribution to the research. For better understand any improvement of the experiment, please fill the questionnaire below. Thank you again for your cooperation in this research.

Points of concern:

- The results of the questionnaire may be published at academic conferences, journal articles, and the laboratory website.
- The data is anonymized, and no personal information can be released.

If you disagree the points of concern above, you do not need to answer the following questions.

Questionnaire:
This is a standard questionnaire that measures the overall usability of a system. Please select the answer that best expresses how you feel about each statement after using the rehabilitation robotic system today.

	Strongly Disagree	Somewhat Disagree	Neutral	Somewhat Agree	Strongly Agree
1. I think I would like to use this rehabilitation robot frequently.	☐	☐	☐	☐	☐
2. I think the rehabilitation robot is complex and difficult to use.	☐	☐	☐	☐	☐
3. I think the rehabilitation robot is easy to use.	☐	☐	☐	☐	☐
4. I think that I would need the technical assistance to be able to use this rehabilitation robot.	☐	☐	☐	☐	☐
5. I think the various functions in this rehabilitation robot are well integrated.	☐	☐	☐	☐	☐
6. I think the functionality of this rehabilitation robot are not organized.	☐	☐	☐	☐	☐
7. I would imagine that most people would learn to use this rehabilitation robot very quickly.	☐	☐	☐	☐	☐
8. I think most of users will have difficulties to learn how to use the rehabilitation robot.	☐	☐	☐	☐	☐
9. I felt very confident when using the rehabilitation robot.	☐	☐	☐	☐	☐
10. I may need to learn a lot of things before I am able to use this rehabilitation robot.	☐	☐	☐	☐	☐

Figure A.1: First page of the questionnaire. (English Version)

11. Did you experience any discomfort or pain when wearing the robot before rehabilitation process?
☐Yes ☐No
If yes, please specify the area where you felt discomfort or pain.
_____

12. Did you experience any discomfort or pain during rehabilitation process?
☐Yes ☐No
If yes, please specify the area where you felt discomfort or pain.
_____

13. Did you experience any discomfort or pain after rehabilitation process?
☐Yes ☐No
If yes, please specify the area where you felt discomfort or pain.
_____

14. During the rehabilitation process, did you encounter any fear of the danger caused by the robot?
☐Yes ☐No
If yes, please describe the reason.
_____

15. What do you think the weight of the robot?
☐Light ☐Normal ☐Heavy

16. Do you find any limitation of the robot?
☐Yes ☐No
If yes, please describe the limitation.
_____

17. Would you recommend the robot to other patients who need rehabilitation?
☐Yes ☐No

18. Please write down your opinion for the robot and the experiment.

Thank you very much for taking the time to answer the questionnaire.

Figure A.2: Second page of the questionnaire. (English Version)

「手首・前腕のリハビリテーション用ウェアラブルロボットの実験的研究」
アンケート

東京工業大学　工学院　機械系
武田・菅原研究室
研究責任者:武田行生 教授
研究担当者: Liu Ying-Chi

本日の実験にご参加いただきまして、誠にありがとうございました。本研究へのご参加とご貢献に感謝を申し上げます。つきましては、本実験の改善点を把握するため、以下のアンケートにご協力いただきますようお願い申し上げます。改めて，ご協力に感謝申し上げます。

留意事項:

- アンケート結果は、学術講演会、雑誌論文、研究室ホームページなどで公表することがあります。
- データは匿名化され、個人情報が公開されることはありません。

上記留意事項にご了承いただけない場合、当アンケートにご回答いただく必要はございません。

アンケート:
このアンケートは今日使用いただいたリハビリ用ロボットシステムの総合的な使い勝手を測るアンケートです。今日、このシステムを使用した後に感じたことに基づいて、以下の質問について最も適切な答えを選んでください。

	全くそう思わない	そう思わない	どちらでもない	そう思う	全くそう思う
1. このリハビリ用ロボットはよく使いたいと思う。	□	□	□	□	□
2. このリハビリ用ロボットは複雑で使い難いと思う。	□	□	□	□	□
3. このリハビリ用ロボットは使いやすいと思う。	□	□	□	□	□
4. このリハビリ用ロボットを使えるようになるには、技術的な支援が必要だと思う。	□	□	□	□	□
5. このリハビリ用ロボットは、さまざまな機能がうまく統合されていると思う。	□	□	□	□	□
6. このリハビリ用ロボットの機能はうまく統合されていないと思う。	□	□	□	□	□
7. このリハビリ用ロボットは、ほとんどの人がすぐに使いこなせるようになると思う。	□	□	□	□	□
8. このリハビリ用ロボットの使い方を覚えるには、ほとんどのユーザーが苦労するのではないかと思う。	□	□	□	□	□
9. このリハビリ用ロボットを使う自信がある。	□	□	□	□	□
10. このリハビリ用ロボットを使いこなすには、いろいろな勉強が必要と思う。	□	□	□	□	□

Figure A.3: First page of the questionnaire. (Japanese Version)

11. リハビリ運動を始める前にロボットを装着した際に、不快感や痛みはありましたか？
□はい □いいえ
「はい」の場合、不快感や痛みを感じた部位を具体的にお教えください。

12. リハビリ運動を行っている間に、不快感や痛みはありましたか？
□はい □いいえ
「はい」の場合、不快感や痛みを感じた部位を具体的にお教えください。

13. リハビリ運動を行った後、不快感や痛みはありましたか？
□はい □いいえ
「はい」の場合、不快感や痛みを感じた部位を具体的にお教えください。

14. リハビリ運動の間、ロボットによる恐怖や危険を感じましたか？
□はい □いいえ
「はい」の場合、その理由をお教えください。

15. ロボットの重さをどのように感じましたか？
□軽い □普通 □重い

16. ロボットに何らかの限界を感じましたか？
□はい □いいえ
「はい」の場合、その内容をご説明ください。

17. リハビリを必要とする他の患者さんにもこのロボットを勧めたいですか？
□はい □いいえ

18. その他、お気づきの点について、自由にご記入ください。

ご協力をいただきまして誠にありがとうございました。

Figure A.4: Second page of the questionnaire. (Japanese Version)

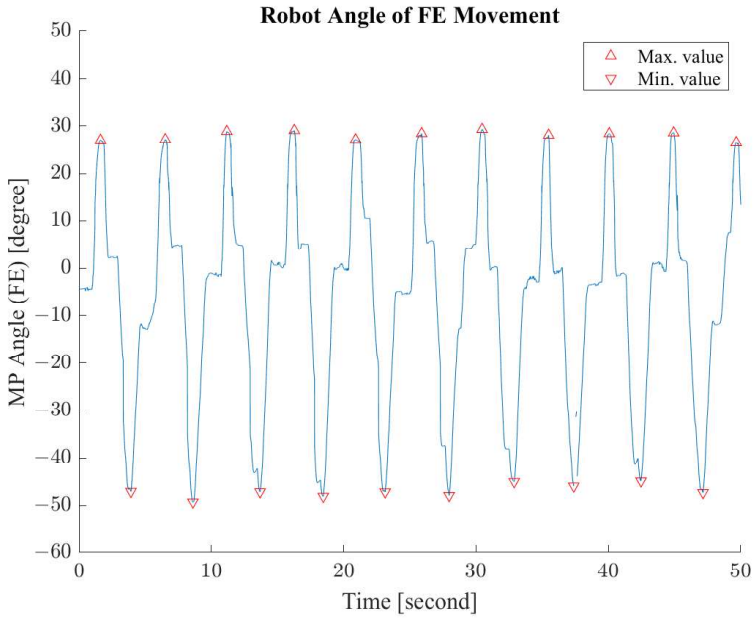

(a) Robot angle of FE movement

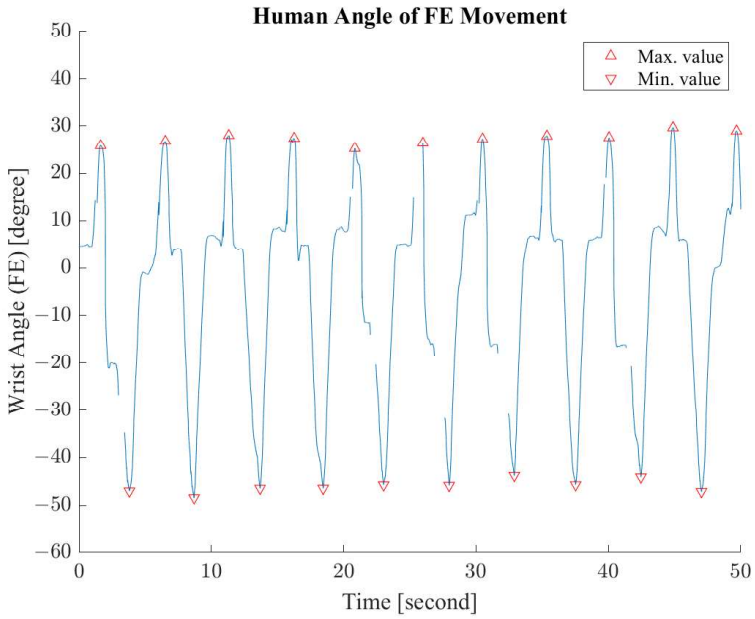

(b) Human angle of FE movement

Figure A.5: Experimental results of FE movement (Subject 2)

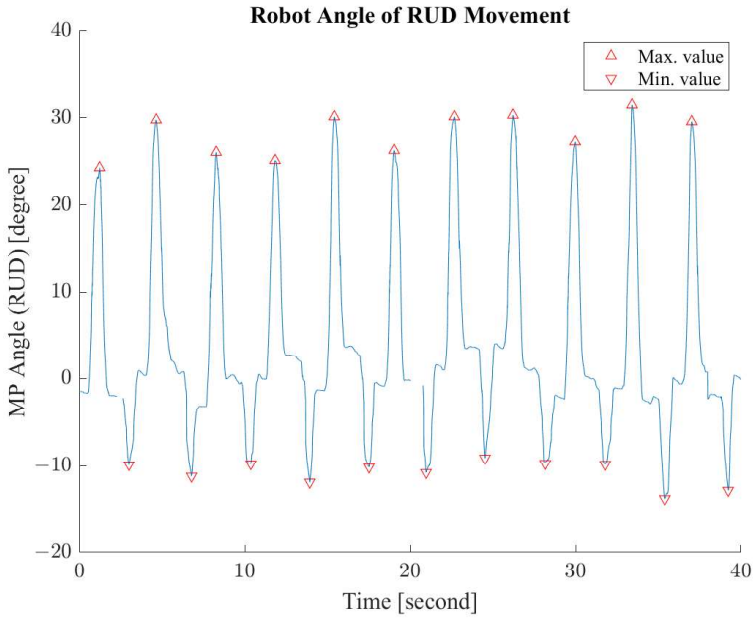

(a) Robot angle of RUD movement

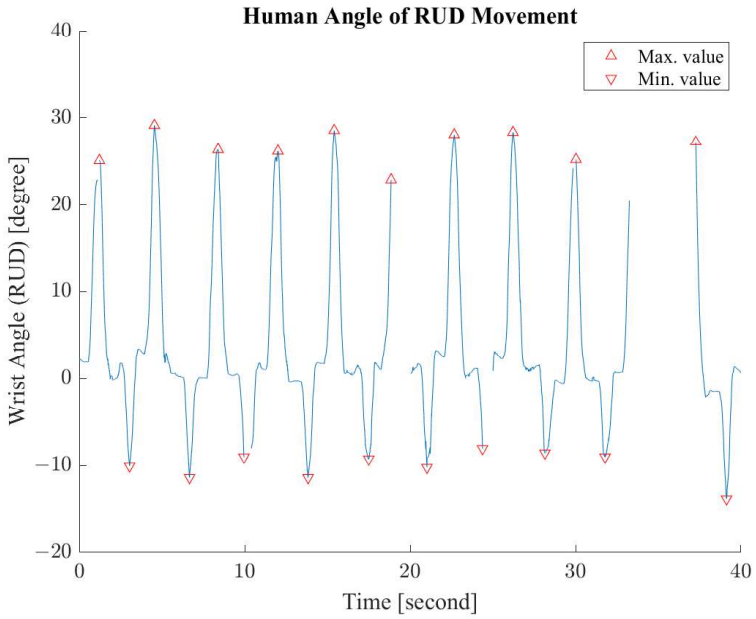

(b) Human angle of RUD movement

Figure A.6: Experimental results of RUD movement (Subject 2)

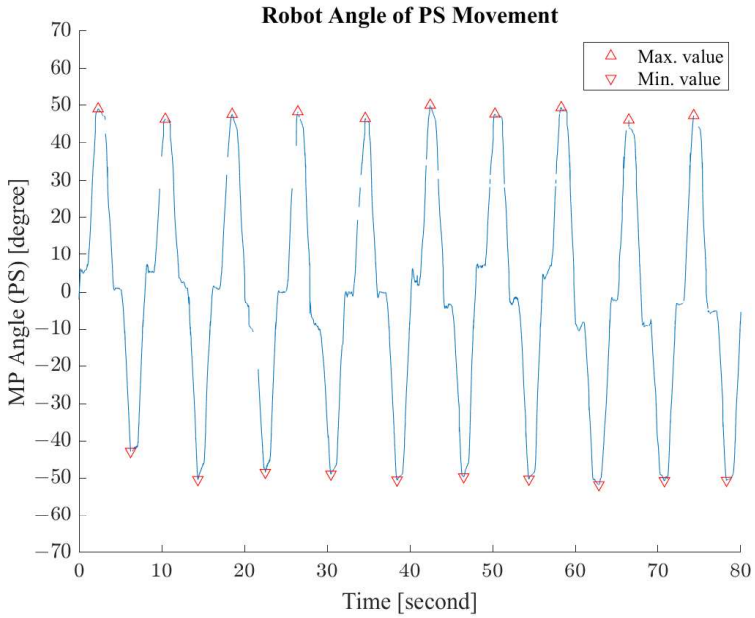

(a) Robot angle of PS movement

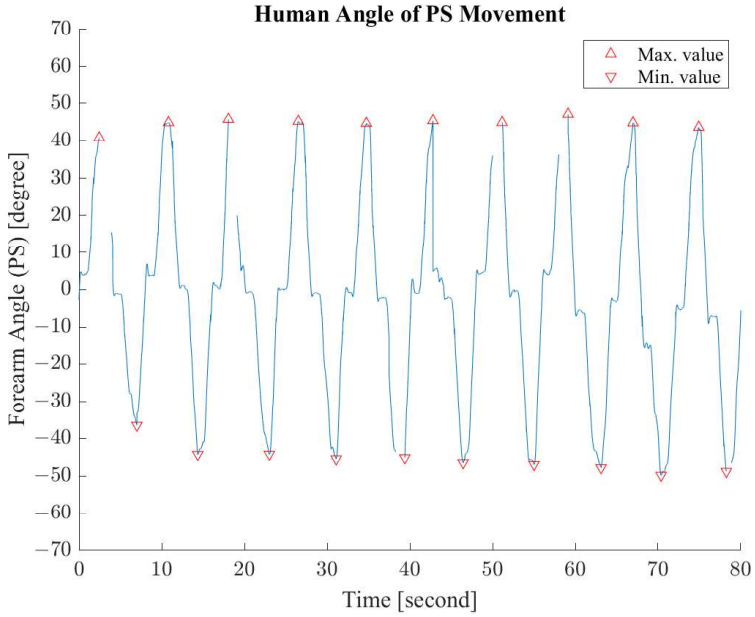

(b) Human angle of PS movement

Figure A.7: Experimental results of PS movement (Subject 2)

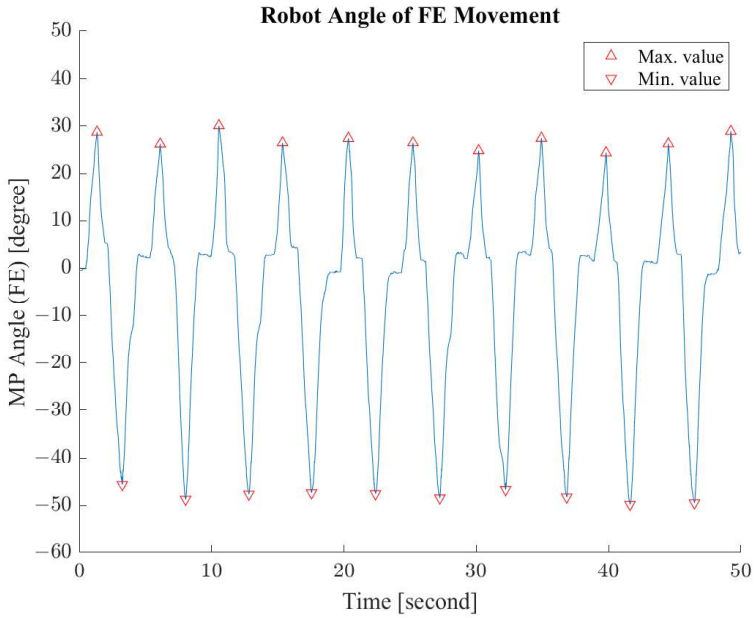

(a) Robot angle of FE movement

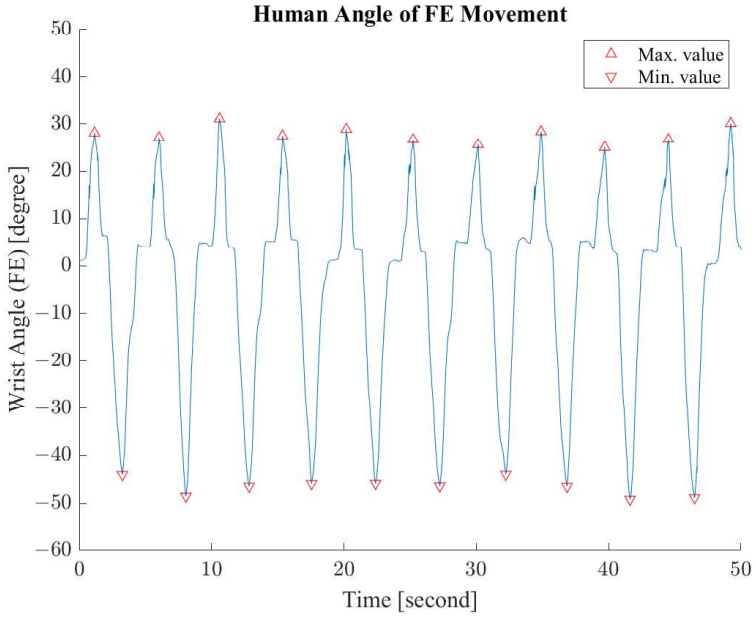

(b) Human angle of FE movement

Figure A.8: Experimental results of FE movement (Subject 3)

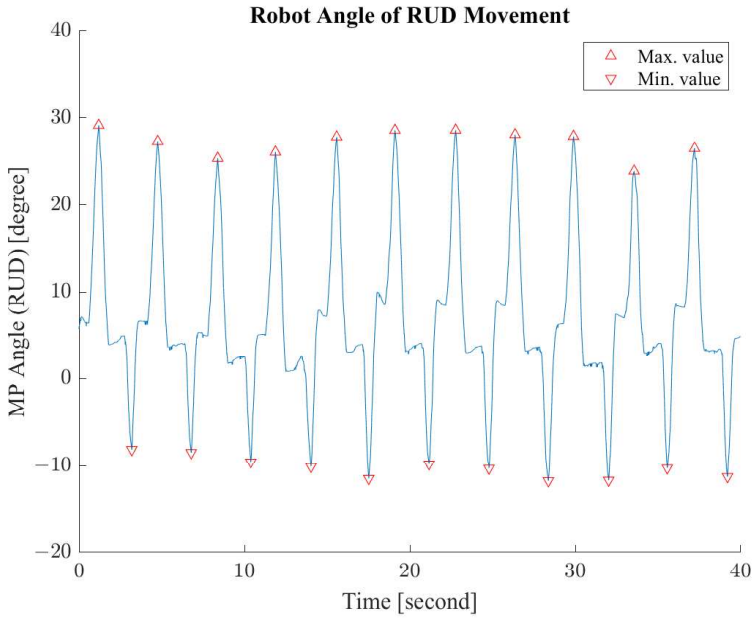

(a) Robot angle of RUD movement

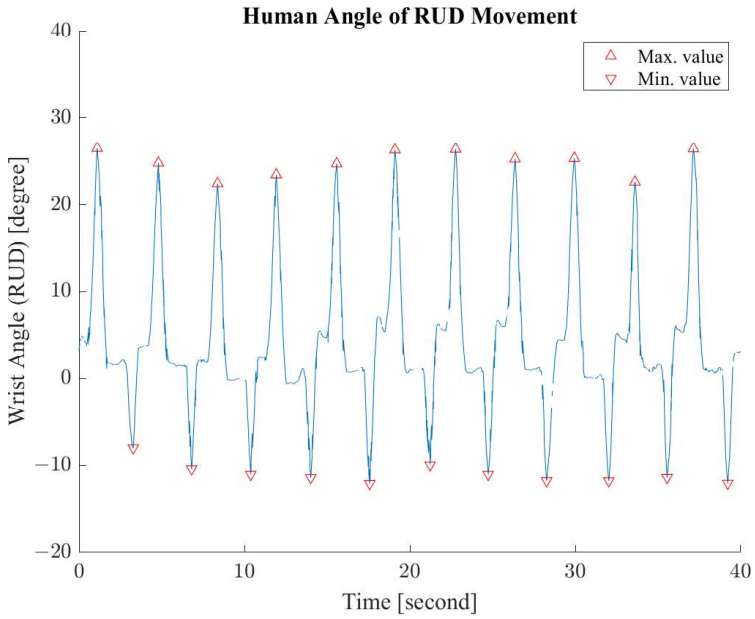

(b) Human angle of RUD movement

Figure A.9: Experimental results of RUD movement (Subject 3)

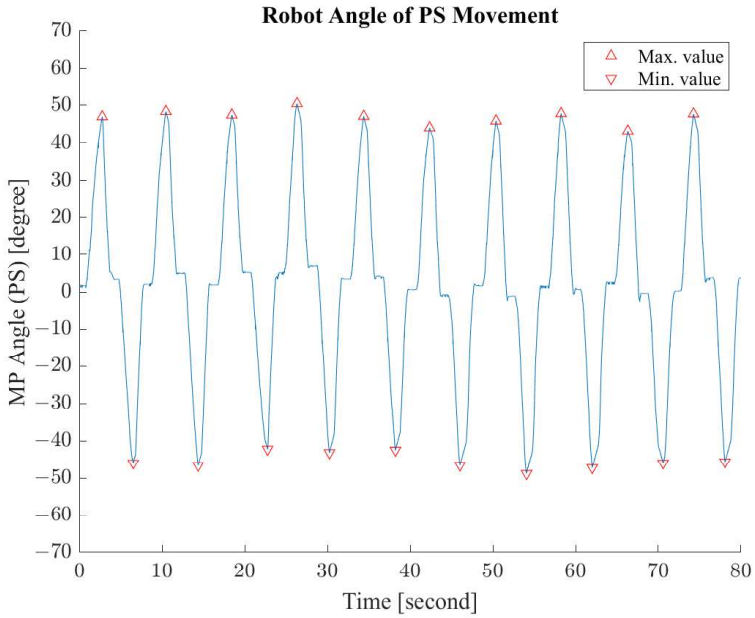

(a) Robot angle of PS movement

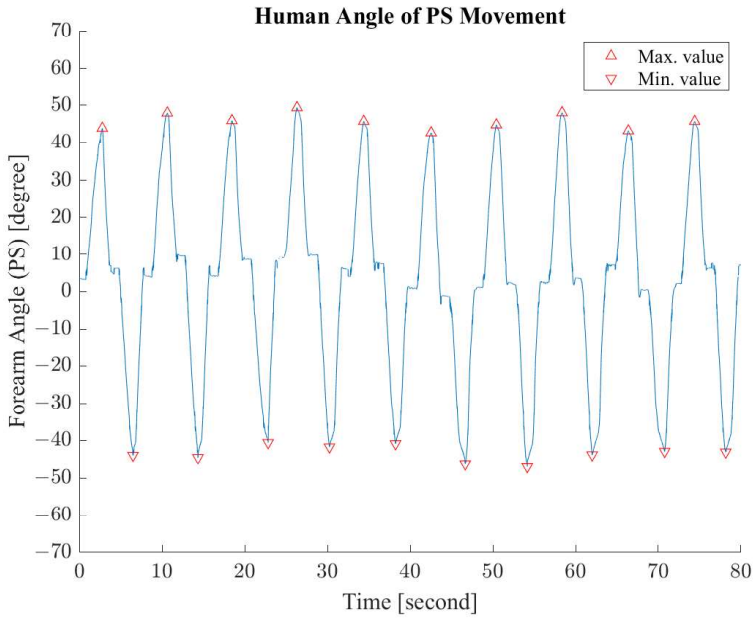

(b) Human angle of PS movement

Figure A.10: Experimental results of PS movement (Subject 3)

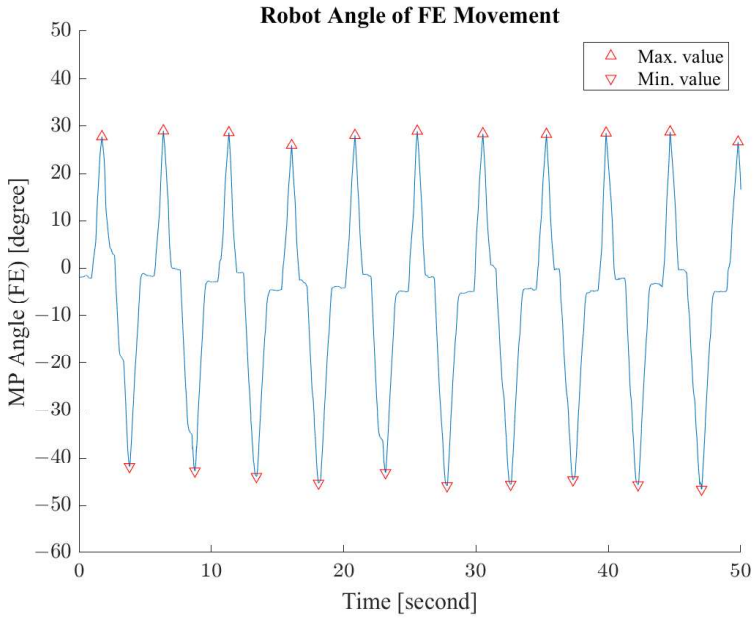

(a) Robot angle of FE movement

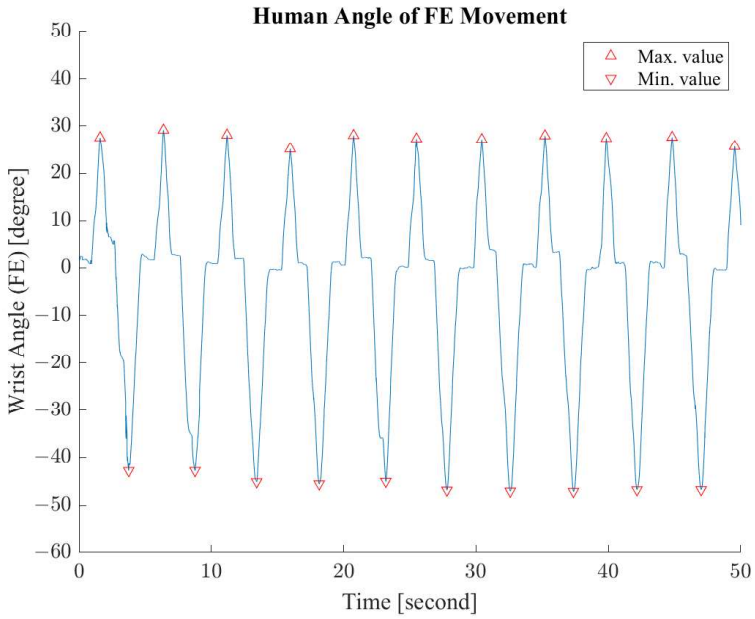

(b) Human angle of FE movement

Figure A.11: Experimental results of FE movement (Subject 4)

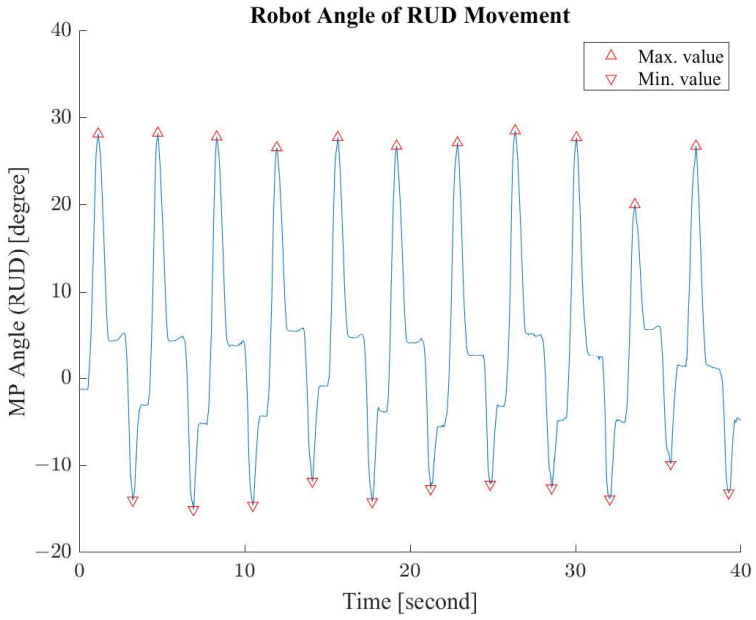

(a) Robot angle of RUD movement

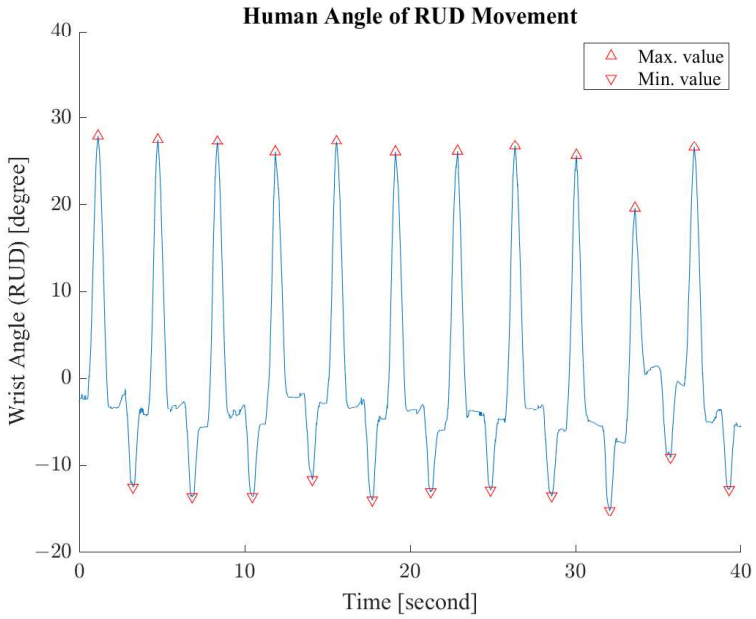

(b) Human angle of RUD movement

Figure A.12: Experimental results of RUD movement (Subject 4)

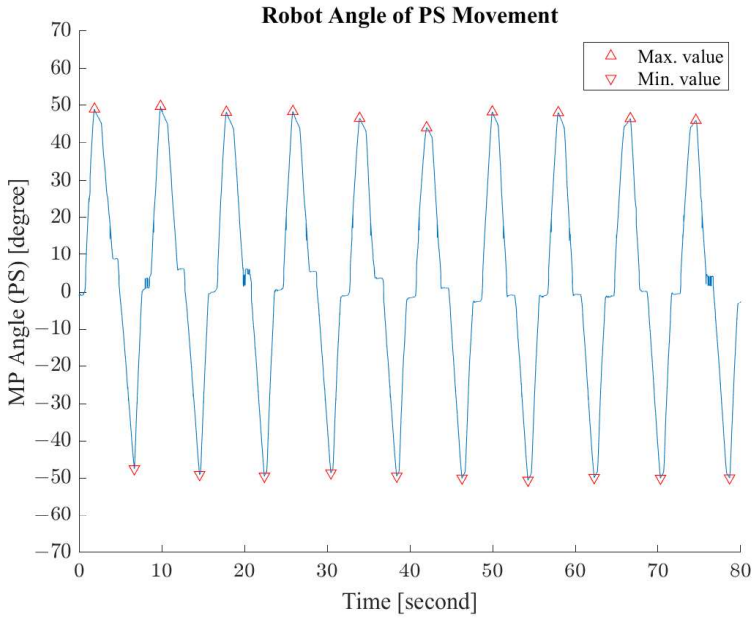

(a) Robot angle of PS movement

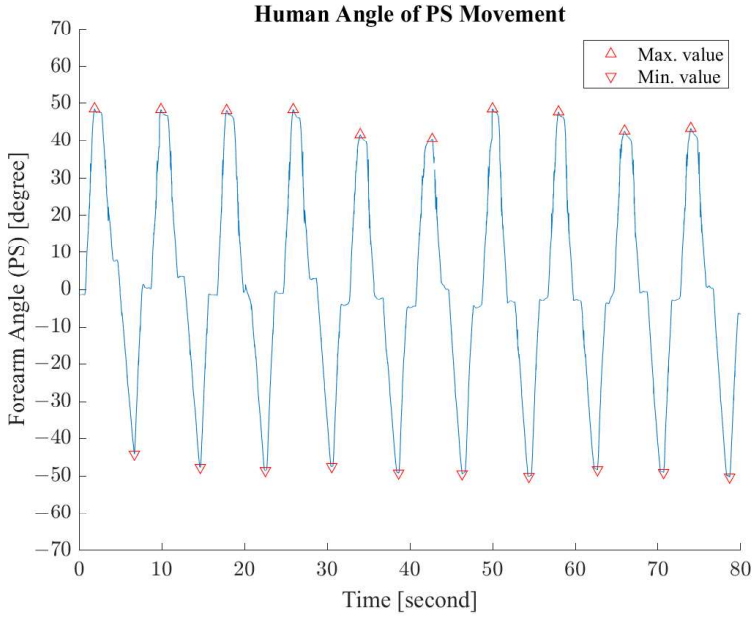

(b) Human angle of PS movement

Figure A.13: Experimental results of PS movement (Subject 4)

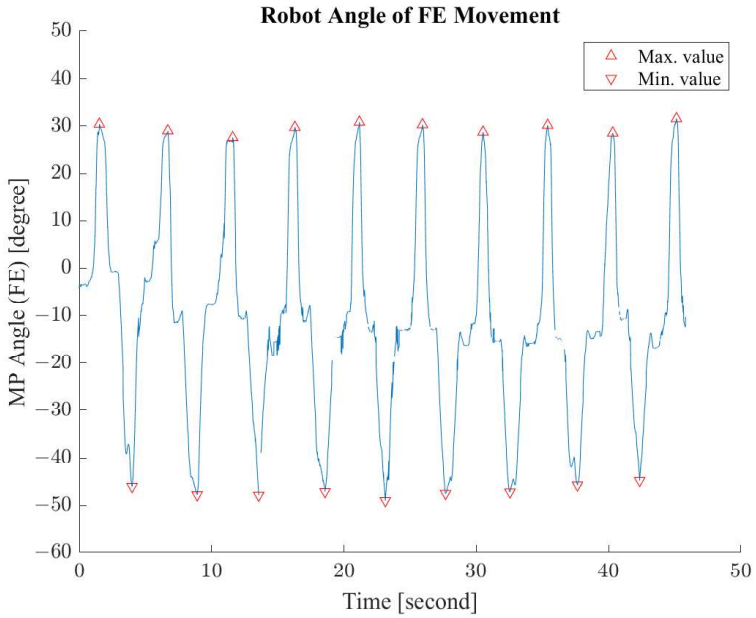

(a) Robot angle of FE movement

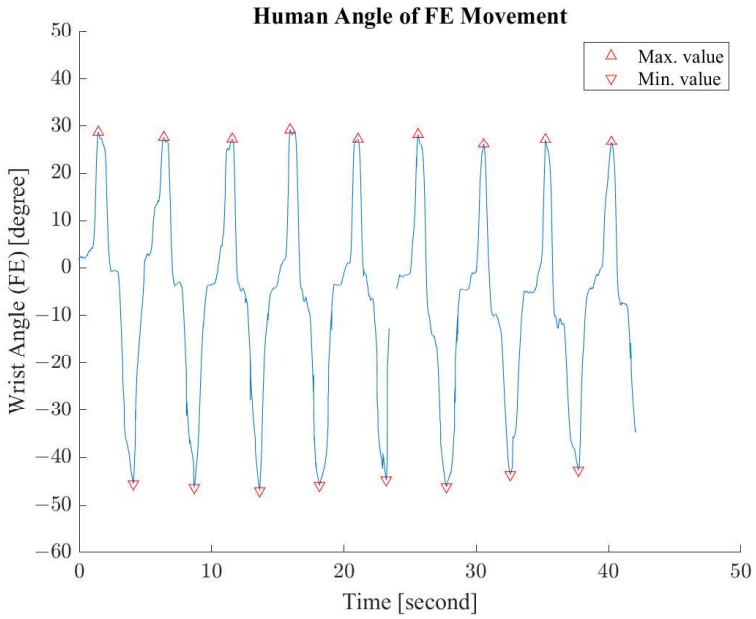

(b) Human angle of FE movement

Figure A.14: Experimental results of FE movement (Subject 5)

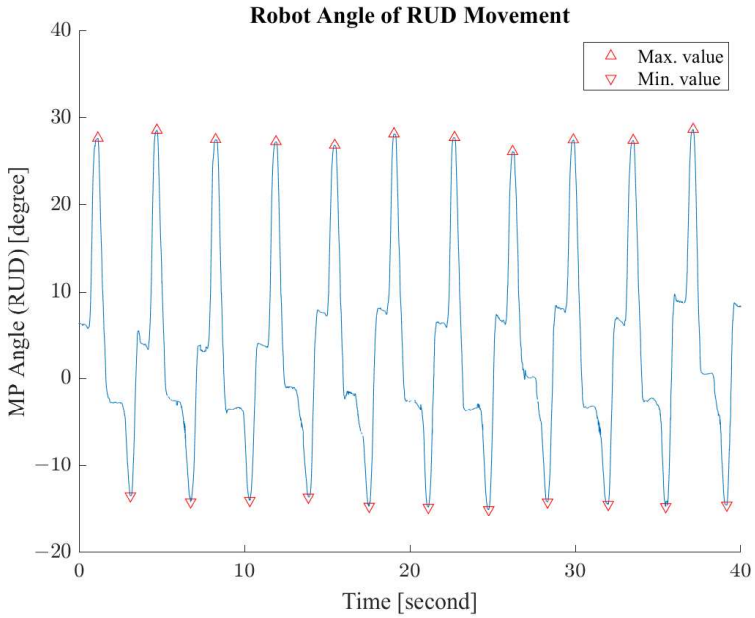

(a) Robot angle of RUD movement

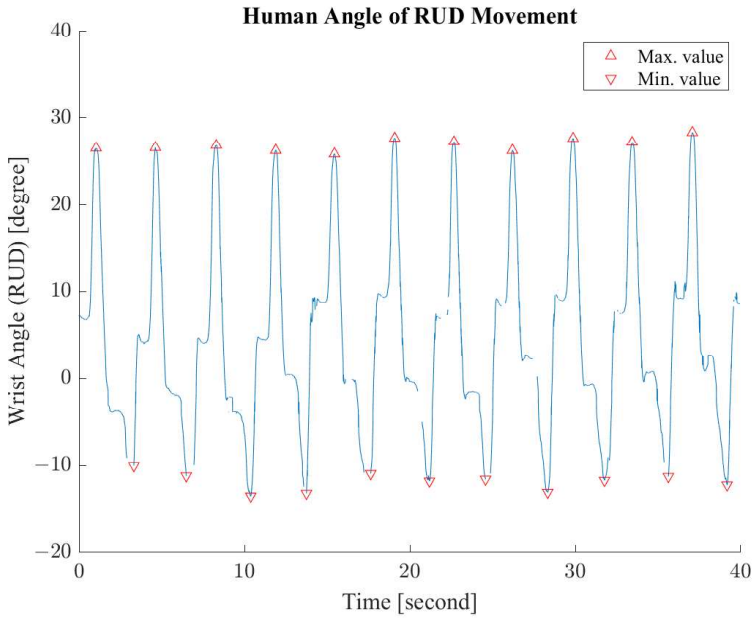

(b) Human angle of RUD movement

Figure A.15: Experimental results of RUD movement (Subject 5)

References

[1] Tai, S.-Y., Cheon, S., Yamaoka, Y., Chien, Y.-W., and Lu, T.-H., 2022. "Changes in the rankings of leading causes of death in japan, korea, and taiwan from 1998 to 2018: a comparison of three ranking lists". *BMC Public Health,* **22**(1), may.

[2] Virani, S. S., Alonso, A., Aparicio, H. J., Benjamin, E. J., Bittencourt, M. S., Callaway, C. W., Carson, A. P., Chamberlain, A. M., Cheng, S., Delling, F. N., Elkind, M. S., Evenson, K. R., Ferguson, J. F., Gupta, D. K., Khan, S. S., Kissela, B. M., Knutson, K. L., Lee, C. D., Lewis, T. T., Liu, J., Loop, M. S., Lutsey, P. L., Ma, J., Mackey, J., Martin, S. S., Matchar, D. B., Mussolino, M. E., Navaneethan, S. D., Perak, A. M., Roth, G. A., Samad, Z., Satou, G. M., Schroeder, E. B., Shah, S. H., Shay, C. M., Stokes, A., VanWagner, L. B., Wang, N.-Y., and and, C. W. T., 2021. "Heart disease and stroke statistics—2021 update". *Circulation,* **143**(8), feb.

[3] Duncan, P. W., Goldstein, L. B., Matchar, D., Divine, G. W., and Feussner, J., 1992. "Measurement of motor recovery after stroke. outcome assessment and sample size requirements.". *Stroke,* **23**(8), aug, pp. 1084–1089.

[4] Wade, D. T., Langton-Hewer, R., Wood, V. A., Skilbeck, C. E., and Ismail, H. M., 1983. "The hemiplegic arm after stroke: mea-

surement and recovery.". *Journal of Neurology, Neurosurgery Psychiatry,* **46**(6), jun, pp. 521–524.

[5] Kwakkel, G., Wagenaar, R. C., Koelman, T. W., Lankhorst, G. J., and Koetsier, J. C., 1997. "Effects of intensity of rehabilitation after stroke". *Stroke,* **28**(8), aug, pp. 1550–1556.

[6] Kwakkel, G., Kollen, B. J., and Wagenaar, R. C., 2002. "Long term effects of intensity of upper and lower limb training after stroke: a randomised trial". *Journal of Neurology, Neurosurgery Psychiatry,* **72**(4), pp. 473–479.

[7] Bütefisch, C., Hummelsheim, H., Denzler, P., and Mauritz, K.-H., 1995. "Repetitive training of isolated movements improves the outcome of motor rehabilitation of the centrally paretic hand". *Journal of the Neurological Sciences,* **130**(1), may, pp. 59–68.

[8] Oujamaa, L., Relave, I., Froger, J., Mottet, D., and Pelissier, J.-Y., 2009. "Rehabilitation of arm function after stroke. literature review". *Annals of Physical and Rehabilitation Medicine,* **52**(3), apr, pp. 269–293.

[9] Calautti, C., and Baron, J.-C., 2003. "Functional neuroimaging studies of motor recovery after stroke in adults". *Stroke,* **34**(6), jun, pp. 1553–1566.

[10] Zimbelman, J., Juraschek, S., Zhang, X., and Lin, N., 2010. "Physical therapy workforce in the united states: Forecasting nationwide shortages". *PM&R: the journal of injury, function, and rehabilitation,* **2**(11), 11, pp. 1021–1029.

[11] Poli, P., Morone, G., Rosati, G., and Masiero, S., 2013. "Robotic technologies and rehabilitation: New tools for stroke patients' therapy". *BioMed Research International,* **2013**, pp. 1–8.

[12] Garcia, D., Arredondo, R., Morris, M., and Tosunoglu, S., 2012. "A review of rehabilitation strategies for stroke recovery". *ASME Early Career Technical Journal,* **11**, 11, pp. 24–31.

[13] Fazekas, G., and Tavaszi, I., 2019. "The future role of robots in neuro-rehabilitation". *Expert Review of Neurotherapeutics,* **19**(6), may, pp. 471–473.

[14] Manjunatha, H., Pareek, S., Jujjavarapu, S. S., Ghobadi, M., Kesavadas, T., and Esfahani, E. T., 2021. "Upper limb home-based robotic rehabilitation during COVID-19 outbreak". *Frontiers in Robotics and AI,* **8**, may.

[15] Qassim, H. M., and Hasan, W. Z. W., 2020. "A review on upper limb rehabilitation robots". *Applied Sciences,* **10**(19), oct, p. 6976.

[16] Gull, M. A., Bai, S., and Bak, T., 2020. "A review on design of upper limb exoskeletons". *Robotics,* **9**(1), mar, p. 16.

[17] Babaiasl, M., Mahdioun, S. H., Jaryani, P., and Yazdani, M., 2015. "A review of technological and clinical aspects of robot-aided rehabilitation of upper-extremity after stroke". *Disability and Rehabilitation: Assistive Technology*, jan, pp. 1–18.

[18] Norouzi-Gheidari, N., Archambault, P. S., and Fung, J., 2012. "Effects of robot-assisted therapy on stroke rehabilitation in upper limbs: Systematic review and meta-analysis of the literature". *The Journal of Rehabilitation Research and Development,* **49**(4), p. 479.

[19] Pereira, M. F., Prahm, C., Kolbenschlag, J., Oliveira, E., and Rodrigues, N. F., 2020. "Application of AR and VR in hand rehabilitation: A systematic review". *Journal of Biomedical Informatics,* **111**, nov, p. 103584.

[20] Faria, A. L., Andrade, A., Soares, L., and i Badia, S. B., 2016. "Benefits of virtual reality based cognitive rehabilitation through simulated activities of daily living: a randomized controlled trial with stroke patients". *Journal of NeuroEngineering and Rehabilitation,* **13**(1), nov.

[21] Maciejasz, P., Eschweiler, J., Gerlach-Hahn, K., Jansen-Troy, A., and Leonhardt, S., 2014. "A survey on robotic devices for upper limb rehabilitation". *Journal of NeuroEngineering and Rehabilitation,* **11**(1), jan.

[22] Shaw, L., Rodgers, H., Price, C., van Wijck, F., Shackley, P., Steen, N., Barnes, M., Ford, G., and Graham, L., 2010. "BoTULS: a multicentre randomised controlled trial to evaluate the clinical effectiveness and cost-effectiveness of treating upper limb spasticity due to stroke with botulinum toxin type a". *Health Technology Assessment,* **14**(26), may.

[23] Lo, H. S., and Xie, S. Q., 2012. "Exoskeleton robots for upper-limb rehabilitation: State of the art and future prospects". *Medical Engineering & Physics,* **34**(3), apr, pp. 261–268.

[24] Krebs, H., Hogan, N., Aisen, M., and Volpe, B., 1998. "Robot-aided neurorehabilitation". *IEEE Transactions on Rehabilitation Engineering,* **6**(1), mar, pp. 75–87.

[25] Krebs, H., Ferraro, M., Buerger, S. P., Newbery, M. J., Makiyama, A., Sandmann, M., Lynch, D., Volpe, B. T., and Hogan, N., 2004. "Rehabilitation robotics: pilot trial of a spatial extension for mit-manus". *Journal of NeuroEngineering and Rehabilitation,* **1**(1), p. 5.

[26] Lum, P. S., Burgar, C. G., Shor, P. C., Majmundar, M., and der Loos, M. V., 2002. "Robot-assisted movement training compared with conventional therapy techniques for the rehabilitation of upper-limb motor function after stroke". *Archives of Physical Medicine and Rehabilitation,* **83**(7), jul, pp. 952–959.

[27] Lum, P. S., Burgar, C. G., der Loos, M. V., Shor, P. C., Majmundar, M., and Yap, R., 2006. "MIME robotic device for upper-limb neurorehabilitation in subacute stroke subjects: A follow-up study". *The Journal of Rehabilitation Research and Development,* **43**(5), p. 631.

[28] Loureiro, R., Amirabdollahian, F., Topping, M., Driessen, B., and Harwin, W., 2003. "Upper limb robot mediated stroke therapy gentle/s approach". *Autonomous Robots,* **15**(1), pp. 35–51.

[29] Hesse, S., Schulte-Tigges, G., Konrad, M., Bardeleben, A., and Werner, C., 2003. "Robot-assisted arm trainer for the passive and active practice of bilateral forearm and wrist movements in hemiparetic subjects11an organization with which 1 or more of the authors is associated has received or will receive financial benefits from a commercial party having a direct financial interest in the results of the research supporting this article.". *Archives of Physical Medicine and Rehabilitation,* **84**(6), jun, pp. 915–920.

[30] Toth, A., Fazekas, G., Arz, G., Jurak, M., and Horvath, M., 2005. "Passive robotic movement therapy of the spastic hemiparetic arm with REHAROB: Report of the first clinical test and the followup system improvement". In 9th International Conference on Rehabilitation Robotics, 2005. ICORR 2005., IEEE.

[31] Reinkensmeyer, D. J., Kahn, L. E., Averbuch, M., McKenna-Cole, A., Schmit, B. D., and Rymer, W. Z., 2000. "Understanding and treating arm movement impairment after chronic brain injury: progress with the arm guide.". *Journal of rehabilitation research and development,* **37**, pp. 653–662.

[32] Gupta, A., and O'Malley, M., 2006. "Design of a haptic arm exoskeleton for training and rehabilitation". *IEEE/ASME Transactions on Mechatronics,* **11**(3), jun, pp. 280–289.

[33] French, J., Rose, C., and O' malley, M., 2014. *System Characterization of MAHI Exo-II: A Robotic Exoskeleton for Upper Extremity Rehabilitation.* American Society of Mechanical Engineers, 10, pp. V003T–43A.

[34] Nef, T., Mihelj, M., and Riener, R., 2007. "ARMin: a robot for patient-cooperative arm therapy". *Medical & Biological Engineering & Computing,* **45**(9), aug, pp. 887–900.

[35] Mihelj, M., Nef, T., and Riener, R., 2007. "ARMin II - 7 DoF rehabilitation robot: mechanics and kinematics". In Proceedings 2007 IEEE International Conference on Robotics and Automation, IEEE.

[36] Nef, T., Guidali, M., and Riener, R., 2009. "ARMin III – arm therapy exoskeleton with an ergonomic shoulder actuation". *Applied Bionics and Biomechanics,* **6**(2), jul, pp. 127–142.

[37] Sanchez, R., Liu, J., Rao, S., Shah, P., Smith, R., Rahman, T., Cramer, S., Bobrow, J., and Reinkensmeyer, D., 2006. "Automating arm movement training following severe stroke: Functional exercises with quantitative feedback in a gravity-reduced environment". *IEEE Transactions on Neural Systems and Rehabilitation Engineering,* **14**(3), sep, pp. 378–389.

[38] Stienen, A. H., Hekman, E. E., der Helm, F. C. V., Prange, G. B., Jannink, M. J., Aalsma, A. M., and der Kooij, H. V., 2007. "Dampace: dynamic force-coordination trainer for the upper extremities". In 2007 IEEE 10th International Conference on Rehabilitation Robotics, IEEE.

[39] Balasubramanian, S., Wei, R., Perez, M., Shepard, B., Koeneman, E., Koeneman, J., and He, J., 2008. "RUPERT: An exoskeleton robot for assisting rehabilitation of arm functions". In 2008 Virtual Rehabilitation, IEEE.

[40] Gopura, R. A. R. C., Kiguchi, K., and Li, Y., 2009. "SUEFUL-7: A 7dof upper-limb exoskeleton robot with muscle-model-oriented EMG-based control". In 2009 IEEE/RSJ International Conference on Intelligent Robots and Systems, IEEE.

[41] Frisoli, A., Borelli, L., Montagner, A., Marcheschi, S., Procopio, C., Salsedo, F., Bergamasco, M., Carboncini, M. C., Tolaini, M., and Rossi, B., 2007. "Arm rehabilitation with a robotic exoskeleleton in virtual reality". In 2007 IEEE 10th International Conference on Rehabilitation Robotics, IEEE.

[42] Perry, J. C., Rosen, J., and Burns, S., 2007. "Upper-limb powered exoskeleton design". *IEEE/ASME Transactions on Mechatronics,* **12**(4), aug, pp. 408–417.

[43] Näf, M. B., Junius, K., Rossini, M., Rodriguez-Guerrero, C., Vanderborght, B., and Lefeber, D., 2018. "Misalignment compensation for full human-exoskeleton kinematic compatibility: State of the art and evaluation". *Applied Mechanics Reviews,* **70**(5), sep.

[44] Tucan, P., Gherman, B., Major, K., Vaida, C., Major, Z., Plitea, N., Carbone, G., and Pisla, D., 2020. "Fuzzy logic-based risk assessment of a parallel robot for elbow and wrist rehabilitation". *International Journal of Environmental Research and Public Health,* **17**(2), jan, p. 654.

[45] Scherer, M. J., 1996. "Outcomes of assistive technology use on quality of life". *Disability and Rehabilitation,* **18**(9), jan, pp. 439–448.

[46] Näf, M. B., Koopman, A. S., Baltrusch, S., Rodriguez-Guerrero, C., Vanderborght, B., and Lefeber, D., 2018. "Passive back support exoskeleton improves range of motion using flexible beams". *Frontiers in Robotics and AI,* **5**, jun.

[47] d'Elia, N., Vanetti, F., Cempini, M., Pasquini, G., Parri, A., Rabuffetti, M., Ferrarin, M., Lova, R. M., and Vitiello, N., 2017. "Physical human-robot interaction of an active pelvis orthosis: toward ergonomic assessment of wearable robots". *Journal of NeuroEngineering and Rehabilitation,* **14**(1), apr.

[48] Cai, V. A. D., Bidaud, P., Nguyen, V. T., Granata, C., and Nguyen, M. T., 2016. "Control of a self-adjusting lower limb

exoskeleton for knee assistance". In *ROMANSY 21 - Robot Design, Dynamics and Control*. Springer International Publishing, pp. 385–392.

[49] Beekhuis, J. H., Westerveld, A. J., van der Kooij, H., and Stienen, A. H. A., 2013. "Design of a self-aligning 3-DOF actuated exoskeleton for diagnosis and training of wrist and forearm after stroke". In 2013 IEEE 13th International Conference on Rehabilitation Robotics (ICORR), IEEE.

[50] Matsuura, D., Ishida, S., Koga, T., and Takeda, Y., 2014. "Design of ankle rehabilitation mechanism using a quantitative measure of load reduction". In *Advances on Theory and Practice of Robots and Manipulators*. Springer International Publishing, pp. 27–36.

[51] Szigeti, A., Takeda, Y., and Matsuura, D., 2015. "Portable design and range of motion control for an ankle rehabilitation mechanism capable of adjusting to changes in joint axis". In *Recent Advances in Mechanism Design for Robotics*. Springer International Publishing, pp. 123–132.

[52] Joodaki, H., and Panzer, M. B., 2018. "Skin mechanical properties and modeling: A review". *Proceedings of the Institution of Mechanical Engineers, Part H: Journal of Engineering in Medicine,* **232**(4), mar, pp. 323–343.

[53] Yu, T. F., and Wilson, A. J., 2014. "A passive movement method for parameter estimation of a musculo-skeletal arm model incorporating a modified hill muscle model". *Computer Methods and Programs in Biomedicine,* **114**(3), may, pp. e46–e59.

[54] Rocon, E., Ruiz, A., Pons, J., Belda-Lois, J., and Sanchez-Lacuesta, J., 2005. "Rehabilitation robotics: a wearable exo-skeleton for tremor assessment and suppression". In Proceedings of the 2005 IEEE International Conference on Robotics and Automation, IEEE.

[55] Lagoda, C., Moreno, J. C., and Pons, J. L., 2012. "Human-robot interfaces in exoskeletons for gait training after stroke: State of the art and challenges". *Applied Bionics and Biomechanics,* **9**(2), pp. 193–203.

[56] KROUSKOP, T., WILLIAMS, R., KREBS, M., HERSZKOWICZ, I., and GARBER, S., 1985. "Effectiveness of mattress overlays in reducing interface pressures during recumbency". *The Journal of Rehabilitation Research and Development,* **22**(3), p. 7.

[57] Boer, M., Duchnik, E., Maleszka, R., and Marchlewicz, M., 2016. "Structural and biophysical characteristics of human skin in maintaining proper epidermal barrier function". *Advances in Dermatology and Allergology,* **1**, pp. 1–5.

[58] Moissl-Eichinger, C., Probst, A. J., Birarda, G., Auerbach, A., Koskinen, K., Wolf, P., and Holman, H.-Y. N., 2017. "Human age and skin physiology shape diversity and abundance of archaea on skin". *Scientific Reports,* **7**(1), jun.

[59] Lees, V., 2016. "The functional anatomy of forearm rotation". *Journal of Hand and Microsurgery,* **01**(02), sep, pp. 92–99.

[60] Haddadin, S., Albu-Schäffer, A., and Hirzinger, G., 2009. "Requirements for safe robots: Measurements, analysis and new in-

sights". *The International Journal of Robotics Research,* **28**(11-12), aug, pp. 1507–1527.

[61] Rosenstrauch, M. J., and Kruger, J., 2017. "Safe human-robot-collaboration-introduction and experiment using ISO/TS 15066". In 2017 3rd International Conference on Control, Automation and Robotics (ICCAR), IEEE.

[62] Yamada, Y., Hirasawa, Y., Huang, S., and Umetani, Y., 1996. "Fail-safe human/robot contact in the safety space". In Proceedings 5th IEEE International Workshop on Robot and Human Communication. RO-MAN'96 TSUKUBA, IEEE.

[63] Biggs, J., and Srinivasan, M., 2022. "Tangential versus normal displacements of skin: relative effectiveness for producing tactile sensations". In Proceedings 10th Symposium on Haptic Interfaces for Virtual Environment and Teleoperator Systems. HAPTICS 2002, IEEE Comput. Soc.

[64] TAKEDA, Y., SUGAHARA, Y., MATSUURA, D., MATSUDA, S., SUZUKI, T., KITAGAWA, M., and LIU, Y.-C., 2019. "Introduction of dynamic pair to modeling and kinemato-dynamic analysis of wearable AssistDevices". *The Proceedings of Mechanical Engineering Congress, Japan,* **2019**(0), p. S11405.

[65] Liang, X., and Takeda, Y., 2019. "An iterative method for the inverse kinematics of lower-mobility parallel mechanism with three RS or SR chains based on kinematically equivalent mechanism". *Mechanism and Machine Theory,* **141**, nov, pp. 40–51.

[66] Ryu, J., Cooney, W. P., Askew, L. J., An, K.-N., and Chao, E. Y., 1991. "Functional ranges of motion of the wrist joint". *The Journal of Hand Surgery,* **16**(3), may, pp. 409–419.

[67] Schiele, A., 2008. "An explicit model to predict and interpret constraint force creation in pHRI with exoskeletons". In 2008 IEEE International Conference on Robotics and Automation, IEEE.

[68] Liu, Y.-C., and Takeda, Y., 2020. "Kineto-static analysis of a wrist rehabilitation robot with compliance and passive joints for joint misalignment compensation". *Machines,* **8**(2), may, p. 23.

[69] Pezent, E., Rose, C. G., Deshpande, A. D., and O'Malley, M. K., 2017. "Design and characterization of the OpenWrist: A robotic wrist exoskeleton for coordinated hand-wrist rehabilitation". In 2017 International Conference on Rehabilitation Robotics (ICORR), IEEE.

[70] McDaid, A. J., 2015. "Development of an anatomical wrist therapy exoskeleton (AW-TEx)". In 2015 IEEE International Conference on Rehabilitation Robotics (ICORR), IEEE.

[71] Holland, J. H., 1992. *Adaptation in Natural and Artificial Systems.* The MIT Press.

[72] Faghihi, A., Haghpanah, S. A., Farahmand, F., and Jafari, M., 2015. "Design and fabrication of a robot for neurorehabilitation : smart RoboWrist". In 2015 2nd International Conference on Knowledge-Based Engineering and Innovation (KBEI), IEEE.

[73] Srinivas, M., and Patnaik, L., 1994. "Adaptive probabilities of crossover and mutation in genetic algorithms". *IEEE Transactions on Systems, Man, and Cybernetics,* **24**(4), apr, pp. 656–667.

[74] Gomi, Koike, and Kawato, 1992. "Human hand stiffness during discrete point-to-point multi-joint movement". In Proceedings of the Annual International Conference of the IEEE Engineering in Medicine and Biology Society, IEEE.

[75] Mckinley, J. R., Rodríguez, E. Y., and Salcedo, M. F. C., 2019. "Multibody approach Matlab GUI for kinematic and dynamic analysis of planar mechanisms". In Scientia Et Technica.

[76] Hüsing, M., Riedel, M., Corves, B., and Nefzi, M., 2011. "Development of tailor-made robots - from concept to realization for small and medium-siz ed enterprise s". In The 13th World Congress in Mechanism and Machine Science.

[77] Kevin M. Lynch, F. C. P., 2017. *Modern Robotics: Mechanics, Planning, and Control*. CAMBRIDGE, May.

[78] Weng, H., Hunt, B., Todes, M., and Schultz, J., 2018. Modern Robotics: Mechanics, Planning, and Control-Code Library-Version 1.1.0. Tech. rep., Cambridge University Press.

[79] Liang, X., Irube, K., and Takeda, Y., 2020. "Kinematic design of a 3-rps parallel mechanism for wrist rehabilitation". In Proceedings of The 4th INTERNATIONAL WORKSHOP ON FUNDAMENTAL ISSUES, APPLICATIONS AND FUTURE RESEARCH DIRECTIONS FOR PARALLEL MECHANISMS / MANIPULATORS / MACHINES, The 4th INTERNATIONAL WORKSHOP ON FUNDAMENTAL ISSUES, APPLICATIONS AND FUTURE RESEARCH DIRECTIONS FOR PARALLEL MECHANISMS / MANIPULATORS / MACHINES.

[80] Palmer, A. K., Werner, F. W., Murphy, D., and Glisson, R., 1985. "Functional wrist motion: A biomechanical study". *The Journal of Hand Surgery,* **10**(1), jan, pp. 39–46.

[81] Morrey, B. F., Askew, L. J., and Chao, E. Y., 1981. "A biomechanical study of normal functional elbow motion.". *The Journal of Bone and Joint Surgery,* **63**(6), jul, pp. 872–877.

[82] Muscolino, J. E., 2016. *Kinesiology - The Skeletal System and Muscle Function.* Elsevier HealthScience EN, Aug.

[83] Neumann, D. A., 2016. *Kinesiology of the Musculoskeletal System: Foundations for Rehabilitation.* Elsevier LTD, Oxford, Nov.

[84] Krebs, H. I., Volpe, B. T., Williams, D., Celestino, J., Charles, S. K., Lynch, D., and Hogan, N., 2007. "Robot-aided neurorehabilitation: A robot for wrist rehabilitation". *IEEE Transactions on Neural Systems and Rehabilitation Engineering,* **15**(3), sep, pp. 327–335.

[85] Lewis, J. R., and Sauro, J., 2009. "The factor structure of the system usability scale". In *Human Centered Design.* Springer Berlin Heidelberg, pp. 94–103.

[86] Bangor, A., Kortum, P. T., and Miller, J. T., 2008. "An empirical evaluation of the system usability scale". *International Journal of Human-Computer Interaction,* **24**(6), jul, pp. 574–594.

[87] Cronbach, L. J., 1951. "Coefficient alpha and the internal structure of tests". *Psychometrika,* **16**(3), sep, pp. 297–334.

[88] Sauro, J., and Lewis, J. R., 2012. *Quantifying the User Experience.* Elsevier.

[89] Merlet, J. P., 2005. "Jacobian, manipulability, condition number, and accuracy of parallel robots". *Journal of Mechanical Design,* **128**(1), jun, pp. 199–206.

[90] Liang, X., and Takeda, Y., 2019. "Transmission index of a class of parallel manipulators with 3-RS(SR) primary structures based on pressure angle and equivalent mechanism with 2-SS chains replacing RS chain". *Mechanism and Machine Theory,* **139**, sep, pp. 359–378.

[91] Takeda, Y., and Funabashi, H., 1995. "Motion transmissibility of in-parallel actuated manipulators". *JSME international journal. Ser. C, Dynamics, control, robotics, design and manufacturing,* **38**(4), pp. 749–755.

[92] Mirmohammadi, S. J., Mehrparvar, A. H., Mostaghaci, M., Davari, M. H., Bahaloo, M., and Mashtizadeh, S., 2016. "Anthropometric hand dimensions in a population of iranian male workers in 2012". *International Journal of Occupational Safety and Ergonomics,* **22**(1), jan, pp. 125–130.

[93] Liu, Y.-C., Irube, K., and Takeda, Y., 2021. "Kineto-static analysis and design optimization of a 3-DOF wrist rehabilitation parallel robot with consideration of the effect of the human limb". *Machines,* **9**(12), nov, p. 323.

[94] Liu, Y.-C., and Takeda, Y., 2021. "Kineto-static analysis of a compact wrist rehabilitation robot including the effect of human soft tissue to compensate for joint misalignment". In ROMANSY 23 - Robot Design, Dynamics and Control, G. Venture, J. Solis, Y. Takeda, and A. Konno, eds., Springer International Publishing, pp. 321–329.

[95] Liu, Y.-C., Botta, A., Quaglia, G., and Takeda, Y., 2022. "Preliminary mechanical design of a wearable parallel-serial hybrid robot for wrist and forearm rehabilitation with consideration of joint misalignment compensation". In ROMANSY 24 - Robot Design, Dynamics and Control, A. Kecskeméthy and V. Parenti-Castelli, eds., Springer International Publishing, pp. 53–61.

[96] Liu, Y.-C., and Takeda, Y., 2019. "Static analysis of a wrist rehabilitation robot with consideration to the compliance and joint misalignment between the robot and human hand". In In Proceedings of the Annual Conference of the Robotics Society of Japan 2019, The 37th Annual Conference of the Robotics Society of Japan, pp. 1F3–05.

[97] Liu, Y.-C., and Takeda, Y., 2019. "Kineto-static analysis of a wrist rehabilitation robot with compliant elements and supplementary passive joints to compensate the joint misalignment". In The 2nd International Jc-IFToMM Symposium, The 2nd International Jc-IFToMM Symposium.

[98] Liu, Y.-C., and Takeda, Y., 2020. "Development of a human-robot dynamic model of a wearable robot for wrist rehabilitation". In In Proceedings of the Annual Conference of the Robotics Society of Japan 2020, The 38th Annual Conference of the Robotics Society of Japan, pp. 1I2–01.

[99] Liu, Y.-C., and Takeda, Y., 2021. "Analysis of a 3-dof parallel robot for wrist rehabilitation with consideration of effect of human limb". In Proceedings of The 3rd Jc-IFToMM International Symposium (The 26th Jc-IFToMM Symposium on Mechanism and Machine Theory, The 3rd Jc-IFToMM International Symposium

(The 26th Jc-IFToMM Symposium on Mechanism and Machine Theory), pp. 49–56.

List of Publications

Journal Paper

1. Liu, Y.-C., and Takeda, Y., 2020. "Kineto-static analysis of a wrist rehabilitation robot with compliance and passive joints for joint misalignment compensation". *Machines,* **8**(2), may, p. 23

2. Liu, Y.-C., Irube, K., and Takeda, Y., 2021. "Kineto-static analysis and design optimization of a 3-DOF wrist rehabilitation parallel robot with consideration of the effect of the human limb". *Machines,* **9**(12), nov, p. 323

Book Chapter

1. Liu, Y.-C., and Takeda, Y., 2021. "Kineto-static analysis of a compact wrist rehabilitation robot including the effect of human soft tissue to compensate for joint misalignment". In ROMANSY 23 - Robot Design, Dynamics and Control, G. Venture, J. Solis, Y. Takeda, and A. Konno, eds., Springer International Publishing, pp. 321–329

2. Liu, Y.-C., Botta, A., Quaglia, G., and Takeda, Y., 2022. "Preliminary mechanical design of a wearable parallel-serial hybrid robot for wrist and forearm rehabilitation with consideration of joint misalignment compensation". In ROMANSY 24 - Robot Design, Dynamics and Control, A. Kecskeméthy and V. Parenti-Castelli, eds., Springer International Publishing, pp. 53–61

Conference Paper

1. Liu, Y.-C., and Takeda, Y., 2019. "Static analysis of a wrist rehabilitation robot with consideration to the compliance and joint misalignment between the robot and human hand". In In Proceedings of the Annual Conference of the Robotics Society of Japan 2019, The 37th Annual Conference of the Robotics Society of Japan, pp. 1F3–05

2. Liu, Y.-C., and Takeda, Y., 2019. "Kineto-static analysis of a wrist rehabilitation robot with compliant elements and supplementary passive joints to compensate the joint misalignment". In The 2nd International Jc-IFToMM Symposium, The 2nd International Jc-IFToMM Symposium

3. Liu, Y.-C., and Takeda, Y., 2020. "Development of a human-robot dynamic model of a wearable robot for wrist rehabilitation". In In Proceedings of the Annual Conference of the Robotics Society of Japan 2020, The 38th Annual Conference of the Robotics Society of Japan, pp. 1I2–01

4. Liu, Y.-C., and Takeda, Y., 2021. "Analysis of a 3-dof parallel robot for wrist rehabilitation with consideration of effect of human limb". In Proceedings of The 3rd Jc-IFToMM International Symposium (The 26th Jc-IFToMM Symposium on Mechanism and Machine Theory, The 3rd Jc-IFToMM International Symposium (The 26th Jc-IFToMM Symposium on Mechanism and Machine Theory), pp. 49–56

Acknowledgements

First and foremost, I would like to thank my supervisor Professor Yukio TAKEDA for his guidance, encouragement and continuous support throughout my research duration at Tokyo Tech. I am grateful to Associate Professor Yusuke SUGAHARA, Associate Professor Daisuke MATSUURA, Assistant Professor Kotaro HOSHIBA and Assistant Professor Ming JIANG for their constructive feedback and guidance for my research and life. I would also like to thank the members of Mechanical Systems Design Laboratory for their advice and assistance.

I would like to thank all the participant who volunteered for our experiment, for sparing their valuable time to contribute for this work. I would also like to thank assistants of our lab, Hiroko TAKANO - san and Taiko ICHINOSE - san, for helping me with the daily life activities.

Finally, I would like to express my deepest gratitude to my parents and family for all their support and understanding throughout my research life.